UNIVERSITY OF Southampton

University of Southampton Research Repository

Copyright © and Moral Rights for this thesis and, where applicable, any accompanying data are retained by the author and/or other copyright owners. A copy can be downloaded for personal non-commercial research or study, without prior permission or charge. This thesis and the accompanying data cannot be reproduced or quoted extensively from without first obtaining permission in writing from the copyright holder/s. The content of the thesis and accompanying research data (where applicable) must not be changed in any way or sold commercially in any format or medium without the formal permission of the copyright holder/s.

When referring to this thesis and any accompanying data, full bibliographic details must be given, e.g.

Thesis: Author (Year of Submission) "Full thesis title", University of Southampton, name of the University Faculty or School or Department, PhD Thesis, pagination.

Data: Author (Year) Title. URI [dataset]

University of Southampton

Faculty of Environmental and Life Sciences

Ocean and Earth Science

Assessing the Capabilities of the ICP-MS/MS for radionuclide analysis

by

Žilvinas Zacharauskas

Thesis for the degree of PhD Ocean and Earth Science

September 2019

University of Southampton

Abstract

Faculty of Environmental and Life Science

Ocean and Earth Science}

Thesis for the degree of Doctor of Philosophy

Assessing the capabilities of the ICP-MS/MS for radionuclide analysis

by

Žilvinas Zacharauskas

The development of robust and routine methods for radionuclide analysis using ICP-MS/MS systems has been investigated for application to nuclear decommissioning and waste characterisation, as well as applications to nuclear forensics and emergency response scenarios. The advances of the Agilent 8800, ICP-MS/MS system have increased the range of potentially measurable radionuclides. Overcoming interferences through the use of the tandem mass spectrometers and the collision/ reaction cell, allowed for a faster throughput than traditional radiometric techniques. The study utilised the ICP-MS/MS in conjunction with robust chemical separation steps both offline and online to achieve the most complete interference removal and apply measurement to real world scenarios and matrixes, with specific interest in nuclear waste assays.

An initial assessment of non-active ground water, stainless steel, air filter and non-active concrete samples were processed and analysed to demonstrate the potential sensitivities achievable by ICP-MS/MS for direct digest solutions, with high matrix concentration. Low instrumental backgrounds were achievable for many of the actinides, including ^{235}U, ^{236}U, ^{237}Np, ^{239}Pu, ^{241}Am as well as ^{59}Ni, ^{93}Zr, ^{99}Tc, ^{126}Sn, ^{135}Cs and ^{151}Sm when operating under no gas, MS/MS demonstrates the potential for emergency response analysis, where minimal sample handling and preparation would reduce sample turn around, and improve response times. The technique also offers a means for characterisation and screening of decommissioning waste and samples from a range of different matrix types including ground waters, steels, air filters and concretes, without the need for extensive separation and purification.

A focused assessment was carried out on concrete samples, with stable concrete direct digest analysis demonstrating that the isotopes of ^{234}U, ^{235}U, ^{236}U, ^{238}U, ^{239}Pu, ^{240}Pu and ^{241}Am could be measured well below their out-of-scope limits as demonstrated by the low background signal measured. The analysis of variable digest procedures utilising variable acid digests showed that in most cases acid attack in the form of concentrated HNO_3, HCl or a combination of (aqua regia) was not sufficient in liberating the majority of the target analytes from the concrete matrixes investigated. Complete sample digest ($LiBO_2$ fusion followed by HNO_3 digest) was utilised on active concretes to demonstrate the need for complete sample digest to ensure all the actinides and specifically the potentially insoluble Pu species, such as PuO_2, would also be incorporated into the solution. The use of collision gases was shown to not have any benefit for actinide analysis and instead increased the uncertainty on the measurements due to signal dampening and reduction in overall signal sensitivity. The use of MS/MS mode, however, was able to reduce the impact from the bulk matrix loading, potential polyatomic interference formation within the cell and tailing from abundant neighbouring radionuclides. The use of no gas mode ensured maximum signal sensitivity for the target radionuclides.

Method development was extended to ^{129}I to further demonstrate the capabilities of the ICP-MS/MS. Iodine-129 is a long-lived radionuclide formed most commonly from anthropogenic activity via nuclear fission, with the majority originating from reprocessing facilities and decommissioning of nuclear sites. The long half-life is theoretically suited to measurement using inductively coupled plasma mass spectrometry (ICP-MS), which offers a rapid alternative to decay counting and AMS techniques. However, previous measurement has been limited by the multiple interferences on m/z = 129. Recent availability of tandem ICP-MS/MS has demonstrated a means to overcoming these interferences using a combination of a collision-reaction cell and tandem mass spectrometer setup. This study builds on previous work with additional improvements in sensitivity (~60% increase) through matrix modification prior to sample introduction and demonstrates the importance of selecting an appropriate internal standard. The method was tested on various decommissioning wastes including silo liquors and slurries, ion exchange resins and graphite, with good agreement between ICP-MS/MS and liquid scintillation counting was observed. A detection limit of 1.05×10^{-4} Bq g^{-1} (0.016 ng g^{-1}) was achieved for ^{129}I, which is two orders of magnitude below the out-of-scope limit of 0.01 Bq

g^{-1} (1.53 ng g^{-1}). The results put ICP-MS/MS in a position where routine out-of-scope measurement of ^{129}I is now a possibility, which is beneficial for rapid assessment of materials at decommissioning nuclear sites, and for long term waste storage and disposal with potential development into environmental monitoring.

Having assessed the instrument for direct digest analysis and method development of a specific radionuclide, the instrument was investigated for its capabilities in assessing isotope ratios which traditionally required extensive offline chemical separation and purification prior to analysis by multi-collector ICP-MS. The ICP-MS/MS offers the capabilities of doing direct digest analysis of samples while still being able to accurately measure isotope ratios. Lead isotope ratios were selected as a representative stable element system which is well understood for the anthropogenic source terms with results compared against MC-ICP-MS data. The technique was able to achieve measurement uncertainties <0.2% for the single quadrupole configuration and <0.6 % for $^{206}Pb/^{204}Pb$ and ~0.25 % for $^{206}Pb/^{207}Pb$ under MS/MS mode, self-aspirated and using NIST SRM 981 Pb standard sample bracketing. The use of MS/MS was shown to increase uncertainty however, for radiometric isotopic systems where interfering ions associated with isobars and neighbouring isotope tailing into the m/z = ±1 and ±2, as well as polyatomic interferences, utilising the MS/MS, mass filtering capabilities of Q1 it is possible to reduce this impact and potentially allow for isotope ratios to be measured with results comparable to those achievable by MC-ICP-MS without the need for extensive sample preparation.

Table of Contents

Table of Tables

Table of Tables

Table of Figures

Table of Figures

Table of Figures

Research Thesis: Declaration of Authorship

Print name: Žilvinas Zacharauskas

Title of thesis: Assessing the capabilities of the ICP-MS/MS for radionuclide analysis

I declare that this thesis and the work presented in it are my own and has been generated by me as the result of my own original research.

I confirm that:

1. This work was done wholly or mainly while in candidature for a research degree at this University;
2. Where any part of this thesis has previously been submitted for a degree or any other qualification at this University or any other institution, this has been clearly stated;
3. Where I have consulted the published work of others, this is always clearly attributed;
4. Where I have quoted from the work of others, the source is always given. With the exception of such quotations, this thesis is entirely my own work;
5. I have acknowledged all main sources of help;
6. Where the thesis is based on work done by myself jointly with others, I have made clear exactly what was done by others and what I have contributed myself;
7. Parts of this work have been published as:-

Warwick, P.E., Russell, B.C., Croudace, I.W., Zacharauskas, Ž., J. Anal. At. Spectrom., 2019, 34 (9),1810-1821 Evaluation of inductively coupled plasma tandem mass spectrometry for radionuclide assay in nuclear waste characterisation

Signature: Date:

Acknowledgements

I would like to express my greatest appreciation and thanks to my supervisors Phil Warwick, Ben Russell and Ian Croudace for their invaluable guidance, patience and drive in helping me achieve the PhD and for shape me into the research scientist that I am today. I would also like to thank the University of Southampton, NPL and GAU radioanalytical for proving the funding and support of.

I would like to thank my parents for being my emotional support during the trying times of the PhD and for their unwavering love and support in helping me achieve my goals and ambitions. Without them making the choice all those years ago to move to the UK in the pursuit of a better life I would not have had the opportunities to discover and pursue own my passion in the sciences, go to university to read chemistry and finally work towards achieving my dream of completing a PhD. They have facilitated my growth not only as scientist but more importantly as a person and for that I will forever be indebted to them.

I am particularly grateful to my friends Žygimantas Kadžiulis, Tanya Beattie, Callum Fry, and many others for their emotional support over the last 4 years, helping me maintain my sanity and reminding me that taking a break is a necessary evil. The many hours spent together have shaped the person that I have become, and I am sure there will be many more moments we will undoubtable spend together.

My thanks are extended to the staff of the GAU, with each and every one of them giving assistance, guidance and advice without hesitation. They made my time in the laboratories that much more enjoyable and productive.

Definitions and Abbreviations

AGR - Advanced Gas-cooled Reactor

AMS - Accelerator Mass Spectrometry

Bq - Becquerel

DTM – Difficult To Measure

HLW – High Level Waste

HMI – High Matrix Introduction

ICP – Inductively Coupled Plasma

ICP-MS – Inductively Coupled Plasma – Mass Spectrometry

ICP-MS/MS – Inductively Coupled Plasma – Tandem Mass Spectrometry

ILW – Intermediate Level Waste

LLW – Low Level Waste

LMI – Low Matrix Introduction

LoD – Limit of Detection

LSC – Liquid Scintillation Counting

MC – Multiple Collectors

MC-ICP-MS – Multiple Collector – Inductively Coupled Plasma - Mass Spectrometry

MS - Mass Spectrometry

NDA – Nuclear Decommissioning Authority

NORM – Naturally Occurring Radioactive Material

ONR – Office for Nuclear Regulation

ORS^3 – Octopole Reaction System

PWR - Pressurized Water Reactor

RF – Radio Frequency

RNAA – Radiochemical Neutron Activation Analysis

SEM – Secondary electron Multiplier

SF-ICP-MS – Sector Field – Inductively Coupled Plasma – Mass Spectrometer

SQ – Single Quadrupole

TDS – Total Dissolved Solid

TIMS – Thermal Ionization Mass Spectrometry

VLLW – Very Low-Level Waste

Chapter 1 Introduction

Globally 115 commercial power reactors, 48 experimental or prototype reactors and over 250 research reactors have been retired from operation and are transitioning to decommissioning and shutdown (WNA 2019). Many of these being first and second generation nuclear facilities that were built between the 1960's and 1970's. The UK has 29 reactors, across 17 sites, Figure 1, with 11 of these sites being the Magnox designed reactors that have shifted across to decommissioning activities with all having been defueled by 2019 (NDA Draft Business Plan 2018). While the remaining 15 operating reactors, advanced gas-cooled reactors (AGR) and pressurized water reactors (PWR), also expected to head towards shutdown and decommissioning between 2023 and 2035 (NDA Draft Business Plan 2018).

Since each of these reactors was built with variations the techniques and technologies developed for one are not always easily transferable to others. The process for decommissioning of a reactors in the UK, Figure 2, requires the removal and transportation of the spent fuel to a reprocessing facility in North West England, Sellafield, making the decommission of this facility a much greater challenge (ukinventory.nda.gov.uk). These challenges come about from the fact that much of the difficult to work with materials from other reactors are brought to its cooling pools and stored under one system. This provides a challenge in characterisation of the radionuclides present in the waste as well as measurement issues associated with the types of radiation and radionuclides within the matrix itself. It is also important to recognise that there is little high level waste (HLW) (<1 %) relative to the intermediate (ILW) (~6%) and low level waste (LLW) (94%) meaning that much of the waste is low activity but makes up a large volume of the total waste, Figure 3 and Table 1, (ww3).

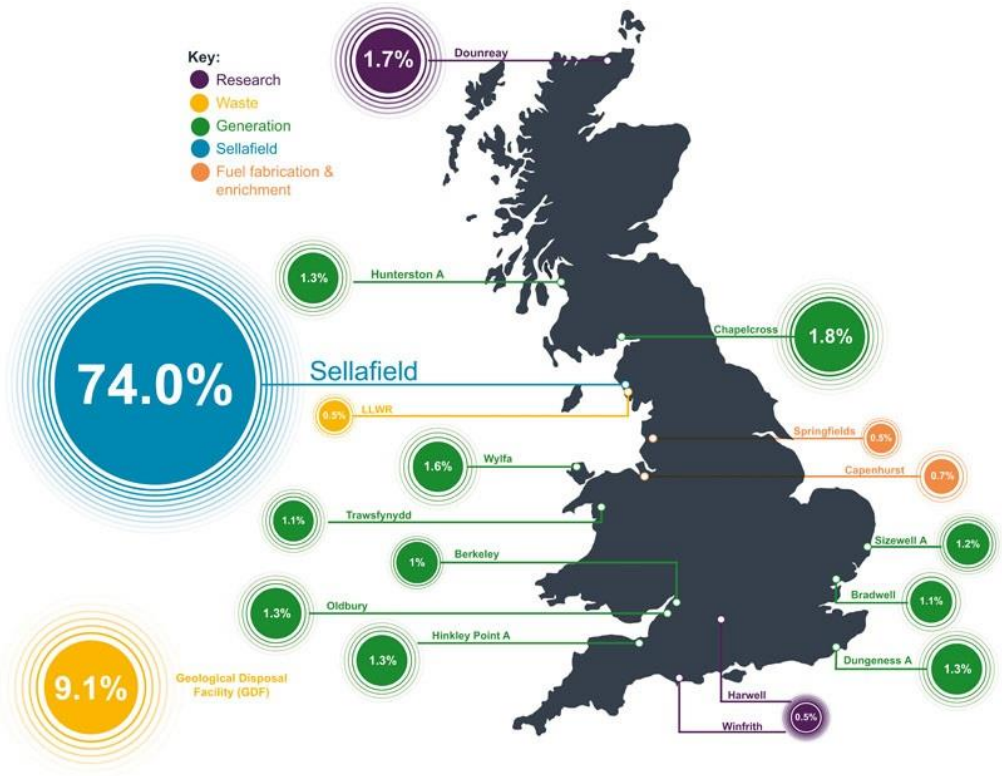

Figure 1: Map showing sites and the percentage of the undiscounted nuclear provision forecast to be spent at each site, 2017 (gov.uk)

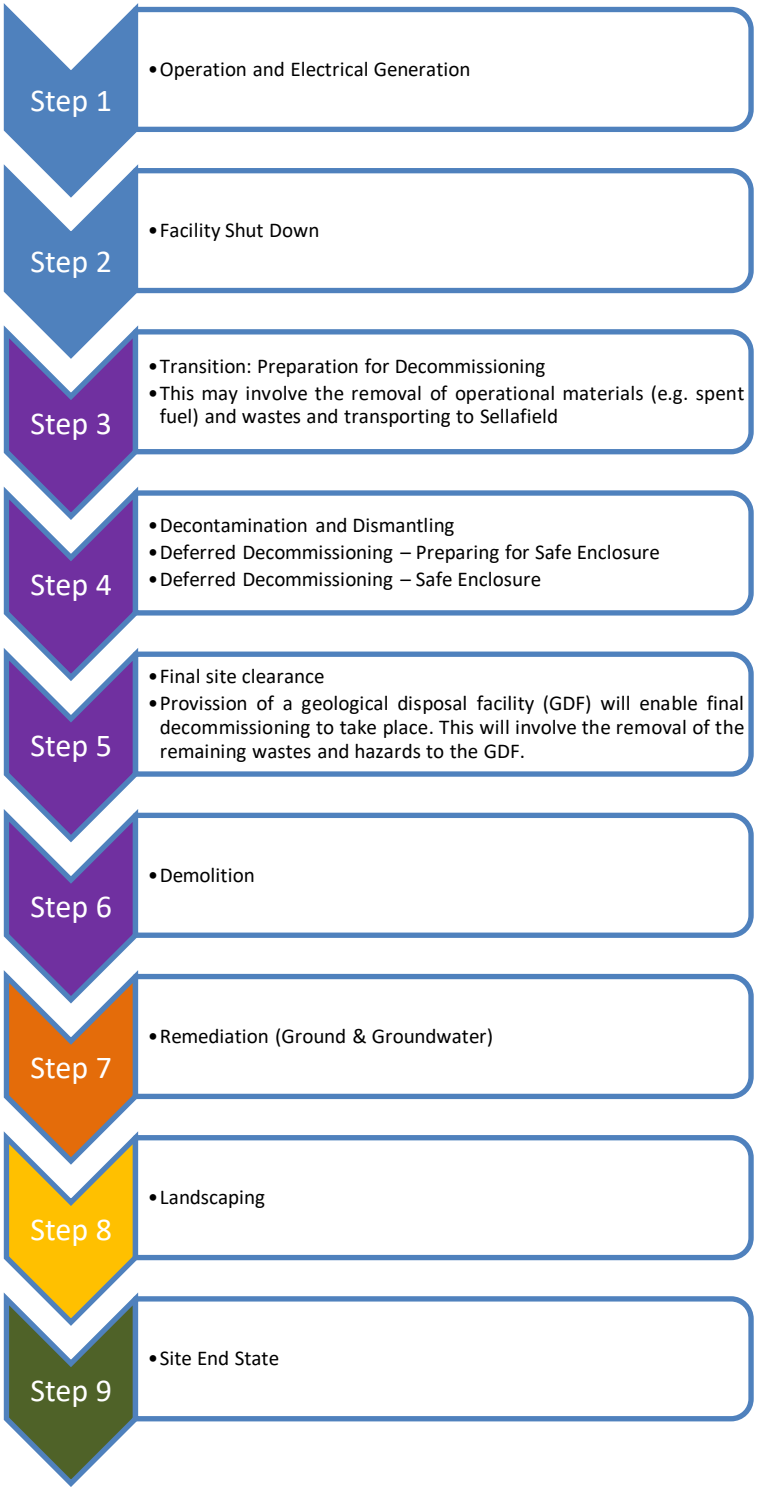

Figure 2: Stages of nuclear facility operation and decommissioning. Adapted from NDA site transition (ukinventory.nda.gov.uk)

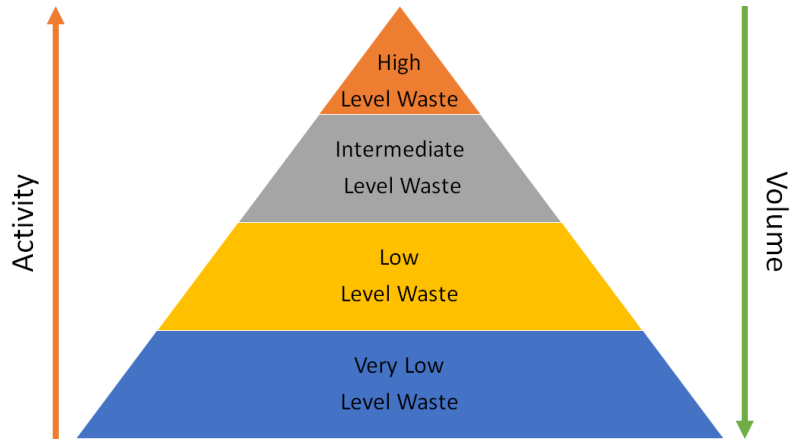

Figure 3: Nuclear waste pyramid, classification, volume and activity

Table 1: Nuclear waste description and characterisation criteria (NDA 2018, Integrated Waste Management Radioactive Waste Strategy, ONR 2015, Basic Principles of Radioactive Waste Management)

Waste category	Type of material	Classification
High Level Waste (HLW)	Used Fuel Reprocessing Fuel Waste Sludge's from Cooling Pools	Temperature may rise significantly due to the radioactivity present and must be taken into consideration for storage and disposal
Intermediate Level Waste (ILW)	Refurbishment Waste Ion Exchange Resins Long Lived Radionuclides Materials Exposed to Neutrons (Concrete, Metals, Construction Materials)	Exceeds the upper limit of LLW but does not generate a significant amount of heat
Low Level Waste (LLW)	Structural Concrete and Steel Protective Shoe Covers, Rags, Mops and Tools Short Lived Radionuclides (<300 years) Contaminated Ground from Leaks	<4 gigabecquerels (GBq) per tonne of alpha activity <12 GBq per tonne of beta/gamma activity
Very Low Level Waste (VLLW)	Rubble, Soil and steel items	A sub-category of LLW with limits permissible for regular household/ industrial waste disposal

Sellafield is a unique level of complexity for the global nuclear sector, especially given that it was developed as a plutonium production facility and then transitioned into a decommissioning and reprocessing facility, meaning that the initial research focused on the measurement of short lived radionuclides (Croudace et al., 2017). The site has since shifted towards the lower abundance longer lived radionuclides in the presence of higher abundance radionuclides. These longer lived radionuclides are a mix of activation, fission and naturally occurring radionuclides and are proving to be of greater importance due to the long term exposure as well as the target of long term storage (Ewing et al., 2015, Croudace et al., 2016, Clases et al., 2017). The analytical challenges for these radionuclides are not only limited to the matrix, but also interfering ions, polyatomic and spectral interference. Many of the existing radiometric techniques have a limited sample throughput, reducing the efficiency of decommissioning and hence faster, robust techniques are being explored as technology advances (Croudace et al., 2017).

Engineering issues associated with Sellafield are also to be taken into consideration when developing decommissioning technique for the radionuclides. The densely packed site and the initial builds had no plans set into motion in regard to decommissioning. Record keeping has also been highlighted as poor relative to modern standards, meaning that the nature and state of the materials both hazardous and constructional are not well documented and further research is required to truly understand the task at hand (gov.uk, NDA 2019). The development of new technologies for this site have already opened up possibilities for future decommissioning projects, however, the process is long, complex and costly.

The current expected cost of the UK's nuclear legacy facilities is £124 billion (gov.uk, NDA 2019), however the nuclear decommissioning authority (NDA) has estimated that it could cost anywhere from £99 billion to £232 billion over the 120 year time scale, with Sellafield taking almost ¾ of the annual budget (gov.uk, NDA 2019).

1.1 Source of radionuclides

Radionuclides are radioactive isotopes of elements found either naturally, as in the case of U decay series, ^{40}K, ^{14}C, as well as many others including all the daughter products of the

decay of these naturally occurring isotopes (Łokas et al., 2017). Through the development of nuclear fission technology, a larger range of radionuclides were introduced into the natural environment. These include activation products formed when materials are exposed to a high neutron flux, as in the case for constructional materials around a nuclear reactor, such as ^{59}Ni, ^{63}Ni and ^{41}Ca (Evans 1979, Taddei et al., 2013). An array of fission products may also be introduced, which form when fissile materials such as ^{235}U within a reactor undergoes spontaneous fission or nuclear weapons are detonated causing a fall out of radioactive materials and radionuclides formed as part of the fission process within them, such as ^{90}Sr, ^{129}I, ^{135}Cs, ^{137}Cs (Hu et al., 2010, Merz et al., 2015). Figure 4 shows the range of radionuclides most likely to form from nuclear fission of variable fissile isotopes including ^{233}U, ^{235}U, ^{239}Pu and ^{241}Pu within light water reactors. Figure 5 is the table of the nuclides showing the complete mass range of all the radionuclide species that can and do form within both nuclear reactors and nuclear weapons, sorted by their neutron and proton number (nucleonica.com).

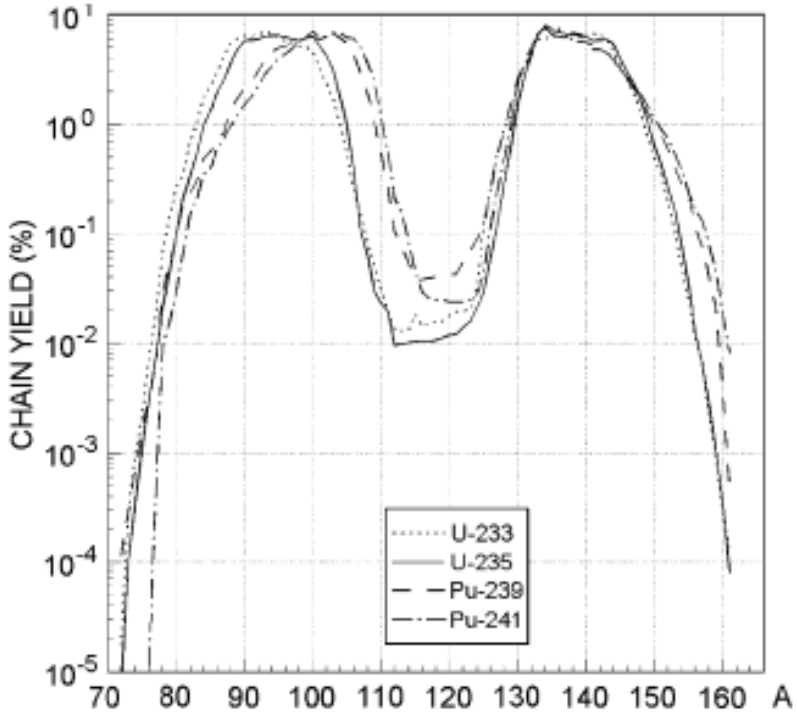

Figure 4: Fission product curve for ^{233}U, ^{235}U, ^{239}Pu and ^{241}Pu (Nuclear Safety in Light Water Reactors, 2012)

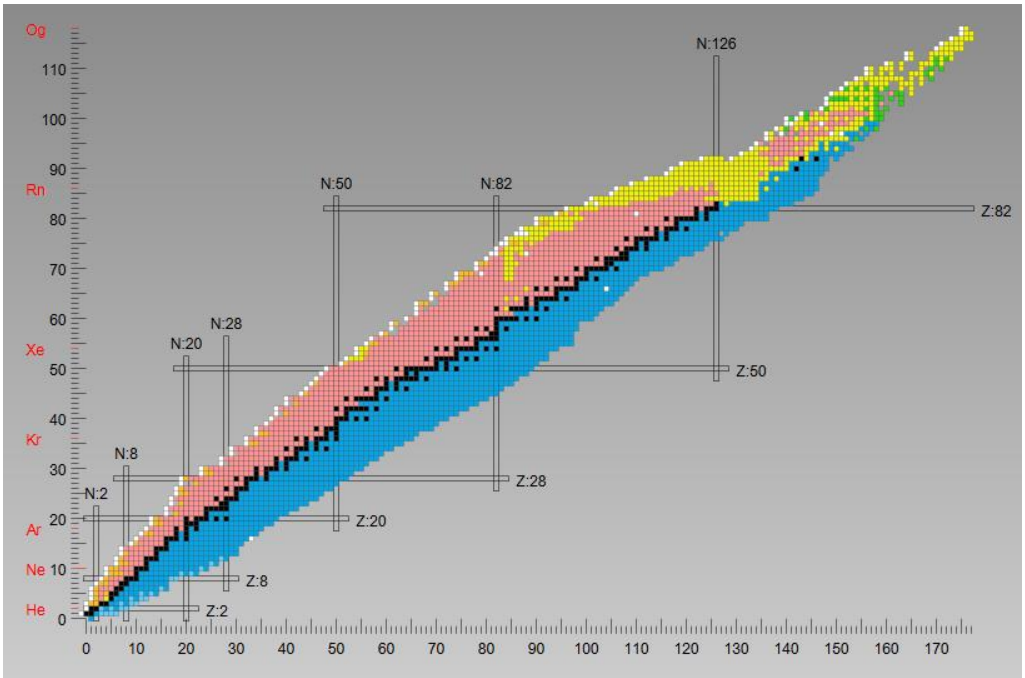

Figure 5: Chart of the nuclides with neutron number posted on the X axis and proton number on the Y axis. Showing the full range of radionuclides which can form via alpha (yellow), or beta decay [beta+ red, beta- blue) or spontaneous fission as well as by gamma

The source of the radionuclide and the locations which it is likely to be found determine what kind of analysis will be best suited for its measurement and which interferences, isobaric, polyatomic, spectral and matrix based will need to be accounted for. Within the reactor itself the proximity to the neutron beam as well as the proximity to the reactor cores will determine if certain materials will have specific radionuclides present.

1.2 Measurement techniques for radionuclides

There has been a shift from operation and reprocessing to decommissioning and waste storage/disposal requiring measurement of a range of medium and long-lived radionuclides. Many of these are considered difficult to measure (DTM), whereby the radionuclide cannot be readily quantified in a waste package using non-destructive techniques such as gamma spectrometry due to the nuclide's emission being low energy beta or alpha radiation, such as ^{14}C, ^{63}Ni and ^{240}Pu, as defined by the IAEA 2009. Many of these DTM radionuclides have not been previously monitored when decommissioning,

with few (if any) routine procedures in place, with some radionuclides requiring a scaling factor based on an easy to measure key radionuclide rather than a direct measurement of the radionuclide itself, for example utilising ^{60}Co to correlate with ^{63}Ni formation and concentration (IAEA, 2007). A comprehensive list of the DTM radionuclides considered for this study can be found in Table 3, which corresponds to radionuclides which the ICP-MS may offer a method for analysis while also being a part of the IAEA 2009 list of DTM radionuclides of interest.

1.2.1 Radiometric analysis of radionuclides

Traditionally radionuclides have been analysed by counting the radiation they give off through nuclear decay. These techniques are known as radiometric techniques and apply to alpha, beta and gamma spectrometry. Gamma emitting radionuclides can be measured without prior separation. Long counting times and complete isolation of radionuclides with complex separation chemistry have meant that alpha and beta counting techniques have limited sample throughput, but can achieve very good limits of detection (LODs) (Kazuhisa and Yasunori, 2004, Komura and Hanahuna, 2004, Rusconi et al., 2006, , Hou, et al., 2009). With many of the DTM radionuclides being alpha and beta emitters, there is a need to improve throughput, which could offer significant economic benefits to decommissioning sites. The increasing importance of DTM radionuclides for decommissioning has led to the use of novel technologies and techniques being investigated to expand the range of radionuclides that can be measured (Hou et al., 2007, IAEA, 2009, Croudace et al., 2017).

1.2.2 Non radiometric analysis of radionuclides

Non radiometric techniques have also been explored as a means to separate radionuclides based on their isotopic mass and count the ions themselves rather than the radiation produced. Techniques such as inductively coupled mass spectrometry (ICP-MS) (Becker, 2005, Croudace et al., 2017), radiochemical neutron activation analysis (RNAA) (Kalmykov et al., 2004, Kučera 2007), accelerator mass spectrometry (AMS) (Zhao et al., 2004, Shozugawa et al., 2015, Terrasi et al., 2018) and thermal ionization mass spectrometry (TIMS) (Meeks et al., 1998), have all been used for analysis of radionuclides in the past. Where activity can be calculated from the number of atoms using, $A = \lambda N$. However, techniques such as RNAA and AMS are not considered routine due to their limited

commercial availability and analytical flexibility. The use of TIMS instrumentation has previously yielded more precise measurements than quadrupole ICP-MS instruments for the actinides but required considerably more operator involvement, reducing sample throughput while making the process impractical for routine analysis at commercial laboratories.

1.2.3 ICP-MS

The development of the first ICP-MS technology in 1983, allowed the rapid and simultaneous measurement of multiple elements and radionuclides (Boomer and Powell, 1987, Hu and Houk, 1993, Potter, 2008). This multi element analysis meant that complete isolation of radionuclides was not necessary as the analysis focused on specific masses rather than the radiation that was produced, meaning that radiometric spectral interferences were no longer an issue (Brown et al., 1988). The use of a plasma source allowed for a more robust routine approach to be used for analysis compared to thermal ionization mass spectrometry (TIMS) which has a limited matrix introduction and long sample preparation times (Meeks et al., 1998). The use of an internal standard for multi-elemental analysis further improved analysis by ICP-MS as it was possible to correct for matrix effects and signal drift and plasma variations throughout the analysis.

Traditionally ICP-MS techniques had been applied to long-lived radionuclides due to the increased efficiency of counting the atoms themselves rather than the relatively weak decay energy (Meeks et al., 1998, Boulyga et al., 2001, Croudace et al., 2017). However, unlike radiometric techniques ICP-MS measurement has been previously limited to interferences from isobaric, polyatomic and abundance sensitivities (Boulyga et al., 2001, Balcaen et al., 2015), Table 2.

Interferences could be removed through either offline chemical separation or online through cell-based separations using collision or reaction gases and the instrumental configurations. The range of gases that can be used is extensive however the premise of collisional gases is to break up polyatomic interferences, while reaction gases are designed to react with the analyte or the interfering ions and either charge transfer or mass shift

them, allowing for an interference free mass to be used and an accurate measurement of the radionuclide to be achieved (May et al., 1998, Balcaen et al., 2015).

Table 2: List of potential instrumental interference on an ICP-MS and how to overcome

Interference	Description and Example	How to Overcome Online
Isobaric	Isotope with similar mass to charge ratio as the ion of interest. e.g. ^{90}Sr and ^{90}Zr, ^{129}I and ^{129}Xe	Reaction gas to shift either the target analyte or interference away, or charge transfer with interfering ion or element. e.g. O_2 mode for Sr/Zr (ZrO forms readily) (Croudace et al., 2017) O_2 mode for I/Xe separation (Charge transfer with Xe) (Ohno et al., 2013)
Polyatomic	A molecular ion with the same mass to charge ratio as the ion of interest. e.g. ^{93}Zr and ^{92}Mo^{1}H (m/z = 93)	Collision gas to break up the polyatomic or a reaction gas to mass shift the target analyte away. e.g. NH_3 and H_2 mode to mass shift the Zr from m/z=93 to m/z=195 as a $^{93}Zr(NH_3)_6$ cluster (Petrov et al., 2018)
Abundance Sensitivity	High abundance isotope one or two mass units either side of the analyte ion, resulting in peak tailing e.g. ^{237}Np and ^{238}U and ^{239}Pu, ^{90}Sr and ^{88}Sr	If tailing isotope is a different element to the analyte, offline chemical separation. If tailing is from an isotope of the same element as the analyte, removal depends on abundance sensitivity of the instrument

Advances in mass spectrometry capabilities have helped with interference removal, through the use of collision/ reaction cells (Fujiwara et al., 2011, Takagi et al., 2014), sector field instruments (Livens and Loveland, 1988, Russell et al., 2014, Russell et al., 2015), variable sample introduction set ups (Scarciglia & Barca 2017) as well as ion beam transitions in the case of using a secondary quadrupole as a mass filter prior to the collision/reaction cell in an ICP-MS/MS (Niu, 1994, Balcaen et al., 2015). The use of these technologies has increased the list of elements and radionuclides that could be analysed. However, reaction cell technology did not allow for complete interference removal, especially in regards to activation products due to the high abundance of stable isotopes present in the matrix analysed, which meant abundance sensitivity has been a limiting factor for many ICP-MS radionuclide measurements (Balcaen et al., 2015).

This limitation lead to further development of high resolution instruments and multi-collector detectors further improved the sensitivity through multiple detector counting,

interference control and removal through reaction cells and cell peak resolving, as well as increasing the range of elements and radionuclides that were measurable through improved understand of reaction gas chemistry that can be carried out online (Tanner et al., 2002, Balcaen et al., 2015,). It should, however, be noted that high peak resolution can improve abundance sensitivity but not resolve isobars (Vonderheide et al., 2004, Becker et al., 2010). These developments reduced the reliance on offline chemical separation and allowed a greater control and separation using the instrument itself (Fujiwara et al., 2011, Yamazaki et al., 2014).

A multi-collector ICP-MS is a combination of an inductively coupled plasma (ICP), an energy filter, a magnetic sector analyser and multiple collectors (MC) for the measurement of ions. The ions are accelerated and focused into a beam via a series of slits, and passed through an energy filter and then a magnetic field where the ion beam is separated based on the m/z ratio before then having the now separated ion beams directed to individual collectors where the ions are converted into voltage and the comparison of voltages can allow for accurate isotopic ratios to be calculated (Figure 6). However, the lack of collision/ reaction cell means that complete resolution of interferences may not be possible if the m/z ratio is too similar, meaning very thorough offline chemical separation is necessary (Baker et al., 2004).

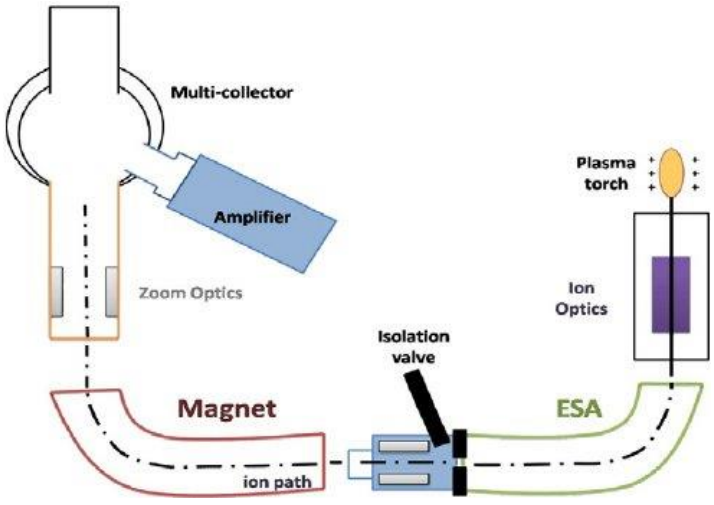

Figure 6: MC-ICP-MS schematic (Ali et al., 2011)

A sector field instrument (Figure 7) utilises a similar configuration to the multi-collector instrument however, it does not have the zoom optics and multiple collectors for the ion

beams but rather it uses both a counting and an analogue detector and electron multiplier which converts the ion charge into a voltage. The use of secondary electron multiplier (SEM) increases the signal sensitivity and increases the dynamic range from 1-10^6 using purely a counting detector to >10^9 using an analogue mode. However, the optimum operational range in analogue mod is 10^4-10^{10} counts per second (ThermoFinnigan Element2 Operating Manual, 2001). This improved signal sensitivity has been shown to be very effective for radionuclides due to the relatively low abundance in samples, however, like the MC-ICP-MS it does not carry a reaction cell to allow for interference removal, relying therefore on offline chemical separation and the magnetic resolution of variable m/z ratios.

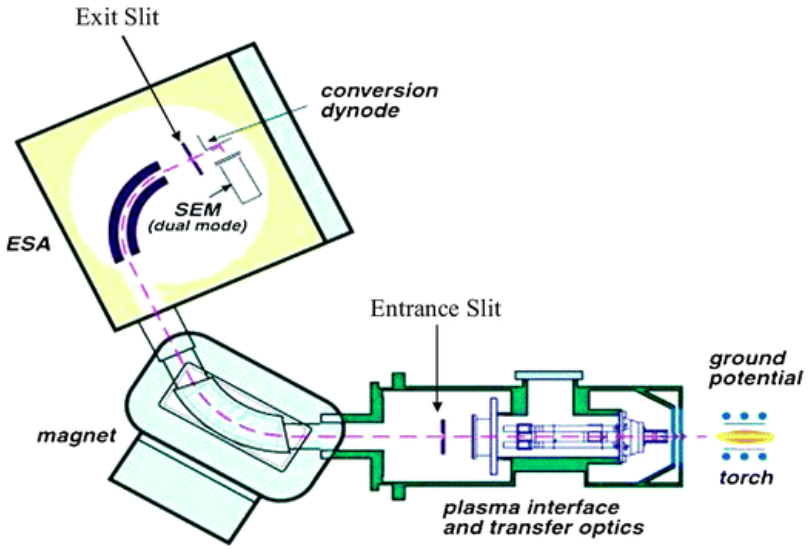

Figure 7: Sector Field ICP-MS schematic - Element 2 (Jakubowski, 2008)

Radiometric techniques favour shorter lived radionuclides as longer-lived radionuclides require longer counting times to get a significant number of radioactive decays which in turn reduces sample throughput. This limited the analysis to shorter lived samples originating from nuclear incidents and meant that longer lived radionuclide analysis was hindered (Figure 8). Longer lived radionuclides are measurable by radiometric techniques but often suffer from spectral interferences of more abundant shorter-lived radionuclides (Croudace et al., 2017). The use of ICP-MS allowed for longer lived radionuclides to be measured in conjunction with the more active shorter lived radionuclides to give a comprehensive assessment of the impact and implications of the nuclear incident or event over a longer timescale (Croudace et al., 2017). It is often important to measure the isotopic signatures of radionuclides as they can be used to determine the source of the

contamination (Dunne et al., 2018), however for certain radionuclides the decay energies cannot be distinguished and therefore must be reported as a sum of the two as in the case of ^{239}Pu and ^{240}Pu where it impossible to distinguish with radiometric analysis and results are reported as $^{239+240}$Pu (Parus and Raab, 1988, Xu et al., 2014). However, the use of an ICP-MS allows for the individual masses to be measured and ratios determined allowed for accurate sources to be determined (Taylor et al., 2015), which is of great importance for both environmental and nuclear facility monitoring as well as nuclear forensics in regards to weapons fallout. The use of the ICP-MS also meant that stable and long lived isotopes could also be measured simultaneously allowing for isotope ratio analysis as is the case for ^{135}Cs/ ^{137}Cs, where radiometric techniques can easily measure ^{137}Cs but rely on mass spectrometric analysis of ^{135}Cs due to the long half-life (Dunne et al., 2017). As ICP-MS technology has developed it has offered a means to measure shorter lived radionuclides in the presence of their interferences, as is the case of ^{135}Cs which has only recently become a routine measurement procedure by ICP-MS due to it previously being a difficult to measure (DTM) nuclide due to the isobaric ^{135}Ba and also the abundance sensitivity issue associated with ^{133}Cs (Dunne et al., 2017, Bu et al., 2018, Bu et al., 2019). The use of N_2O as a reaction gas is able to remove the Ba interference and allow for a clean Cs signal to be measured while the instrumental set up of the ICP-MS/MS resolves the abundance sensitivity issue associated with the stable isotope that is present in much greater abundance (Bu et al., 2018). The analysis of ^{134}Cs/^{137}Cs was previously used however, due to the short half-life of ^{134}Cs, it limited analysis to those directly following a nuclear incident and did not allow for long term monitoring of the surrounding environment (Dunne et al., 2017).

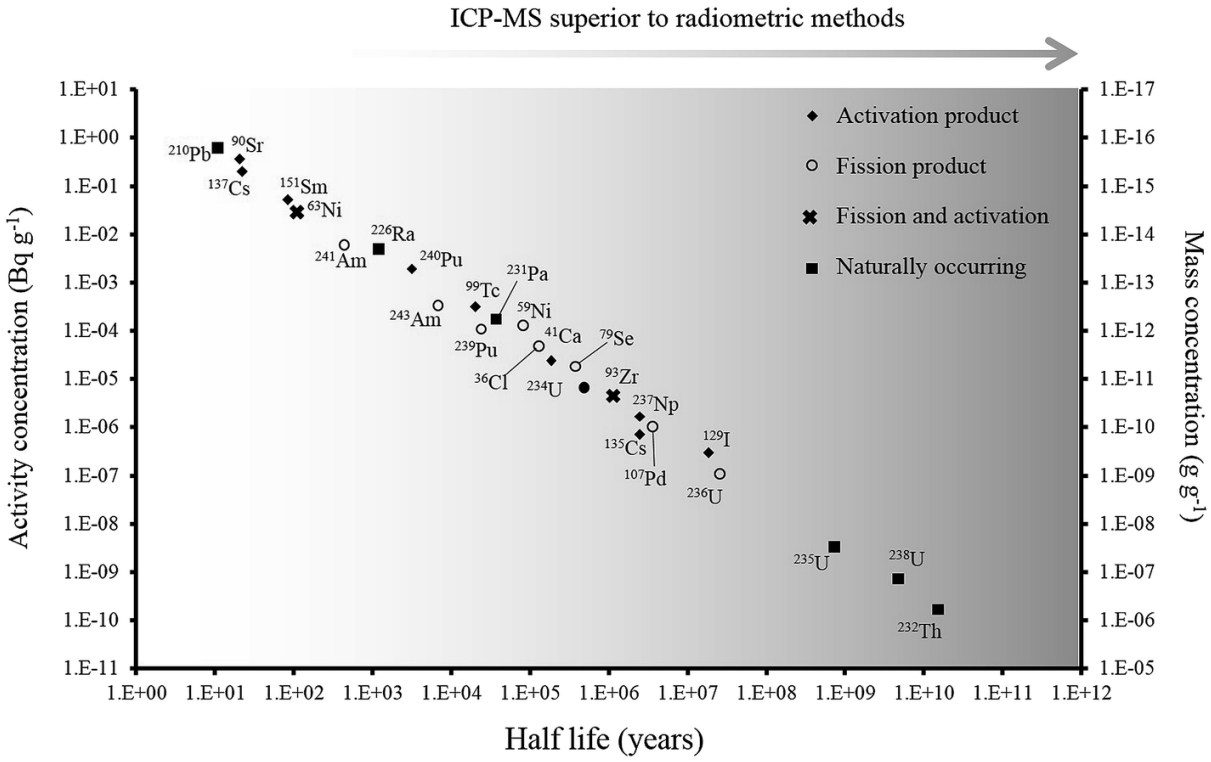

Figure 8: Half-life versus minimum detection activity (activity that gives count rate that is >3 times the standard deviation of the background count rate) and concentrations of selected radionuclides, labelled according to their method of production. Taken from Russell et al., (2014) – Croudace et al., (2017)

1.3 Decommissioning of radionuclides

As previously stated, the range of radionuclides that now need routine and robust methods of analysis has expanded to take into account the long-lived, low abundance radionuclides in the presence of medium-lived radionuclides. The radionuclides that require analysis are fission products, ^{90}Sr, ^{129}I, and activation products, ^{59}Ni, ^{63}Ni, naturally occurring radioactive materials (NORMs), ^{226}Ra, ^{238}U, as well as isotope ratios, ^{129}I/^{127}I, ^{135}Cs/^{137}Cs, of environmental samples that may have been contaminated with radioactive material for environmental site monitoring (Steinhauser et al., 2014) (Table 3).

Table 3: Radionuclides of interest for nuclear decommissioning (Warwick et al., 2019)

Origin	Nuclide	Half-life (a)	SpA (Bq g^{-1})	Mass equivalent to 1 Bq g^{-1} (pg g^{-1})
Activation products	^{36}Cl	$302(4)\times10^{3}$	1.2×10^{9}	821.8
	^{41}Ca	$100.2(17)\times10^{3}$	2.5×10^{9}	402.9
	^{59}Ni	$76(5)\times10^{3}$	3.0×10^{9}	339.0
	^{63}Ni	98.7(24)	2.1×10^{12}	0.5
	^{94}Nb	$20.0(24)\times10^{3}$	7.0×10^{9}	1.4×10^{2}
Fission products	^{79}Se	$356(40)\times10^{3}$	2.8×10^{8}	3583.0
	^{90}Sr	28.8(7)	5.1×10^{12}	0.2
	^{93}Zr	$1.61(6)\times10^{6}$	9.3×10^{7}	1.1×10^{4}
	^{99}Tc	$211.5(11)\times10^{3}$	6.3×10^{8}	1.6×10^{3}
	^{107}Pd	$6.5(3)\times10^{6}$	1.9×10^{7}	5.3×10^{4}
	^{126}Sn	$2.3(14)\times10^{5}$	1.0×10^{9}	952.4
	^{129}I	$16.1(7)\times10^{6}$	6.5×10^{6}	1.5×10^{5}
	^{135}Cs	$2.3(3)\times10^{6}$	4.1×10^{7}	2.4×10^{4}
	^{137}Cs	30.1(8)	3.2×10^{12}	0.3
	^{151}Sm	94.7(6)	9.7×10^{11}	1.1
Naturally occurring radioactive material (NORM)	^{226}Ra	$1.6(7)\times10^{3}$	3.7×10^{10}	27.3
Actinides	^{235}U	$704(1)\times10^{6}$	8.0×10^{4}	1.3×10^{7}
	^{236}U	$23.4(6)\times10^{6}$	1.7×10^{6}	4.2×10^{5}
	^{237}Np	$2.1(7)\times10^{6}$	2.6×10^{7}	3.8×10^{4}
	^{238}U	$4.5(5)\times10^{9}$	1.2×10^{4}	8.0×10^{7}
	^{239}Pu	24.1×10^{3}	2.3×10^{9}	4.4×10^{2}
	^{240}Pu	$6.6(7)\times10^{3}$	8.4×10^{9}	1.2×10^{2}
	^{241}Pu	14.3	3.8×10^{12}	0.3
	^{241}Am	432.6(6)	1.3×10^{11}	7.9

1.4 ICP-MS/MS

The recent commercial availability of tandem mass spectrometers (ICP-MS/MS) offers a potential improvement in interference removal capabilities over alternative instrument

designs with regards to radionuclide measurement. Such instruments are equipped with a quadrupole mass filter positioned in front of a collision-reaction cell, followed by a second quadrupole mass filter (Figure 9). The use of two mass filters improves the abundance sensitivity compared to single quadrupole instruments (~10^{-10}) (Agilent application handbook) compared to single quadrupole designs (~10^{-7}) (Boulyga and Becker, 2002), which improves tailing removal, as can be seen with the analysis of ^{237}Np in the presence of ^{238}U (Duckworth and Woods, 2016, Croudace et al., 2017). Additionally, filtering the ion beam entering the collision/reaction cell improves efficiency of the cell chemistry, and prevents the formation of secondary polyatomic interferences through interactions of ions with the reaction gas. ICP-MS/MS may reduce the extent of chemical separation required prior to sample introduction, further reducing the total procedural time and improving the sample throughput, as well as reducing the number of reagents used and analyst working time.

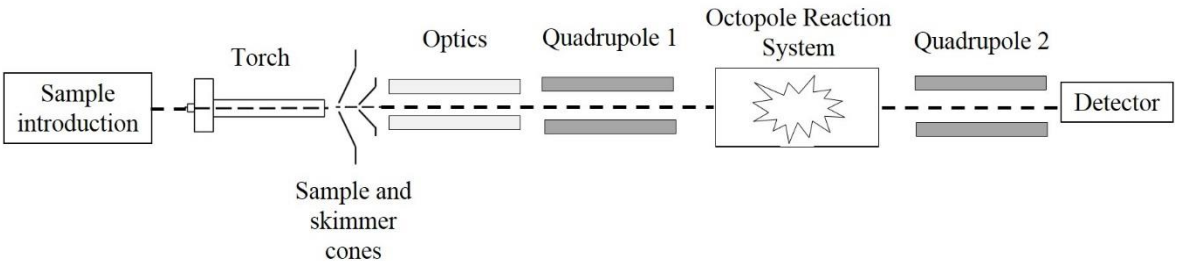

Figure 9: ICP-MS/MS layout (Agilent 8800/8900)

The improved interference removal capability has allowed for a greater range of radionuclides to be analysed with less reliance on offline separation of radionuclides isolation, ^{90}Sr, ^{135}Cs/^{137}Cs, ^{129}I, ^{226}Ra, ^{236}U/^{238}U and ^{239}Pu (Shikamori et al., 2012, Tanimizu et al., 2013, Ohno et al., 2013, Zheng et al., 2014, Amr et al., 2016, Russell et al., 2017, Van Es et al., 2017). This approach also allows for activation and difficult to measure radionuclides to be measured due to their specific mass. It should also be noted that the range of reaction gases, including O_2, NH_3, CH_3F as well as others listed in Table 4, allows for a greater range of isobaric and polyatomic interferences to either be reacted away or the target analyte be moved to an interference free mass (Agilent application handbook).

Table 4: Collision and reaction gases that can be used with the ICP-MS/MS

Type of Gas	Example
Collision	He, H_2
Reaction (Non corrosive)	O_2, NO, N_2O, CO_2
Reaction (Corrosive)	NH_3, CH_4, C_2H_2, C_3H_4, CH_3F

The independent control of the two quadrupoles allows for this separation to be carried out internally rather than relying solely on offline chemical separation of elements and radionuclides, which may be required when using alternative techniques, while also offering an improved understanding of the cell chemistry, with improved isotope isolation and tailing removal (Agilent application handbook).

All experimental work was carried out using two separate Agilent 8800 instruments operated by GAU-Radioanalytical Laboratories (based at the National Oceanography Centre, Southampton) and the Nuclear Metrology Group at the National Physical Laboratory, Teddington. As standard, the instruments were fitted with a collision-reaction cell (Octopole Reaction System, ORS^3) positioned between two quadrupole mass filters (termed Q1 and Q2) (Figure 9). The instruments also incorporated a Scott double pass spray chamber, Micromist nebuliser, quartz torch, and nickel sample and skimmer cones. Both instruments were fitted with four cell gas lines- Lines 1 and 2 are dedicated to hydrogen and helium, respectively, Line 3 is for corrosive gases (in this study NH_3) and Line 4 is for non-corrosive gases (in this study O_2) (Table 5). The corrosive gas is balanced with at least 90% He to protect the ORS. When operating cell Line 3, the helium line automatically runs at a flow rate of 1 mL/min. All gases were provided by BOC with a purity of 99.9999% (N6.0). The major operational modes are termed ‘Single Quad’ (with only Q2 operating as a mass filter) and ‘MS/MS’ (with both Q1 and Q2 operating as mass filters).

Table 5: General operating conditions of the Agilent 8800, ICP-MS/MS, for different setups

Instrument parameter	MS/MS	H_2	He	O_2	NH_3
RF power (W)			1550		
Plasma gas (L/min)			15		
Carrier gas (L/min)			1.05		
Extraction lens 1 (V)			0		
Extraction lens 2 (V)			-200 to -140		
Omega Bias (V)			-120 to -70		
Omega lens (V)			5-18		
Octopole bias (V)	-8	-18	-18	-5	
Energy Discrimination (V)	5	5	0	-7	
Cell gas flow rate range (mL min^{-1})	-	0-10	0-12	0-1	0-10

1.5 Characterisation of ICP-MS/MS performance

Appendix 1

"Evaluation of inductively coupled plasma tandem mass spectrometry for radionuclide assay in nuclear waste characterisation"

P.E. Warwick, B.C. Russell, I.W. Croudace, Ž. Zacharauskas

J. Anal. At. Spectrom., 2019, DOI: 10.1039/C8JA00411K

Contribution from Ž. Zacharauskas included instrument background, sensitivity, abundance sensitivity and hydride formation assessment, as well as case studies of Stronium-90, Iodine-129 and Neptunium-237. Further corrections and drafts where completed as part of a group effort by everyone involved.

1.6 Conclusion

ICP-MS is an increasingly used technique for radionuclide detection with regards to nuclear waste characterisation, expanding the range of radionuclides routinely measurable at nuclear sites, whilst offering an improvement in sample throughput as a result of reduced measurement time compared to decay counting techniques. The removal of isobaric, polyatomic and tailing interferences prior to detection remains the major factor preventing accurate measurement using this technique. The commercial availability of ICP-MS/MS offers improved interference removal over alternative instrument designs, which can be used to support or even replace relatively time-consuming and labour-intensive offline chemical separation techniques, further improving the sample throughput. ICP-MS/MS has been successfully applied to measurement of multiple radionuclides of interest to nuclear sites in a range of sample matrices, including ^{90}Sr, ^{93}Zr, ^{129}I, ^{135}Cs, ^{151}Sm, ^{236}U and ^{237}Np, as well as NORM-relevant ^{226}Ra. The flexibility of the instrument allows the setup to be varied depending on the analytical requirements e.g. sensitivity, tailing removal, or target decontamination factors for interferences. ICP-MS/MS is potentially applicable to detection of a number of other difficult-to-measure radionuclides relevant to nuclear waste clean-up, but for which no routine measurement technique currently exists. Reactive gases can be used to remove isobaric / polyatomic interferences and permit effective measurement of ^{126}Sn and ^{239}Pu. Reactive gases may also benefit ^{99}Tc measurement although no suitable reactive gases have been identified to separate ^{99}Tc from ^{99}Ru. The significant improvement in abundance sensitivity achieved by ICP-MS/MS is beneficial to the measurement of ^{59}Ni, ^{79}Se, ^{94}Nb and ^{107}Pd in the presence of stable isotopes of the element. However, hydride formation is still a dominant contributor to m/z+1 signal and does not appear to be significantly affected by the introduction of a collision gas. For fission products ^{79}Se and ^{107}Pd it is likely that the stable isotopes will not be present in significant concentrations to result in problematic levels of hydride generation. However, for activation products ^{59}Ni and ^{94}Nb, the stable analogues will always be associated with the nuclide of interest and desolvation is required to suppress hydride formation to acceptable levels. For ^{36}Cl and ^{41}Ca, sufficiently sensitive ICP-MS/MS measurement is considered unviable given the high background signals observed.

A comprehensive assessment of the radionuclides measured by ICP-MS/MS can be found in “Evaluation of inductively coupled plasma tandem mass spectrometry for radionuclide

assay in decommissioning and nuclear wastes" by Warwick et al., 2019, (Appendices 1).The challenges associated with these radionuclides could benefit from the ICP-MS/MS setup to overcome them.

This PhD thesis aims to assess the capabilities of the ICP-MS/MS for radionuclide analysis by further developing methods for analysing a range of radionuclides in representative active samples relevant to the nuclear industry. The results of this thesis are presented in scientific paper format, with relevant methods detailed in each chapter. Methods proposed are used to determine the capabilities and the limitations for the ICP-MS/MS in regards to its tolerances to a range of relevant non active matrix digests, including ground water, stainless steel, air filters and concretes, and interferences arising from them (Chapter 2). Once the limitations were determined, comprehensive assessment of active material were carried out in the form of active concretes from nuclear facilities around the UK, supplied by GAU radioanalytical, with the ICP-MS/MS utilised as a rapid screening and characterisation technique (Chapter 3). A difficult to measure radionuclide was selected, ^{129}I, to showcase the capabilities of the ICP-MS/MS configuration over traditional ICP-MS instrumentation with work expanding and optimising existing research, utilising the MS/MS mode, reaction gases, matrix modification and internal standard optimisation, as well as completing a comprehensive custom parameter assessment and tune, with the technique then applied to active waste samples relevant to the nuclear decommissioning industry (Chapter 4). To ensure a thorough assessment of the instrument's capabilities, isotope ratio assessment was completed focusing on Pb isotopes with core material collected from lakes and saltmarshes around the UK. Results were compared against the leading isotope ratio measurements collected on the Neptune MC-ICP-MS, with the methods developed applicable to radionuclide systems as well as waste characterisation and source term assessment within the nuclear decommission industries and potential for emergency response (Chapter 5).

All samples, data collection, processing and writing was completed by Žilvinas Zacharauskas, unless stated otherwise, with feedback, corrections and guidance provided by Phil Warwick, Ben Russell and Ian Croudace. The results of this thesis are presented in scientific paper format, with relevant methods detailed in each chapter.

Chapter 2 Potential for direct measurement of decommissioning samples with limited or no sample preparation

2.1 Introduction

Commercial production of nuclear power produces an unavoidable by product of radioactive waste. When a nuclear facility is permanently shut down and the spent fuel rods removed, 99 % of the radioactivity is accounted for. However, everything from the construction materials, concretes and metals, to the filters used for radionuclide trapping as part of the cooling circuits in both LWRs and AGRs, to the waters used in the cooling circuits in LWR and the cooling ponds, require characterisation to their correct waste streams (Figure 11).

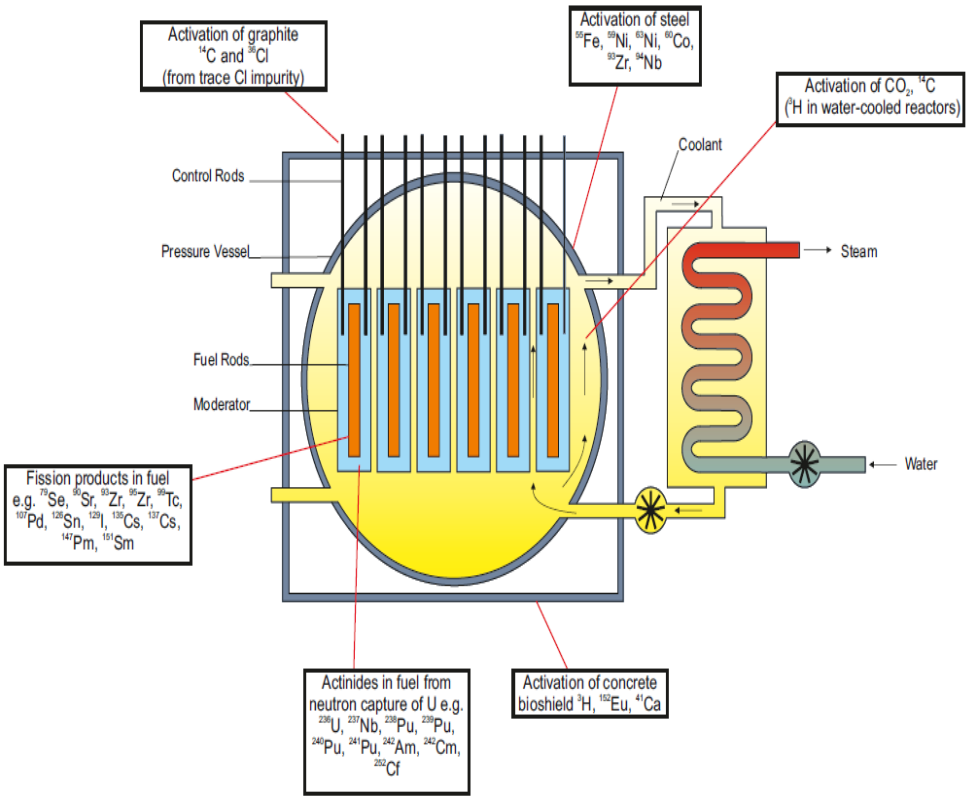

Figure 10: Outline of potential pathways for radionuclides within a nuclear reactor and cooling circuit

The UK radioactive waste inventory (NDA 2013) lays out that the radioactive waste composition is originating mostly from its Magnox reactors. The highest contribution of waste materials originates from the steels, cellulosic (air filter materials), concrete, cement and sand as well as graphite which combined equate to ~74 % of all waste within the inventory. Each of these materials and matrixes require characterisation to ensure that they are allocated to their correct waste stream and disposed and/ or stored appropriately. Each of the matrixes is exposed to varying sources of radioactive contamination ranging from direct interaction from the neutron beam, as is the case of the graphite in the moderators and fuel sleeves which then produce activation products from the impurities present within them, to being exposed to the fission products that are being carried away from the fuel rods through the cooling circuits and into the filter materials (Trojanowicz et al., 2018).

Nuclear decommissioning must abide by comprehensive assessment and characterisation of a range of radionuclides in a range of complex matrixes. Certain radionuclides can be directly measured using direct radiometric scanning as is the case with gamma emitting radionuclides and gamma spectrometry. However, many difficult-to-measure (DTM) radionuclides require further chemical separation and purification for analysis either via liquid scintillation counting (LSC) or potential assessment via mass spectrometry (MS), specifically for some of the longer-lived radionuclides.

Traditional ICP-MS instrumentation allows an advantage over radiometric measurements in that analysis is fast and does not suffer from any radiometric spectral overlap. However, due to the complexity of these matrixes isobaric and polyatomic interferences may start to limit sample analysis. Current advances in ICP-MS technology has led to the development of the ICP-MS/MS.

The ICP-MS/MS instrument configuration consists of two quadrupole mass filters separated by a collision/ reaction cell (Figure 12). The quadrupole prior to the cell entrance improves abundance sensitivity compared to single quadrupole designs from ~10^{-7} to <10^{-10} (Shikamori et al., 2012, Ohno et al., 2013), which is beneficial for stable isotope tailing removal. The first quadrupole also filters the ion beam prior to the cell entrance, giving a greater control and selectivity of reaction / collision cell chemistry, and minimising the formation of cell-based polyatomic interferences (Shikamori et al., 2012, Ohno et al., 2013, Yang et al., 2018). Isobaric and polyatomic interferences formed in the plasma can be removed using the collision-reaction cell through the use of variable collision (e.g. H_2 and He) and/or reactive (e.g. O_2 and NH_3) gases (Shikamori et al., 2012, Ohno et al., 2013, Yang et al., 2018). The instrument also has the capabilities for tolerating high total dissolved solids (TDS) through the use of its high matrix introduction (HMI) configuration. This would reduce the levels of sample handling and allow the instrument itself to carry out dilutions to compensate for the high matrix being introduced from the digestions. These developments put ICP-MS/MS in a position to support or even replace much of the offline chemical separation procedures, increasing the sample throughput and potentially allowing direct analysis of sample digests.

The aim of this study is to assess the capabilities of the ICP-MS/MS, Agilent 8800, for analysing unseparated digests of matrixes relevant to nuclear decommissioning, with specific focus on the difficult-to-measure (DTM) radionuclides. An assessment of

instrumental tolerance and background signal on mass of the DTM radionuclides was carried out on stable analogue digests on ground water, stainless steel, air filter (cellulose) and concrete samples. Signal sensitivity was calculated relative to the background present within the samples on mass of the DTM radionuclides, allowing a means to determine which radionuclides were measurable with no offline chemical separation and could therefore be used as screen and characterisation methods for active waste samples. The study also aimed to address the impact that TDS plays on signal sensitivity following matrix digest specifically focusing on $LiBO_2$ fusion of concretes and comparing to traditional acid leached and/or digest samples.

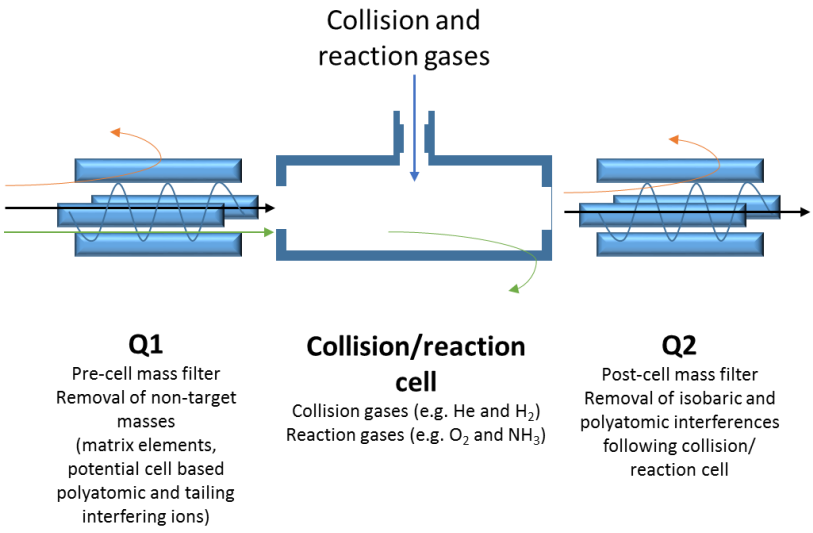

Figure 11: ICP-MS/MS layout and potential benefits of the tandem mass spectrometry configuration

2.2 Methodology

2.2.1 Reagents and Materials

Primar Plus^{TM} HNO_3 (68 %), Aristar grade HCl (37 %), Extra pure H_2O_2 (30 %) were obtained from Fisher Scientific, UK. An Agilent multi element standard (Al, Cr, Mn, Co, Ni, Cu, Zn, As, Se, Sr, Mo, Cd, Ba, Pb) (1 µg g^{-1}) as well as a multi element PA tuning solution (Zn, Be, Cd, As 20 µg g^{-1} each, Ni, Pb, Mg 10 µg g^{-1} each, Tl, Na, Al, U, Cu, Th, Ba, Co, Sr, V, Cr, Mn, Li, Sc, In, Lu, Bi 5µg g^{-1} each, Y, Yb, 2.5 µg g^{-1} each) from Agilent, UK and standard single element standard solutions (10 mg g^{-1}) of Be and U were sourced from Sigma Aldrich, UK. Dilutions

were prepared using deionised water (>18.2 MΩ·cm), produced from a Q-Pod Millipore System (Merck, York, UK).

2.2.2 Instrumentation

All ICPMS measurements were performed using an Agilent 8800, ICP-MS/MS. The instrument is equipped with a collision-reaction cell (termed an Octopole Reaction System, ORS^3) positioned between two quadrupole mass filters (termed Q1 and Q2). The instrument was fitted with a Scott double pass spray chamber, Micromist nebuliser, quartz torch and nickel sample and skimmer cones. The instrument was fitted with four cell gas lines (Table 7) - dedicated H_2 and He lines in line 1 and 2, NH_3 in line 3 (for corrosive gases) and O_2 in line 4 (for non-corrosive gases). The corrosive gas must be balanced with at least 90% He to protect the ORS^3, and when operating cell line 3, the He line is automatically run at a flow rate of 1 mL/min (Table 7). High purity H_2, He, NH_3, O_2 and Ar were supplied by BOC (UK), with a purity of 99.9999% (N6.0).

Table 6: Agilent 8800 gas modes and flow rates available

Cell line	Gas used	Flow rate range (mL/min)
Hydrogen	H_2	0-10
Helium	He	0-12
Line 3 (corrosive)	NH_3 (balanced in 90% He)	0-10
Line 4 (non-corrosive)	O_2	0-1

The instrument was tuned each day in single quadrupole (SQ) mode (only Q2 operating) with no cell gas using a 1 ng g^{-1} stable element standard mixture of Ce, Co, Li, Tl and Y in 0.6 M HNO_3, to ensure criteria for sensitivity, measurement uncertainty, interference formation and peak axes alignment were achieved.

2.2.3 Experimental

2.2.3.1 Background assessment

An assessment of the m/z values of the DTM radionuclides of interest (Table 8) was carried out on the blank acids used in the digestion and dilution procedure. An assessment HNO_3 background was carried out by evaporating off 20 mL of concentrated HNO_3 in a Teflon pot. The residue was then dissolved in HNO_3 (0.6 M) before analysing on the ICP-MS/MS. The signal at the m/z values of the DTM radionuclides was monitored to determine the potential instrumental interferences that may arise from the acid itself and to determine the instrumental detection limits for the radionuclides of interest.

A select set of radionuclides were chosen to demonstrate the variation in background and potential interferences arising from stable element interferences, both isobaric and polyatomic, for activation and fission product analysis as well as naturally occurring radionuclides and the actinides.

Table 7: List of difficult to measure radionuclides by source

Radionuclide	Activation	Fission	Natural	Actinides
Cl-36	X			
Ca-41	X			
Ni-59	X			
Se-79		X		
Sr-90		X		
Zr-93		X		
Nb-94	X			
Tc-99		X		
Pd-107		X		
Sn-126		X		
Cs-135		X		
Cs-137		X		
Sm-151		X		
Ra-226			X	
U-235			X	X
U-236				X
Np-237	X			X
U-238			X	X
Pu-239				X
Am-241				X

The assessment of the $LiBO_2$ fusion digests were assessed for their impact on signal sensitivity due to the high TDS in the solutions.

An assessment of the acid blanks and stable waste analogues was used to determine the potential background and interference signals measured along with the impact that the high TDS and matrix loading would have on the plasma stability and signal sensitivity.

The acid samples were spiked with and internal standard tracer containing In and Re (10 ng g^{-1}). The internal standards were used to monitor the initial changes in signal sensitivity arising from the impurities and TDS present within the acids themselves. The initial assessment demonstrated that there were variation between In and Re signals relative to the reference solution (HNO_3, 0.6 M, spiked with In and Re (10 ng g^{-1}) and therefore a more complete mass range internal standard assessment was carried out using a multi-element spike (Be, Al, Cr, Mn, Co, Ni, Cu, Zn, As, Se, Sr, Mo, Cd, Ba, Pb, U) (10 ng g^{-1})). A reference standard prepared in HNO_3 (0.6 M) with and without the multi element solution spike was used as the background reference value for the HNO_3 used in the dilutions and for low TDS sample sensitivity and background.

The un-spiked and spiked acid digest solutions were analysed in no gas, MS/MS mode on m/z = 9, 27, 52, 55, 59, 60, 63, 66, 75, 77, 78, 82, 88, 95, 111, 137, 208, 238. The signal sensitivity was monitored and compared against the HNO_3 (0.6 M) spiked reference solution.

2.2.3.2 Representative matrix processing

A range of representative stable matrix analogues for the nuclear decommissioning industry were processed following standard practice for each matrix type. Non active ground water, stainless steel and air filter samples were processed and analysed at NPL, Teddington, while the non-active concrete samples were processed and analysed at the NOC, Southampton.

Ground water samples were acidified and diluted by a factor of 10, with HNO_3 (0.6 M) and directly analysed by ICP-MS/MS. Stainless steel samples were acid digested in concentrated

HNO_3 before being diluted by a factor of 12x in HNO_3 (0.6 M) and analysed by ICP-MS/MS. Air filter samples were microwave digested using a combination of HNO_3 (11.2 %) and H_2O_2 (1.2 %). Samples were then diluted by a factor of 1000 in HNO_3 (0.6 M) before being analysed by ICP-MS/MS. Crushed concrete samples (0.5 g) were fused with $LiBO_2$ (2 g) at 1050 ^oC, followed by an acid digestion with HNO_3 (8 M, 100 mL). Samples were evaporated to dryness, with the residue re-dissolved in HNO_3 (0.6 M, 50 mL). A subsample was taken and diluted by a factor of 100 and 10, and analysed by ICP-MS/MS.

An assessment of the instruments ability to tolerate samples with a high total dissolved solid (TDS) was carried out by producing ^{238}U calibration standards (0-100 ng g^{-1}) with clean acids, low TDS, spiked with In and Re internal tracers (5 ng g^{-1}), as well as 1 % Ca ($CaCl_2.2H_2O$) and a separate 1 % Fe ($Fe(NO_3)_3.9H_2O$), high TDS, spiked with In and Re internal tracers (5 ng g^{-1}). The calibration standards were analysed under no gas, MS/MS, mode operating under HMI (high matrix introduction) mode, as well as LMI (low matrix introduction). The use of Ca was chosen to represent concrete digest samples, while Fe was chosen to represent stainless steel digest samples, with the two matrixes mentioned making up a large majority of the representative decommissioning waste material that requires processing and characterisation, while ^{238}U was chosen to represent a high sensitivity, low interference isotope, relative to nuclear decommissioning.

2.2.3.3 Determination of potential radionuclides for direct measurement

An assessment of the un-spiked solutions background in no gas, MS/MS mode and He, MS/MS mode was done analysing the signal on m/z = 36, 41, 59, 79, 90, 93, 94, 99, 107, 126, 135, 137, 151, 226, 235, 236, 237, 238, 239, 241, representative of the radionuclides of interest for this study, ^{36}Cl, ^{41}Ca, ^{59}Ni, ^{79}Se, ^{90}Sr, ^{93}Zr, ^{94}Nb, ^{99}Tc, ^{107}Pd, ^{126}Sn, ^{135}Cs, ^{137}Cs, ^{151}Sm, ^{226}Ra, ^{235}U, ^{236}U, ^{237}Np, ^{238}U, ^{239}Pu, ^{241}Am. An assessment of the isobaric and polyatomic interferences present on the masses of the difficult to measure radionuclide was used to determine which radionuclides had instrumental backgrounds that could and could not be resolved through the use of MS/MS and collision gas, He.

An initial assessment of which radionuclides would be of interest in which matrix was first carried out to ensure assessment was kept relevant to the matrix types that were being used as stable analogues (Table 9).

Table 8: Difficult to measure radionuclides by matrix where they would be expected and of interest for analysis (*all values not listed by EPR 2018 are then set at a conservative low out-of-scope limit of 0.01 Bq g-1, ** ^{41}Ca is a calculated proposed out-of-scope limit produced by the Clearance and Exemptions working group on behalf of the Nuclear Industry Safety Directors Forum (SDF 2017), due to ^{41}Ca not being covered by the EPR 2018.

Radionuclide		Matrix			
	Out-of-scope Limits (Bq g^{-1})	Ground Water	Stainless Steel	Air Filter (cellulosic material)	Concrete
^{36}Cl	1	X	X	X	
^{41}Ca	100**				X
^{59}Ni	1000		X		
^{79}Se	0.01*				X
^{90}Sr	1	X	X	X	X
^{93}Zr	10		X		X
^{94}Nb	0.1		X		
^{99}Tc	1	X	X		
^{107}Pd	0.01*		X	X	X
^{126}Sn	0.01*		X	X	X
^{135}Cs	1000			X	
^{137}Cs	1			X	
^{151}Sm	1000				
^{226}Ra	0.01	X			
^{235}U	1	X			X
^{236}U	10	X			X
^{237}Np	1				X
^{238}U	1	X			X
^{239}Pu	0.1		X	X	X
^{241}Am	0.1		X	X	X

2.3 Results and Discussions

2.3.1 Background assessment

2.3.1.1 Acid blank background

Acid background assessment was used to demonstrate which mass regions had an inherent instrumental and acid related background signal which may limit specific radionuclide assessment. The background assessment showed an elevated signal at m/z = 36 relative to all other signals, of 1.51×10^{8} CPS. This was associated with the ^{36}Ar signal present as part of the plasma gas, therefore contributing to the instrumental background. All other background signals were at least 5 orders of magnitude below that. The second largest background signal was associated with m/z = 63, of 7.60×10^{3} CPS, suggesting that there is an impact from either ^{63}Cu or $^{23}Na^{40}Ar$. All other background signals were <500 CPS with the higher mass region of 126-241 showing backgrounds of <30 CPS (Figure 13).

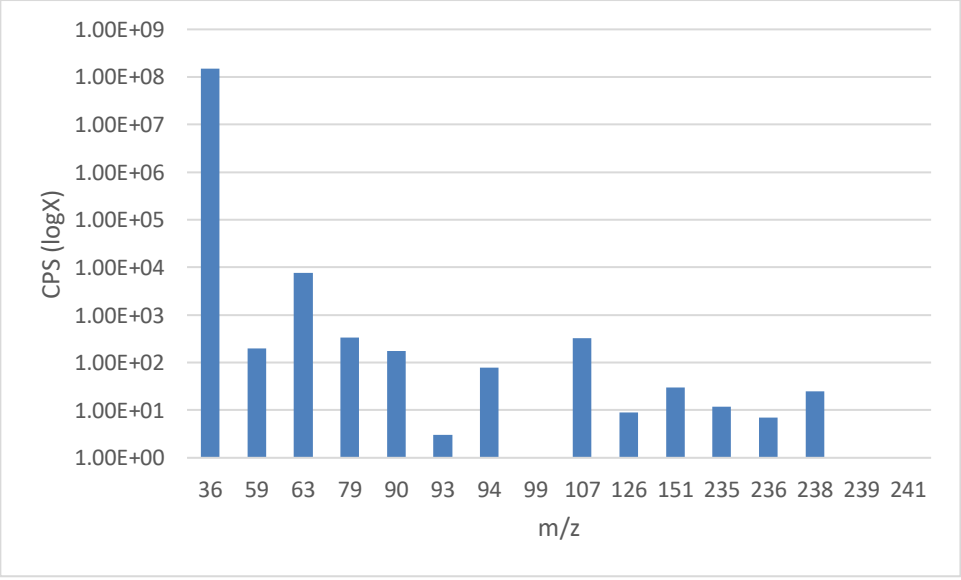

Figure 12: Background signal measured at the masses of the DTM radionuclides in HNO_3 (0.6 M) acid blank

2.3.1.2 Representative matrix backgrounds

The background signal across all the sample types showed heightened signals on m/z = 36, 41, 88, 135, 137. The signals were representative of interferences associated with isobaric, ^{36}Ar, ^{88}Sr, ^{135}Ba and ^{137}Ba, and polyatomic, $^{20}Ne^{16}O$, $^{40}Ca^{1}H$, $^{40}Ar^{1}H$, as well as tailing from ^{40}Ca (96.941 % relative abundance) and ^{40}Ar (99.60 % relative abundance). These interferences are present in the instrument due to being the make-up of the plasma gas, Ar, as trace impurities within the plasma gas, Ne, as well as environmental contaminants Ca, Sr, Ba, which could not be removed.

Ground water samples were analysed across the mass range of the DTM radionuclides (Figure 14, 15 and 16,) with further focus put to the radionuclides expected within the active samples themselves (Figure 17, 18 and 19). Overall, the use of He mode reduced the signal when looking at the full mass range, this is due to any polyatomic interferences stemming from the bulk matrix being broken up by the collision gas (Figures 14,15 and 15), however, this does mean that if lower mass radionuclides do want to be investigated He mode would offer a means to reduce and remove much of the polyatomic interferences present in that mass range. The focused background assessment (Figures 17, 18 and 19) showed a large background signal at m/z =36 associated with the Ar carrier gas, with variations above background signal within the samples being associated to the variations of the plasma gas composition, as the use of He SQ vs MS/MS mode showed no improvement in background removal, but rather an increased signal associated with collisional focusing of the carrier gas and the analytes present. Under no gas mode m/z = 36 could not be monitored due to instrumental limitations preventing the Ar signal from overwhelming the detector. However, the use of He mode both SQ and MS/MS did show a reduction in signal on m/z = 90 associated with the stable Sr in the water samples which would have been forming $^{88}Sr^{1}H_2^{+}$. The use of He reduced the interference by over 1 order of magnitude relative to no gas MS/MS mode. The signal on m/z = 99 was also improved by the use of He mode which would have reduced the signal from polyatomic interferences such as those arising from trace $^{83}Kr^{16}O^{+}$ and $^{98}Mo^{1}H^{+}$, forming within the plasma gas. The DTM radionuclides expected to be present within the active ground waters, including 99, 226, 235, 236 and 238 all showed backgrounds both instrumentally and within their blank analogues within the range expected for instrumental variation and noise of $<10^2$ CPS.

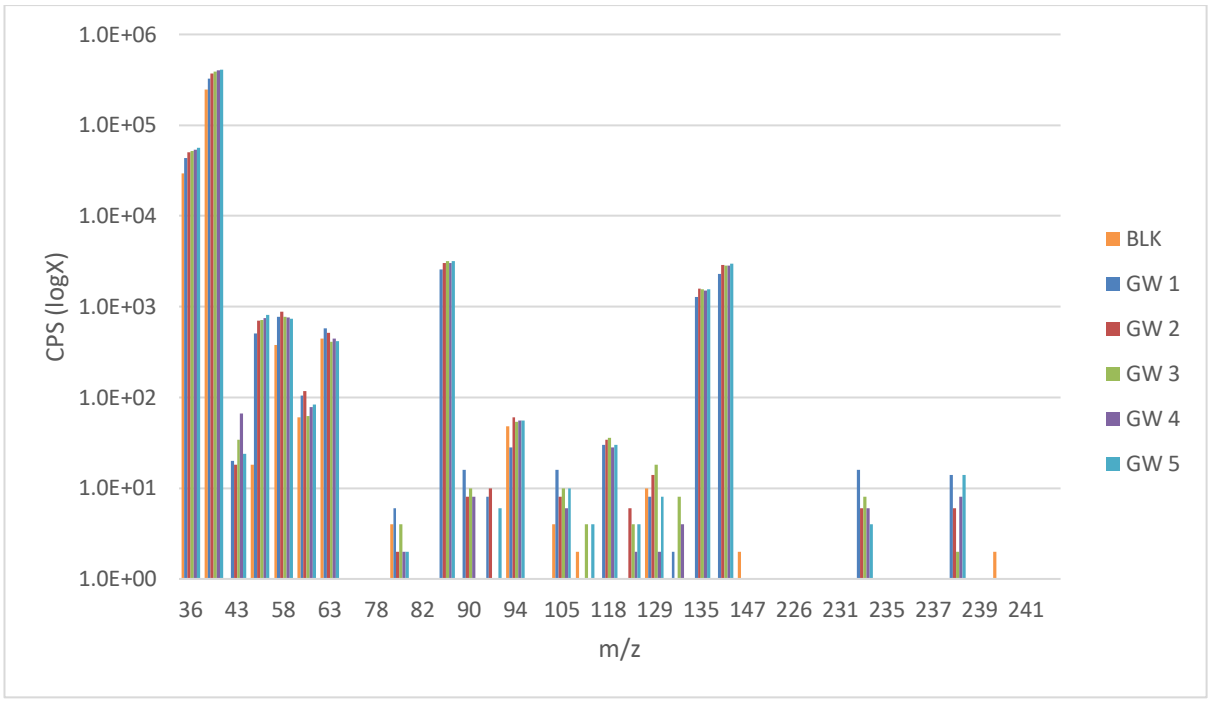

Figure 13: Ground water sample background measured across the mass range of DTM radionuclides – He SQ

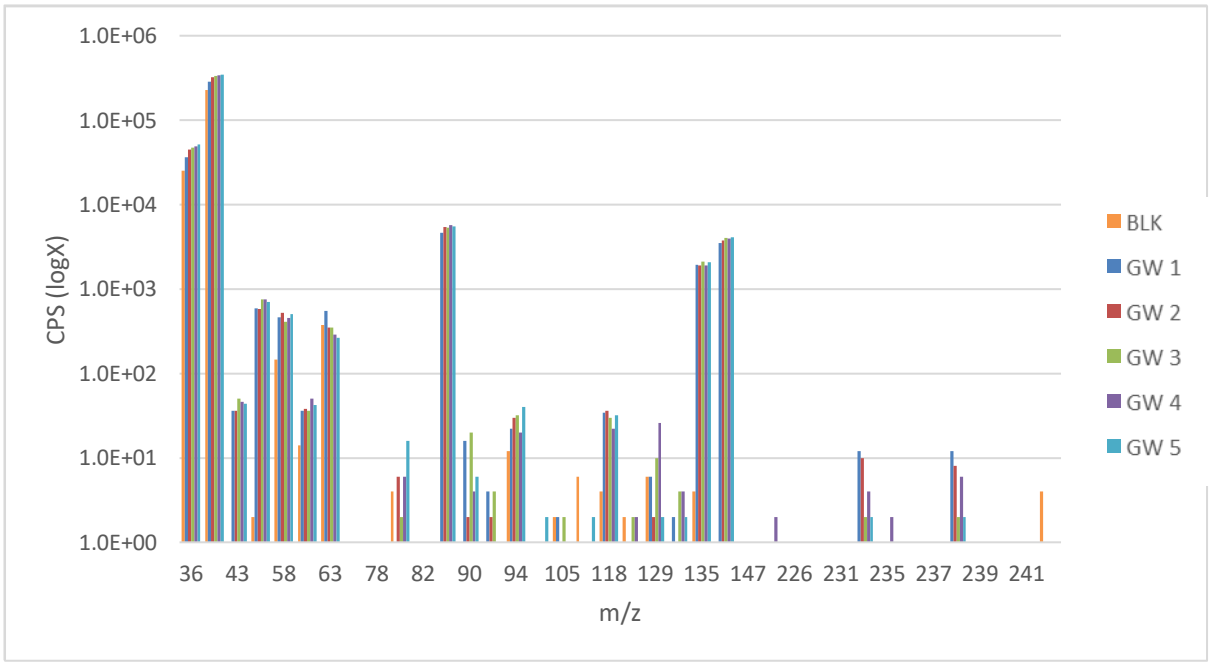

Figure 14: Ground water sample background measured across the mass range of DTM radionuclides - He MS/MS

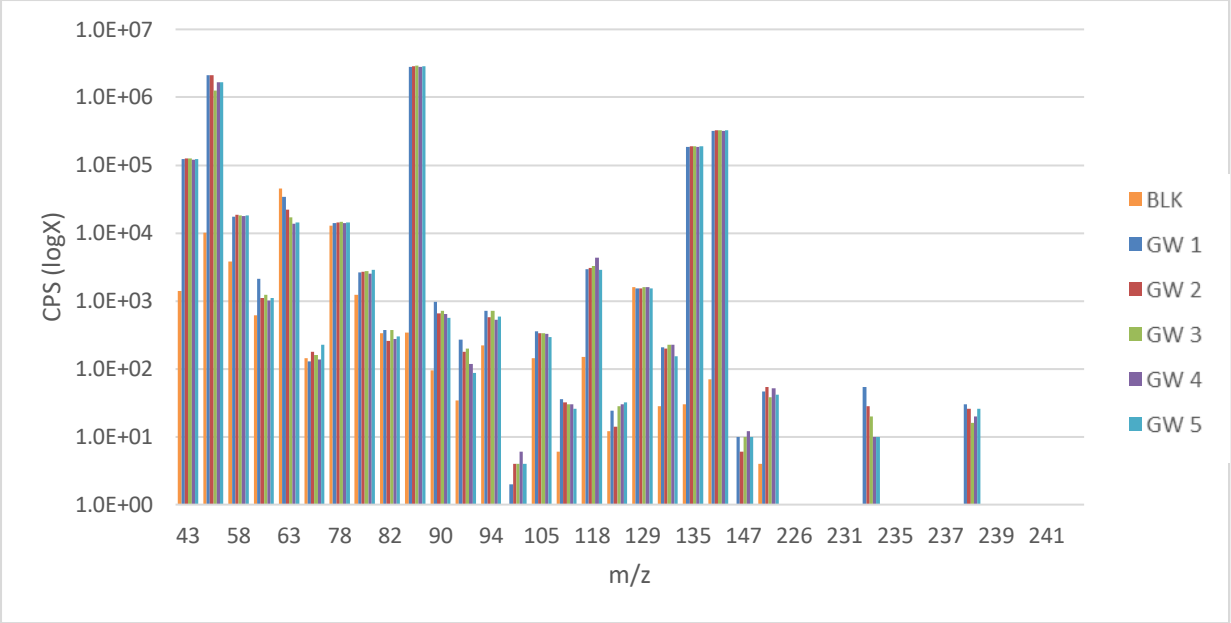

Figure 15: Ground water sample background measured across the mass range of DTM radionuclides - no gas MS/MS

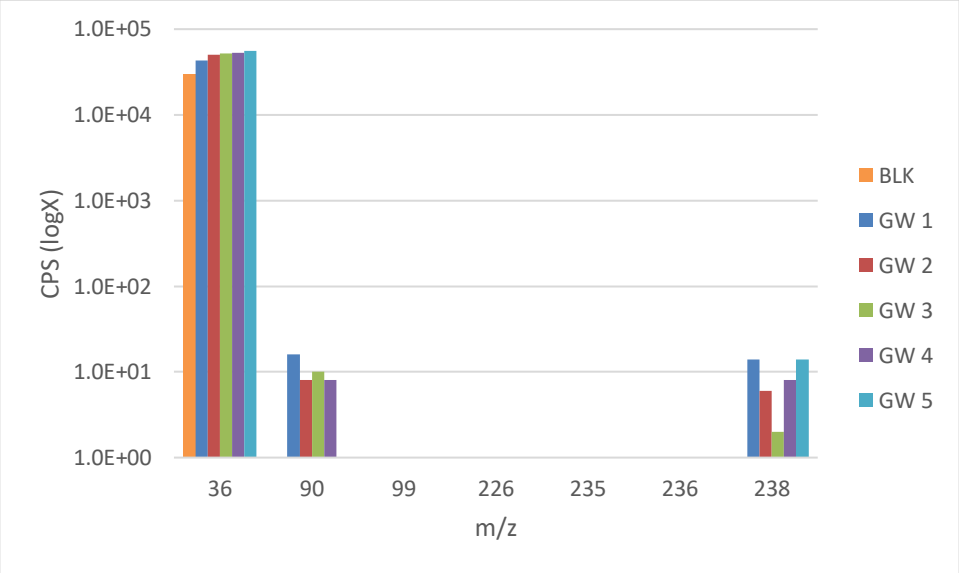

Figure 16: Ground water sample background measured on the masses of expected radionuclides to be present in active ground water samples – He SQ

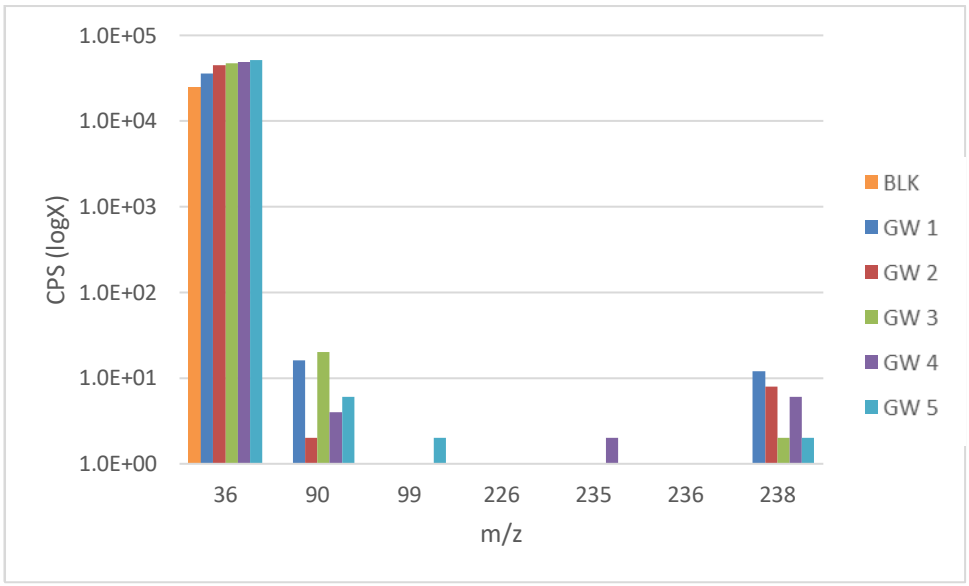

Figure 17: Ground Water sample background measured on the masses of expected radionuclides to be present in active ground water samples - He MS/MS

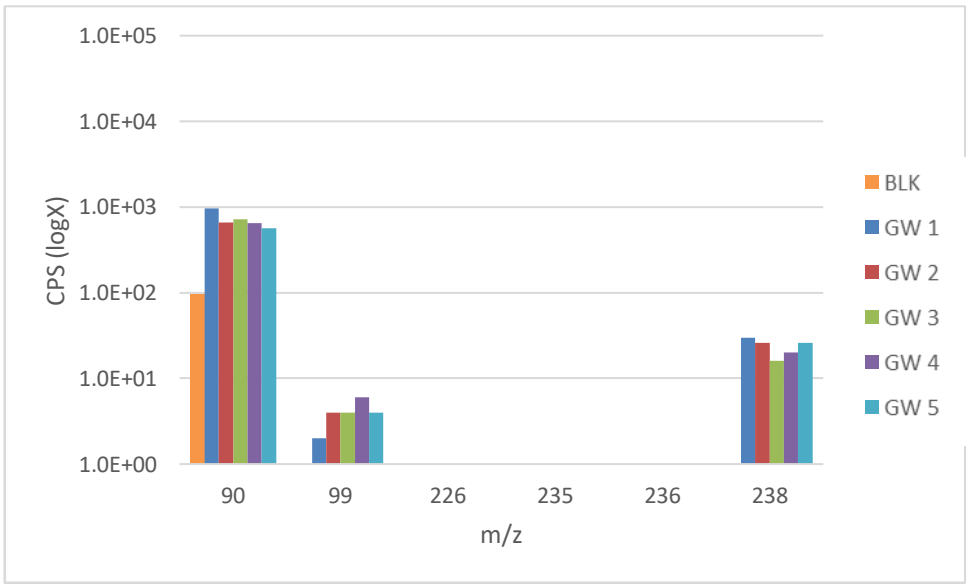

Figure 18: Ground water samples background measured on the masses of expected radionuclides to be present in active ground water samples - no gas MS/MS

Stainless steel samples were analysed across the mass range of the DTM radionuclides (Figure 20, 21 and 22) with further focus of the mass range of expected radionuclides (Figure 23, 24 and 25) showing a heightened background associated with the matrix itself, specifically at m/z = 58, 59, 63, 93, 94 and 118, representative of isobaric interference from ^{58}Fe, ^{59}Co, ^{63}Co, ^{94}Zr and ^{118}Sn, as well as potential tailing from ^{60}Ni, ^{92}Zr, ^{94}Zr, and hydride formation from $^{58}Fe^{1}H$, $^{92}Zr^{1}H$. The interferences mean that direct stainless-steel digest and analysis of ^{59}Ni, ^{63}Ni and ^{60}Co would not be possible without extensive separation and

purification of the radionuclides of interest, therefore reducing the applicability of the technique for rapid screen and characterisation of those particular activation products. Analysis of Zr was improved through the use of He mode as this would break up any potential $^{92}Zr^{1}H^{+}$ that may have formed, while operating in MS/MS mode improves the overall abundance sensitivity and reduces the impact of tailing from ^{92}Zr and ^{94}Zr within the sample. Analysis at m/z = 107 was also improved by three orders of magnitude when operating in He MS/MS mode compared to either He SQ mode or no gas MS/MS mode, due to the He breaking up the polyatomic interference associated with $^{91}Zr^{16}O^{+}$. The signal on m/z = 126 shows an increased signal when operating under MS/MS mode suggesting that MS/MS mode is improving the formation of a polyatomic interference, potentially MoO_2^{+}. The signal on m/z = 239 and 241 are both below the detection limit of the instrument and show that ICP-MS/MS analysis could be utilised for actinide characterisation and screening of active stainless-steel samples.

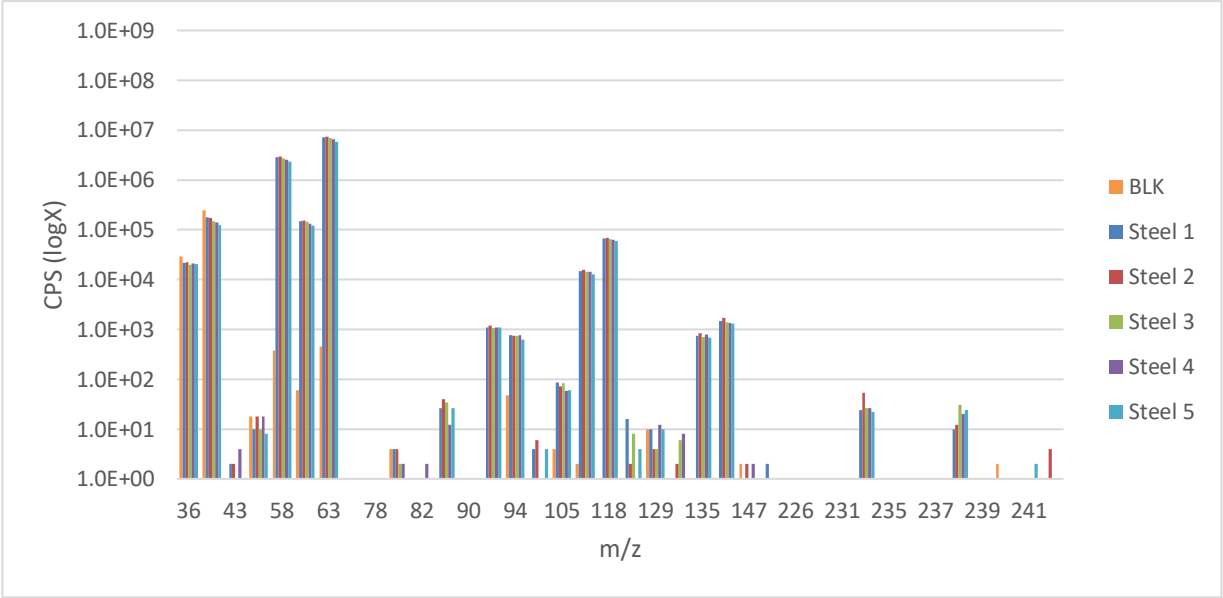

Figure 19: Stainless steel samples backgrounds across all DTM radionuclides m/z values – He SQ

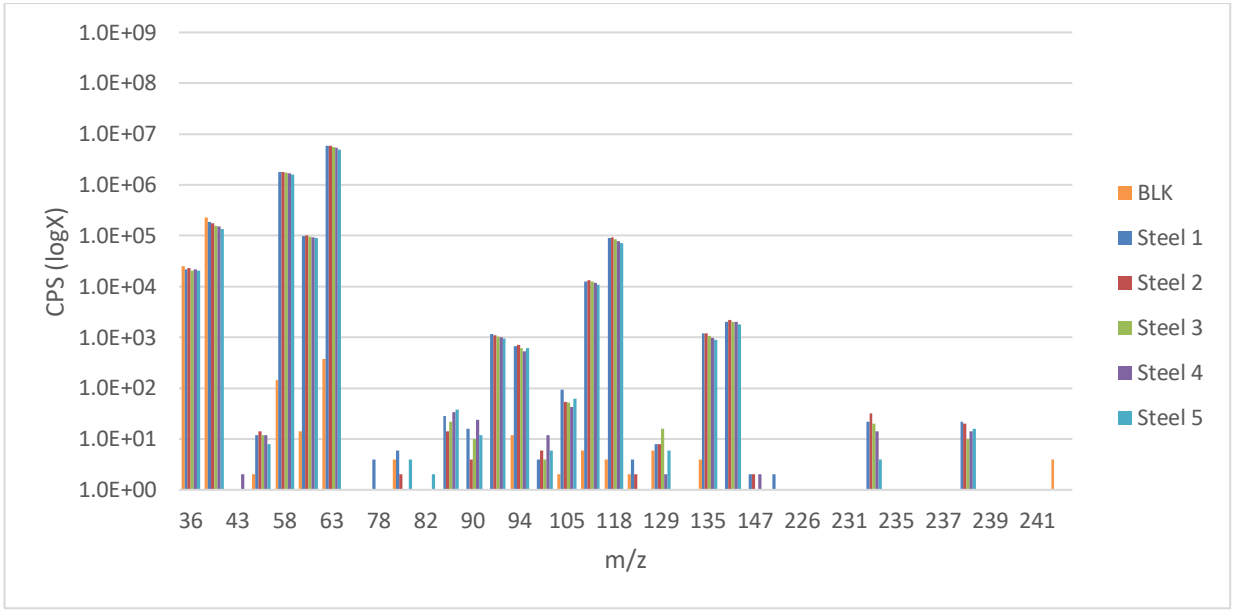

Figure 20: Stainless steel samples backgrounds across all DTM radionuclides m/z values - He MS/MS

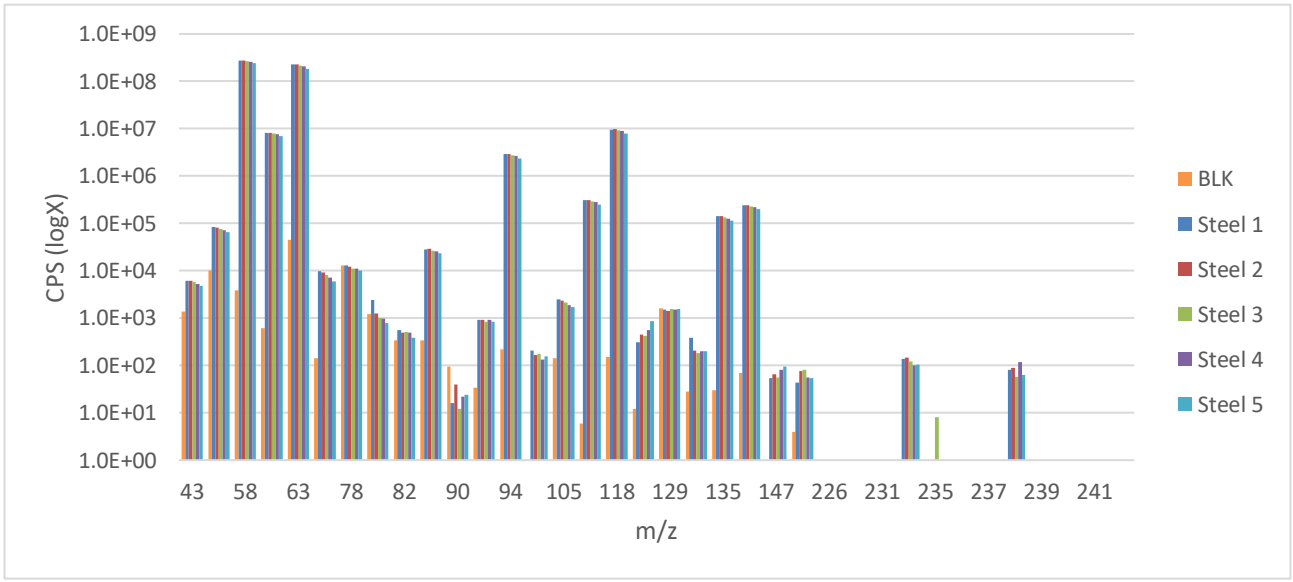

Figure 21: Stainless steel samples backgrounds across all DTM radionuclides m/z values - no gas MS/MS

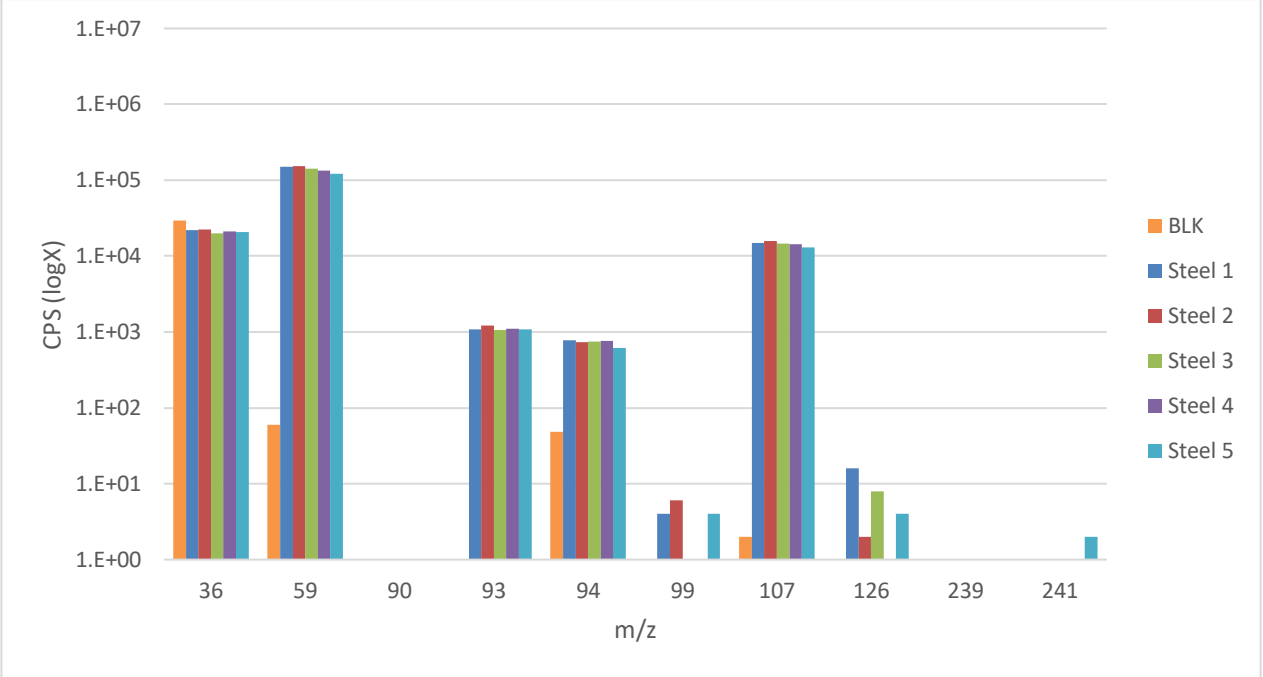

Figure 22: Stainless steel sample backgrounds measured at the m/z values of the expected radionuclides to be present – He SQ

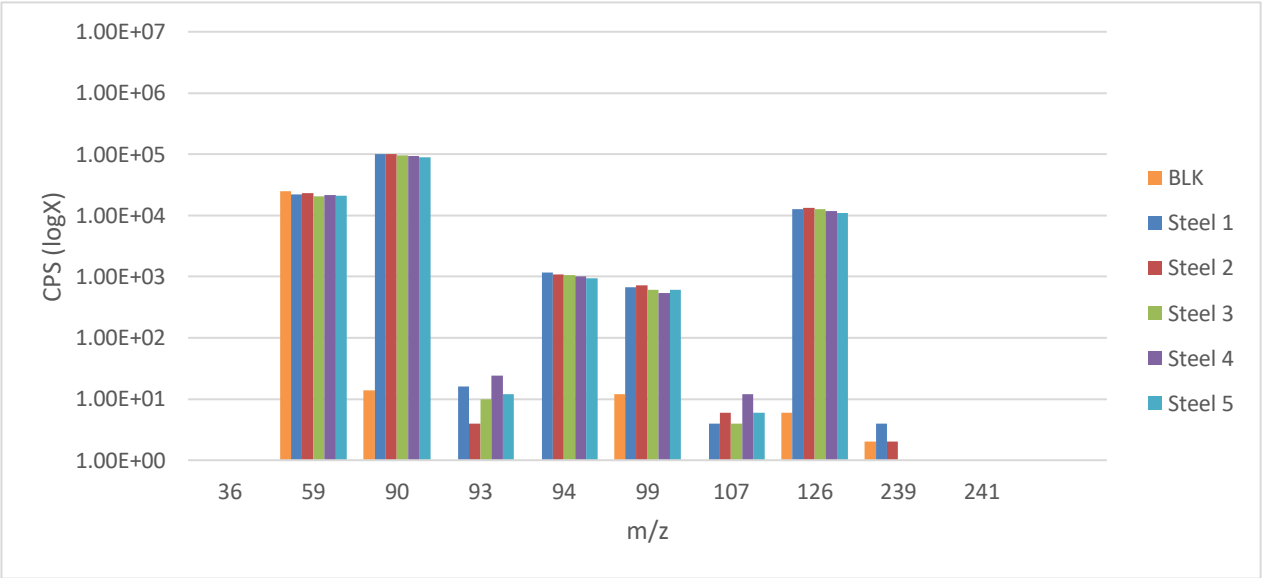

Figure 23: Stainless steel sample backgrounds measured at the m/z values of the expected radionuclides to be present - He MS/MS

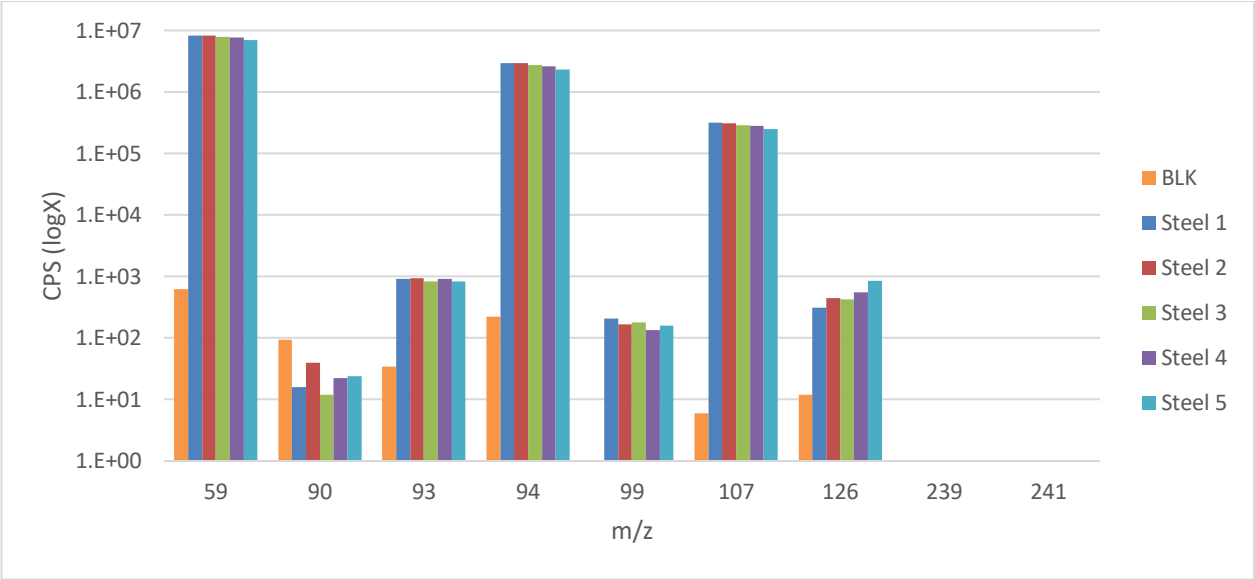

Figure 24: Stainless steel sample backgrounds measured at the m/z values of the expected radionuclides to be present - no gas MS/MS

Air filter (cellulose material) samples were analysed across the mass range of the DTM radionuclides (Figure 26, 27) with further focus of the mass range of expected radionuclides (Figure 28, 29). Operating under SQ and MS/MS He mode was used to distinguish if any of the interferences were forming within the cell, however, there was no significant change on the isotopes of interest. All the background signals observed were associated with either the plasma gas, ^{36}Ar, or atmospheric contaminates such as Zr resulting in interferences on m/z = 90 from $^{90}Zr^{+}$ and on m/z = 107 from $^{91}Zr^{16}O^{+}$, as well as atmospheric Ba contamination at m/z = 135 and 137, ^{135}Ba and ^{137}Ba respectively. However, the largest background observed was associated with <0.2 ng g^{-1} Ba, which would equate to <0.009 Bq g^{-1} of ^{135}Cs and <645 Bq g^{-1} of ^{137}Cs, which would require more extensive chemical separation as well as the use of N_2O to completely remove the background Ba signal at m/z = 135 and 137 (Cao et al., 2016).

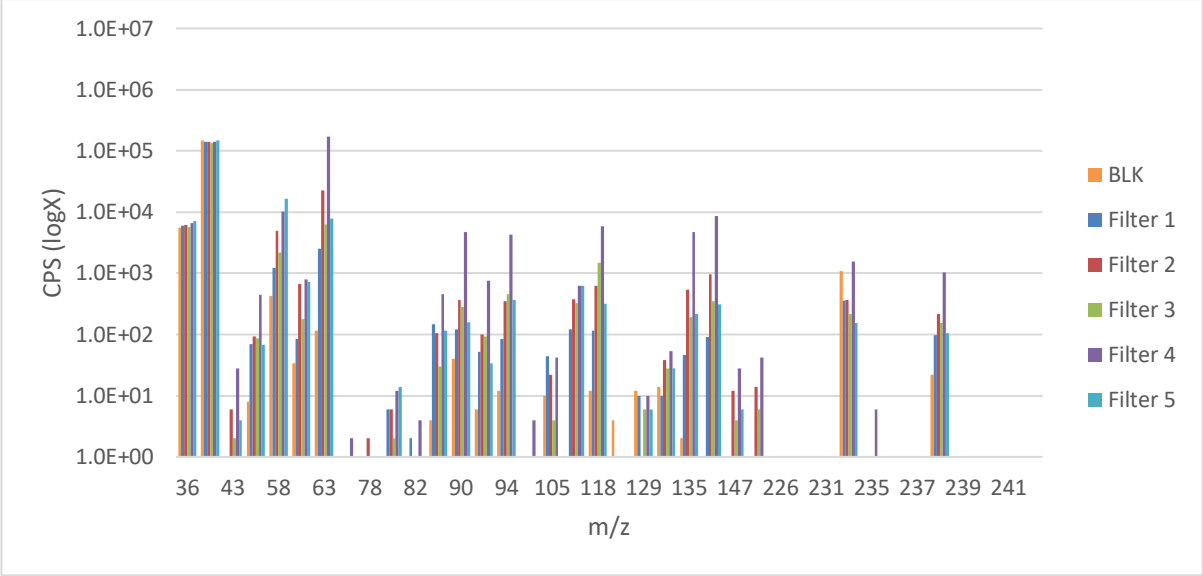

Figure 25: Air filter (cellulose) samples, analysed for all DTM radionuclide m/z values - He SQ

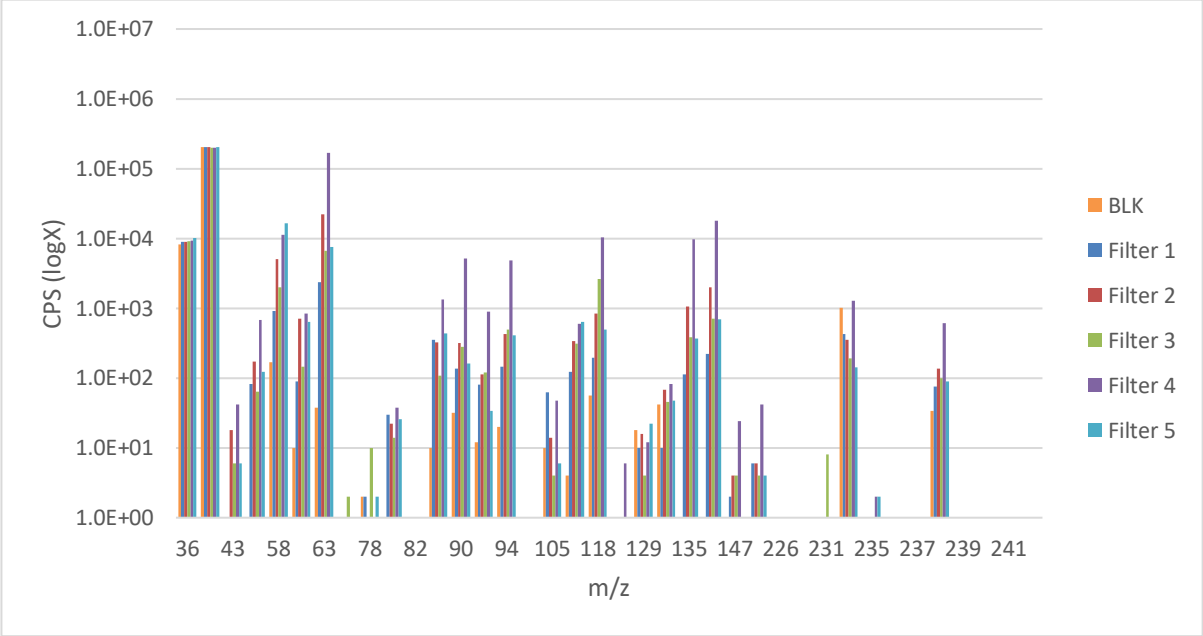

Figure 26: Air filter (cellulose) samples, analysed for all DTM radionuclides m/z values - He MS/MS

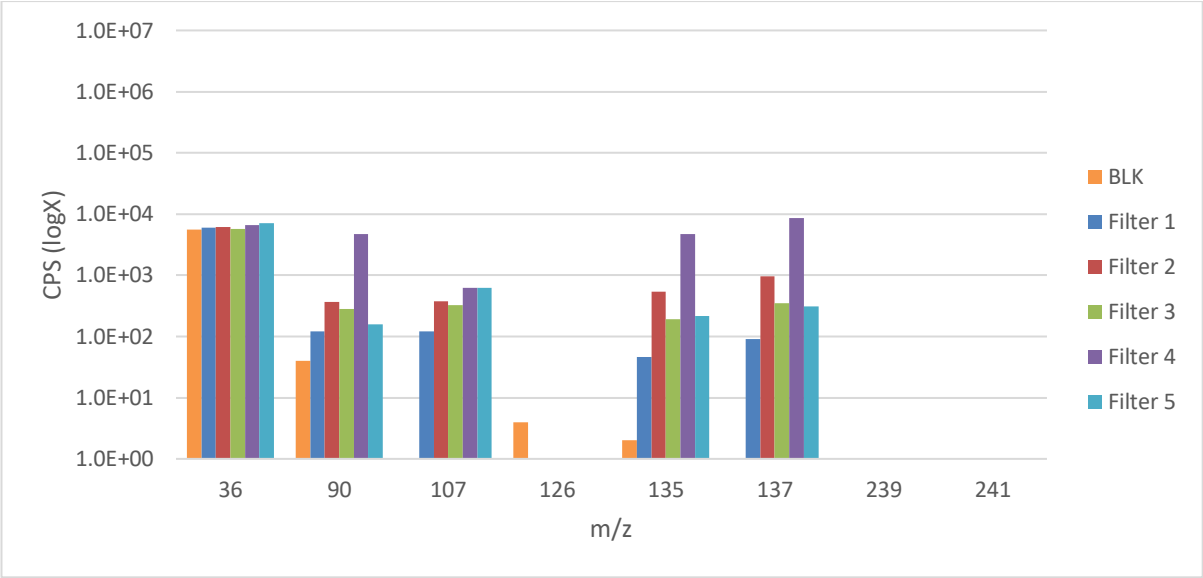

Figure 27: Air filter (cellulose) samples, analysed for the select radionuclides that are expected to be present in active samples - He SQ

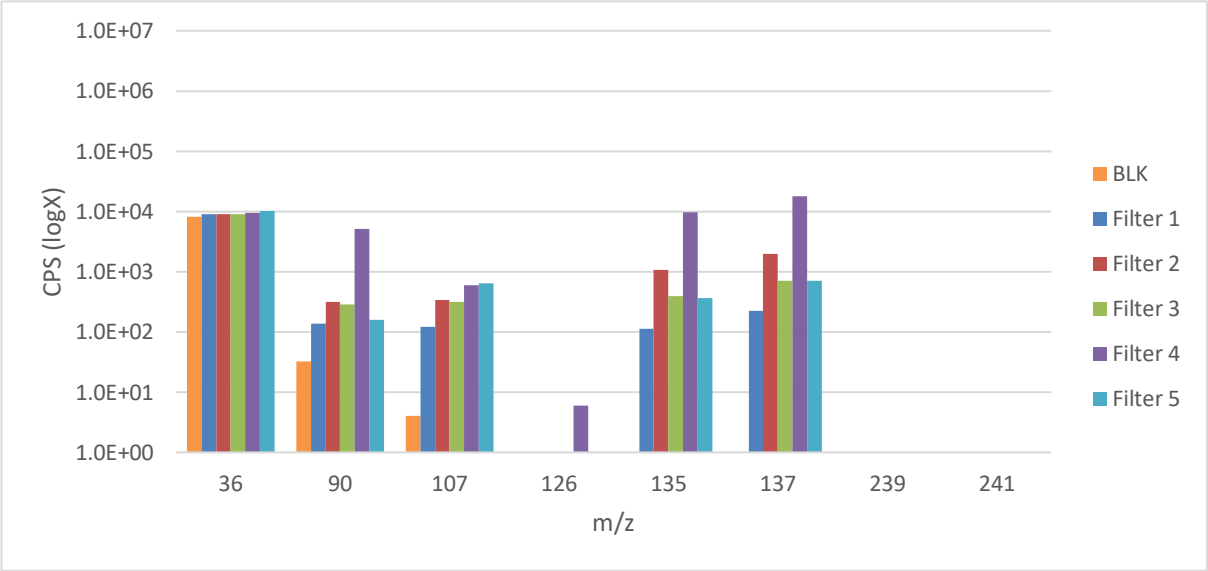

Figure 28: Air filter (cellulose) samples, analysed for the select radionuclides that are expected to be present in active samples - He MS/MS

Concrete samples were analysed across the mass range of the DTM radionuclides (Figure 30) with further focus of the mass range of expected radionuclides (Figure 31) digests also struggled with the elevated backgrounds stemming from the matrix itself as well as the instrumental backgrounds from the plasma gas meaning low to mid mass elements in the m/z = 36 to 63 range were unfavourable for analysis by ICP-MS/MS direct digest analysis. Analysis of actinide isotopes specifically those of ^{235}U and ^{238}U would be impacted by the

presence of naturally uranium isotopes within the concrete itself, however, the presence of any other actinides, at m/z = 236, 237, 239 and 241, were below the detection limit of the instrument and could be measured within the sample following sample digestion with no visible interference on the measurement.

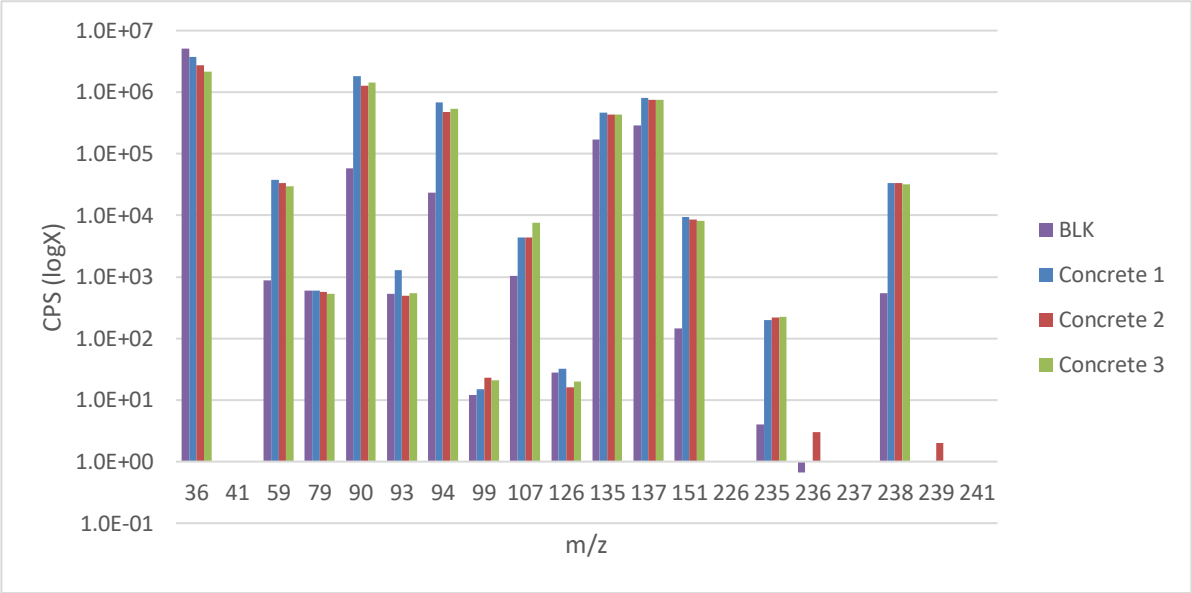

Figure 29: Concrete sample backgrounds across all the m/z values in $LiBO_2$ fussed samples with fussed blank background – No gas MS/MS

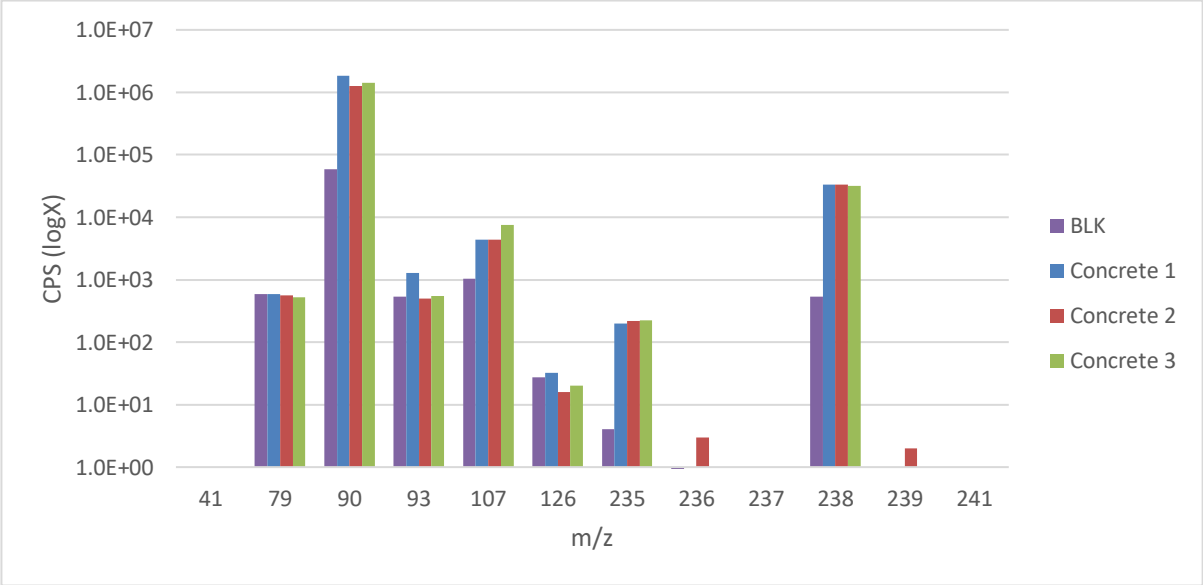

Figure 30: Concrete sample backgrounds across the expected m/z values following $LiBO_2$ fusion, compared against the fussed blank background - no gas MS/MS

Overall, all the matrix types analysed found that many of the higher mass elements, specifically the actinides, had little to no background interferences either from the matrix itself, the instrument or the sample preparation procedure. This therefore opens up the possibility of using the ICP-MS/MS for direct acid digest analysis of a range of matrix compositions for actinide characterisation. The use of He mode also highlighted the possibility of removing much of the polyatomic interferences present from within the bulk matrix, specifically those at the lower mass ranges allowing for a greater number of radionuclides to be investigated than just the expected target radionuclides in each matrix type. It should however be noted that the use of He mode also reduces overall signal sensitivity meaning detection limits and uncertainties may be impacted.

2.3.2 Sensitivity assessment

Calibration standards prepared in clean acid (0.6 M HNO_3), low TDS, were analysed using low matrix introduction (LMI), no gas, MS/MS mode. This resulted in an average signal per ng g^{-1} ^{238}U of ~160,000 CPS, while analysing the 1 % Ca samples in LMI, no gas, MS/MS mode the average signal per ng g^{-1} was reduced to ~65,000 CPS (60 % signal loss) (Figure 32), with replicate runs blocking the instrument due to the high level of TDS in the samples building up on the interface cones, specifically the sampling cone and blocking the orifice and obstructing sample transfer through the instrument. Samples containing 1 % Fe were also investigated however, it was found that the instrument was unable to tolerate this level of Fe in solution with the internal standard dropping to <2 % following the 1 % Fe containing 1 ng g^{-1} ^{238}U standard, resulting in the nebulizer blocking. Further assessment was therefore carried out on the 1 % Ca containing standards only for the purpose of determining the impact of TDS in concrete equivalent samples.

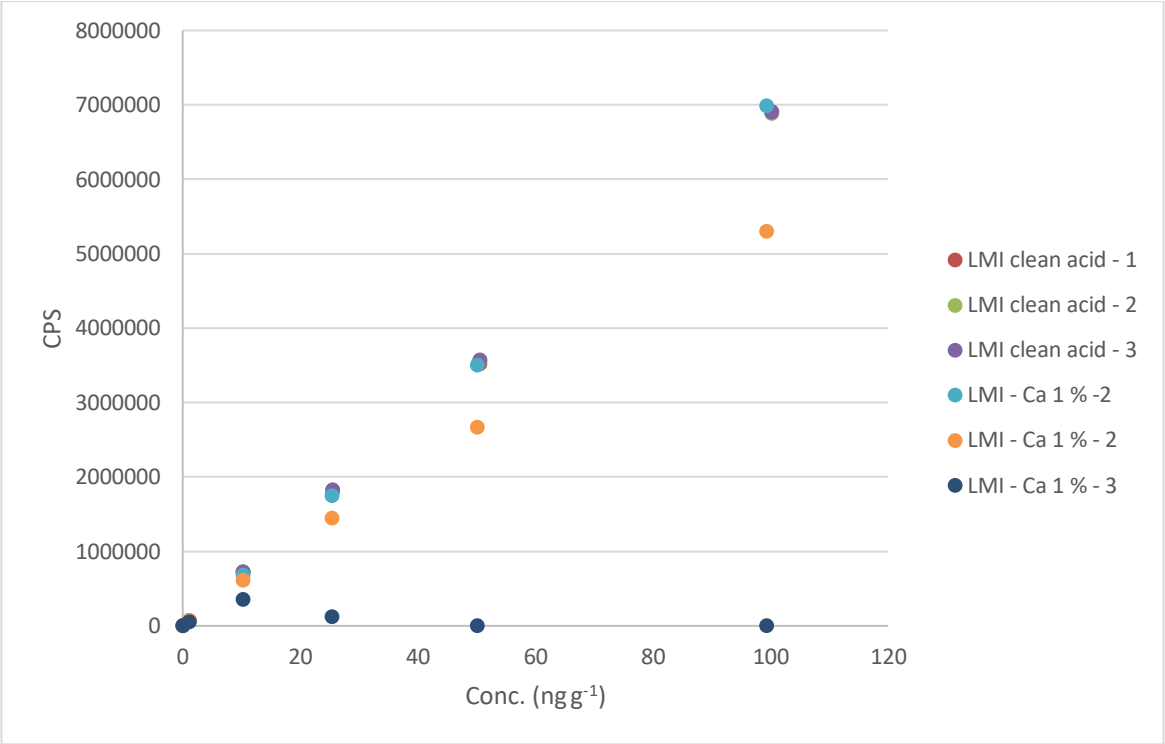

Figure 31: ^{238}U calibration analysed under LMI mode, prepared in clean acid (0.6 M HNO_3) compared against High TDS containing samples with 1 % Ca

When operating the instrument in HMI mode however, the impact on signal variability between the clean acid calibration standards and those containing 1 % Ca only varied by ~15 % (Figure 33), which is an improvement over LMI mode for consistency of sample concentration to TDS content. It should be noted that the overall signal sensitivity did also drop relative to the LMI mode with >90 % overall signal sensitivity reduction, ~160,000 CPS to ~9000 CPS for 1 ng g^{-1} (Figure 34) ^{238}U standard, when operating under HMI mode. This is due to the HMI mode acting as an online dilution stage to reduce the impact of high matrix by diluting the samples with a carrier gas. This approach is beneficial for increasing sample throughput and reducing sample preparation allowing for more concentrated samples with elevated TDS to be analysed. However, it does not improve overall detection limits as the samples are still being analysed at their diluted levels, which could alternatively have been prepared offline to reduce instrument contamination.

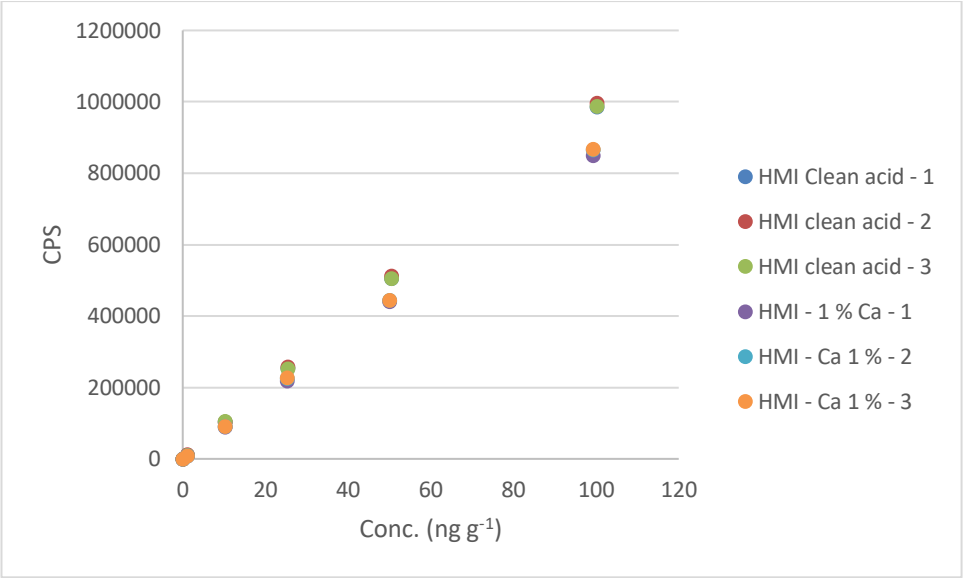

Figure 32: ^{238}U calibration analysed under HMI mode, prepared in clean acid (0.6 M HNO_3) compared against High TDS containing samples with 1 % Ca

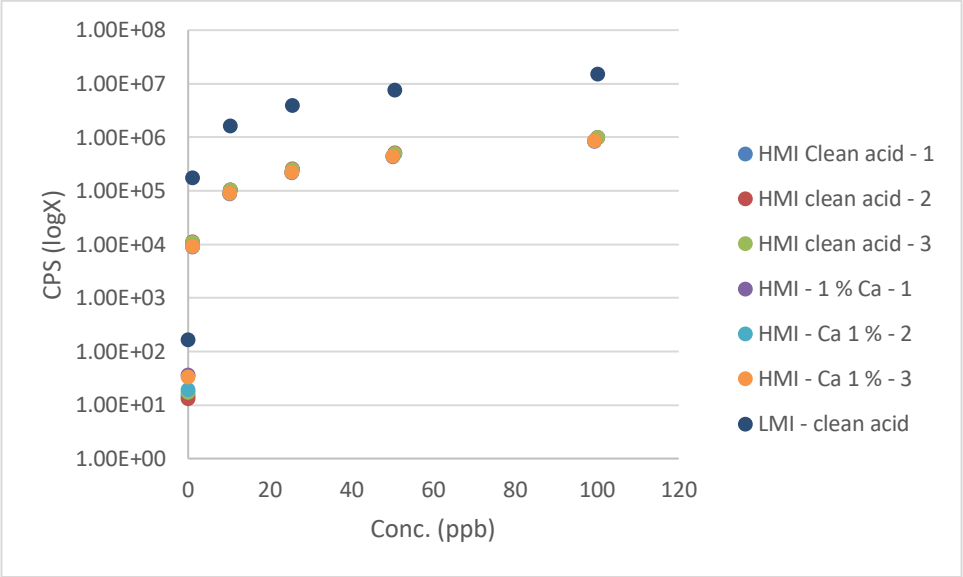

Figure 33: ^{238}U calibration analysed under HMI mode, prepared in clean acid (0.6 M HNO_3) compared against High TDS containing samples with 1 % Ca compared against LMI mode, clean acid ^{238}U calibration.

Signal sensitivity and stability was monitored using In and Re across the range of digestion techniques used for most samples, including HNO_3 and $LiBO_2$ fusion. It was found that the impact of using concentrated HNO_3, for the initial sample digest made no significant impact on the instrumental response for In and Re. However, when $LiBO_2$ flux digests were used

there was a significant drop in signal sensitivity for internal tracers used, specifically the In, ~15 % reduction (Figure 35). This was thought to be due to the high matrix loading, both reducing the ionization efficiency of the plasma, causing plasma dampening, while also disrupting the ion beam further reducing the efficient transfer of the lighter In tracer.

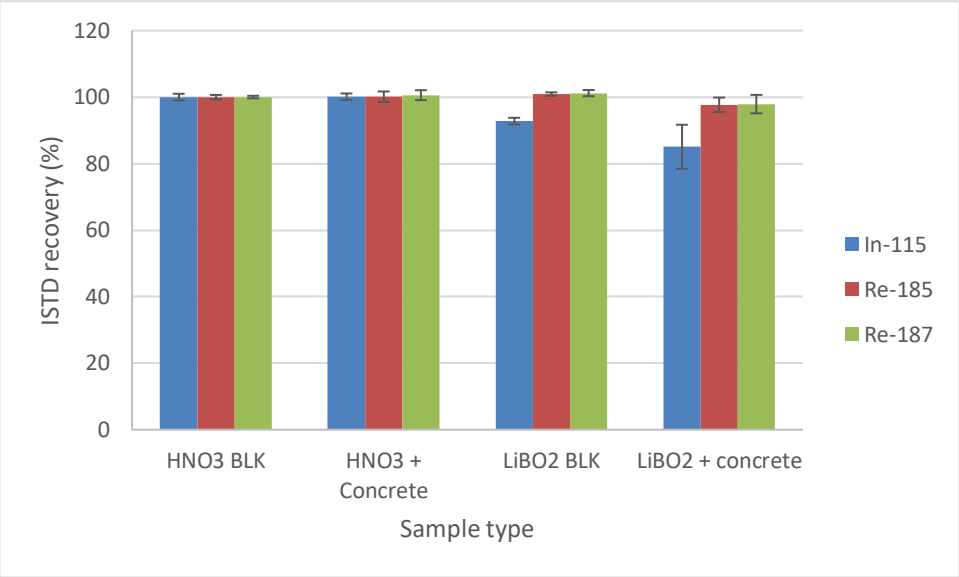

Figure 34: Changes in internal standard comparing HNO_3 standards against HNO_3 concrete digests, $LiBO_2$ blank digests and $LiBO_2$ concrete digests

Further assessment across the mass range using a mixed element standard containing, Be, Al, Cr, Mn, Co, Ni, Cu, Zn, As, Se, Sr, Mo, Cd, Ba, Pb and U was carried out to confirm whether this effect was being observed on other lighter and smaller elements other than In in addition to whether there was any variation in measurement sensitivity across the mass range that would have to be accounted for, for some of the target radionuclide measurement. The stable multi element spiked solutions were analysed under no gas, MS/MS (Figure 36). The HNO_3 solution prepared from concentrated HNO_3, showed good agreement between the mixed element standard solution and the digest solution, with a few exceptions. The $LiBO_2$ digest solution spiked with the mixed element standard showed greater variation than the HNO_3 however on many of the same isotopes. The signals on m/z = 27, 55, 60, 63, 66, 88 and 137, had an increased signal sensitivity. This was thought to be due to impurities and interferences, both isobaric and polyatomic, arising from the acid itself as both solutions used a higher concentration of HNO_3 for their initial preparation than the mixed element standard. The signal on m/z = 27 was thought to be associated

with either an Al^+ impurity or a $^{11}B^{16}O^+$ forming due to the high presence of B in the solution originating from the $LiBO_2$ fusion itself. The elevated signal on m/z = 55, specifically for the $LiBO_2$ fused solution with mixed element standard is thought to be a K impurity within the $LiBO_2$ itself, forming $^{39}K^{16}O^+$ within the plasma. Similarly, the elevated signal at m/z = 60 is thought to be from the $LiBO_2$ flux, as a Ca impurity which formed a polyatomic interference as $^{44}Ca^{16}O^+$. Alternatively, this interference may be from isobaric Ni, which along with Cu and Zn which would produce the interferences on m/z = 60, 63 and 66 respectively. The presence of these three elements in the $LiBO_2$ fused solution specifically suggests a metal impurity in the $LiBO_2$, rather than instrumental background. The elevated signal at m/z = 137 is thought to be ^{137}Ba with a significantly higher signal in the $LiBO_2$ digested solution than the HNO_3 solution.

Overall however, there was no significant signal suppression observed other than the for ^9Be which in the $LiBO_2$ digest lost 75 % of its signal sensitivity (~1600 cps to ~400 cps), however for active sample analysis the low m/z range is not of particular significance especially given the levels of background interferences stemming from oxides, nitrides and argides, all of which are present within the solution and the environment.

This assessment shows the importance for accurately determining both the signal sensitivity of the target analytes as well as the background associated with the digestion technique used, as this may impact the overall measurement if a range of different digests are analysed in tandem.

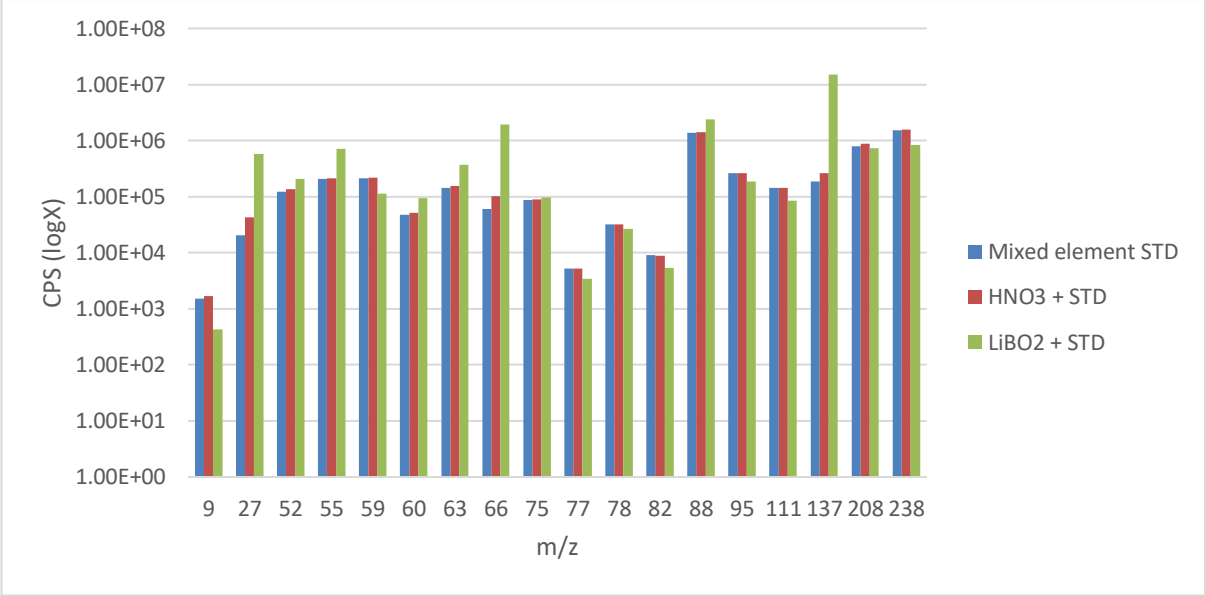

Figure 35: Sensitivity assessment using a mixed element standard solution spiked into representative digest solutions, concentrated HNO_3 and $LiBO_2$ fused solutions compared against the mixed element standard solution itself prepared in 0.6 M HNO_3

2.3.3 Determination of potential radionuclides for direct measurement

The limits of detection (LoD) for the variable radionuclides was calculated based on the matrix digest backgrounds and compared against the out-of-scope limits for the radionuclides, as proposed by EPR 2018, under both no gas, MS/MS mode (Figure 37) and He, MS/MS mode (Figure 38). This analysis highlighted the interferences present across the variable matrix types which would therefore be associated with the instrumental backgrounds that require an alternative approach to resolve such as reaction cell chemistry, as well as radionuclides which require significant purification and separation to remove the bulk matrix interference presence from stable isotopes forming isobaric and polyatomic interferences. The actinide series including ^{235}U, ^{236}U, ^{237}Np, ^{238}U, ^{239}Pu, ^{240}Pu and ^{241}Am all had LoD values below the out-of-scope limits meaning that analysis could be carried out without the need for complex multiple step separation and purification when utilising the ICP-MS/MS under either no gas or He mode. The benefits across all matrix types highlights the capabilities of the ICP-MS/MS for rapid characterisation and screening of decommissioning matrix materials following industry standard digest procedures. The

use of He mode may also have the added potentially benefit of breaking up polyatomic interferences present allowing for some of the lighter radionuclides to be measured below their out-of-scope limits including analysis of both ^{36}Cl and ^{41}Ca, which could not be monitored under no gas mode. Analysis of ^{59}Ni, ^{93}Zr, ^{99}Tc, ^{126}Sn, ^{135}Cs and ^{151}Sm were also below their out-of-scope limits for all the matrix types investigated under both no gas and He mode meaning a larger fingerprint analysis could be utilised following direct digest analysis. However, of the selected DTM radionuclides ^{79}Se, ^{90}Sr, ^{94}Nb, ^{137}Cs and ^{226}Ra were all measurable however all of them were above their out-of-scope limits with exception of ^{107}Pd which was only above its out-of-scope limit in the steel samples associated with $^{91}Zr^{16}O$ and ^{107}Ag interference present as a component within the matrix itself.

Figure 36: LoD of measured DTM radionuclides, scaled to the out-of-scope limits, measured under no gas MS/MS mode

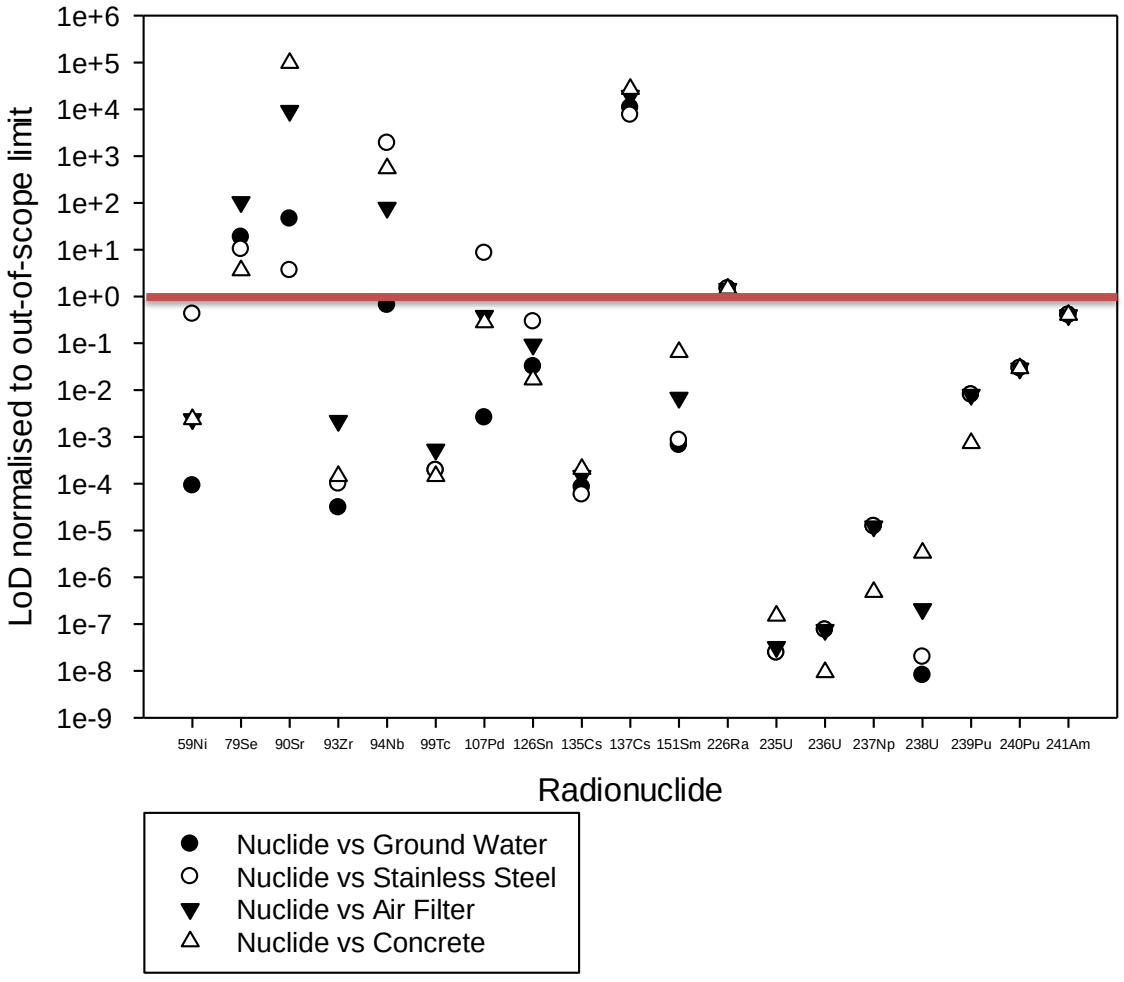

Figure 37: LoD of measured DTM radionuclides, scaled to the out-of-scope limits, measured under He (4.3 mL min-1) MS/MS mode.

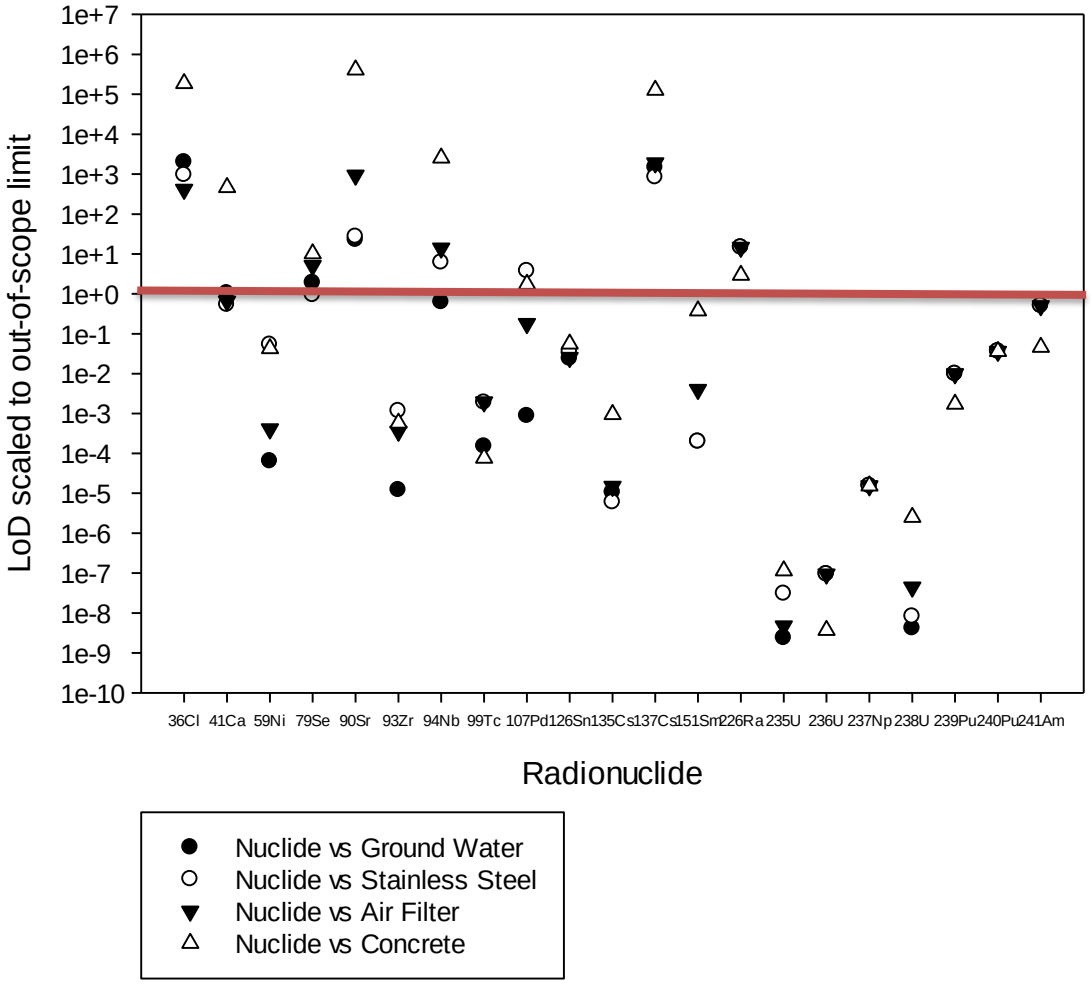

2.4 Conclusion

The assessment of the relevant matrix types analysed shows that there is a potential set of radionuclides that would benefit from direct digest and analysis, specifically those at the higher mass range associated with the actinides, where overall background is <10 cps. The lower mass range on the other hand is limited to accurate direct digest analysis due to both the instrumental background from the plasma gas, the acids, and more importantly the bulk matrix which would be adding a significantly larger concentration of stable isobaric and polyatomic interferences onto the m/z values of interest for the DTM radionuclides. The use of He mode in both SQ and MS/MS has shown the possibility of breaking up some of the polyatomic interferences present within the samples, specifically in the case of

stainless steel where the signal on m/z = 90 was reduced from 10^5 cps to 10^2 cps, however the LoD versus the out-of-scope limit highlights that further separation would be required to achieve $^{90}Sr^+$ measurements below the out-of-scope limits. Samples rich in $^{90}Zr^+$ such as the concrete would also require further separation as the signal at m/z = 90 would not be reduced and would require further reaction through the use of O_2 reaction gas specifically to react and move the Zr^+ off mass as $^{90}Zr^{16}O^+$. The use of HMI was demonstrated as a means to reduce the impact of TDS specifically in the case of $LiBO_2$ fused samples whereby the online instrumental dilution is able to reduce sample preparation time and increase sample throughput. It should however be noted that the impact of HMI mode on signal sensitivity is ~90 % signal reduction due to the online dilution, in which case offline dilution could also be utilised to reduce the TDS concentration and reduce the high matrix loading on the instruments introduction.

Overall the ability for the ICP-MS/MS to tolerate direct digest solutions, with high matrix concentrations while able to achieve low background for many of the actinides, including ^{235}U, ^{236}U, ^{237}Np, ^{239}Pu, ^{241}Am as well as ^{59}Ni, ^{93}Zr, ^{99}Tc, ^{126}Sn, ^{135}Cs and ^{151}Sm when operating under no gas, MS/MS demonstrates the potential for emergency response analysis, where minimal sample handling and preparation will reduce sample turn around, and improve response times. The technique also offers a means for characterisation and screening of decommissioning waste and samples from a range of different matrix types including ground waters, steels, air filters and concretes, without the need for extensive separation and purification.

Chapter 3 Specific application of radionuclide measurement with limited or no sample preparation

3.1 Introduction

All nuclear reactors and facilities have a finite operational life after which they require decommissioning. This involves defueling the reactors themselves and removing any active heat transport fluids, followed by the decontamination of contaminated areas with higher activity areas sealed off. The following stages require all materials, equipment and structures where the radioactivity exists above prescribed levels to be analysed and characterised prior to storage or disposal, before the site itself can be released for other purposes. Within the UK, the largest source of active waste comes in the form of constructional materials specifically concrete, which make up ~60 % of all nuclear waste, with >70 % of all concretes present as VLLW waste (NDA 2016). Concrete is used for a range of different constructional purposes from being the fundamental material in constructing the nuclear facility to creating the bioshield for the reactor (NEA 2011, RAENG 2012). Similarly, any radionuclides that are volatilised or solubilised into the cooling circuit within a nuclear reactor are then circulated and potentially deposited onto the surface of the concrete. However, unlike other construction materials such as steel (Lang 2017), which have relatively poor porosity, concrete is far more porous and radionuclides may deposit deeper into the surface structure (Dae et al., 2008, Maeda et al., 2014). Along with the surface contamination concrete is a combination of cement, aggregate and water meaning that there are a range of different elements present within it that when exposed to a neutron flux can be neutron activated and form a range of activation products (Field et al., 2015). In the UK the most commonly used cement for nuclear facilities is Portland cement which is manufactured from a calcareous material, where limestone and chalk are the two principal examples of such. The addition of clay or shale introduces aluminium oxide, Al_2O_3, and silicon dioxide, SiO_2, to Portland cement (Aïtcin, 2015, Field et al., 2015). The aggregates used for the construction of the reactor can vary greatly based on the location of the facility being constructed as sand or grave is often sourced from local quarries. Since aggregate accounts for approximately 75 % of the total concrete volume, concrete

compositions and the activation products that may arise following the effect of irradiation may be variable between different reactor facilities. Structural demolition is a large scale, late stage procedure for nuclear decommissioning meaning it is important to have a means to rapidly characterise the concrete to allow for rapid waste characterisation and either disposal or storage. Due to the range of radionuclide sources, being able to characterise the waste based of major radionuclides, specifically for low activity concrete, would reduce the time and cost of decommissioning and allow waste to be designated to their specific waste streams more effectively without the need for extensive chemical separation procedure. The use of gamma spectrometry allows for gamma emitting radionuclides to be measured within the matrix however this limits the list of potential fingerprint radionuclides which can be used. For a more complete characterisation, chemical digestion, separation and purification is required to allow for individual isotopic analysis specifically by ICP-MS as well as radiometric analysis by LSC, where complete isotope separation and purification is required.

The most effective way of ensuring complete sample digestion of concretes is by fusing the material with $LiBO_2$ at 1050 ^oC turning it into a glass before digesting further with HNO_3 (8 M) (Braysher et al., 2019), however, doing so introduces all the sample matrix into the solution along with the sample flux, increasing the TDS of the solution itself and the number of interferences present. Direct digest analysis of concretes by ICP-MS is limited due to both the high levels of matrix that would be introduced into the plasma, specifically group 1 and 2 elements in the form of Li, Na, Cs, Mg, Ca and Ba as well as group 3, Al, which would cause signal suppression due to the low 1^{st} ionization energies of these elements (and the high concentrations present within the sample and plasma (Bryant et al., 2002), and the range of interferences that would arise on the radionuclides of interest, both isobaric and polyatomic.

In recent years the development of the ICP-MS/MS, with a quadrupole prior to the cell entrance has introduced a way to potentially reduce or remove the interference by acting as a mass filter, and allow for rapid screening of sample digested to be utilised for characterisation of active concretes.

The aim of this study is to assess the capabilities of the ICP-MS/MS, Agilent 8800, as a means to carry out fingerprint characterisation and screening of active sample digests. Previous assessment of a range of representative matrix analogues demonstrated the

background interferences arising from the instrument and matrix itself, following industry standard sample digestions. Concrete was chosen as a matrix to investigate further and to assess the effects of acid digest and leaching using a range of acids including HNO_3, HCl and aqua regia and comparing against the complete sample digest of $LiBO_2$ fusion and HNO_3 dissolution to determine if specific radionuclides could better be isolated and extracted without the presence of the majority of the matrix and consequent interferences.

Analysis of stable concretes under the varying acid digests was used to better understand the potential background interferences and to further allow for specific radionuclides to be selected for characterisation and screening purposes.

3.2 Methodology

3.2.1 Reagents and Materials

Primar Plus^{TM} HNO_3 (68 %) and Aristar grade HCl (37 %) were obtained from Fisher Scientific, UK. An Agilent multi element standard (Al, Cr, Mn, Co, Ni, Cu, Zn, As, Se, Sr, Mo, Cd, Ba, Pb) (1 µg g^{-1}) from Agilent, UK and standard single element standard solutions (10 mg g^{-1}) of Be and U were sourced from Sigma Aldrich, UK. Dilutions were prepared using deionised water (>18.2 MΩ·cm), produced from a Q-Pod Millipore System (Merck, York, UK).

Active concrete samples were obtained from GAU-radio analytical, Southampton, including bioshield concrete (1433) and active constructional concretes (1132 – 1135) sourced from nuclear facilities around the UK.

3.2.2 Instrumentation

High resolution gamma spectrometric analysis was performed using HPGe detectors. Detectors were calibrated against a mixed radionuclide standard solution. The standard was used to prepare a source of identical geometry to that of the samples. Gamma spectra

were analysed and individual radionuclides quantified using Fitzpeaks spectral deconvolution software (JF Computing Services).

All ICPMS measurements were performed using an Agilent 8800 ICP-MS/MS. The instrument is equipped with a collision-reaction cell (termed an Octopole Reaction System, ORS^3) positioned between two quadrupole mass filters (termed Q1 and Q2). The instrument was fitted with a Scott double pass spray chamber, Micromist nebuliser, quartz torch and nickel sample and skimmer cones. The instrument was fitted with four cell gas lines (Table 10) - dedicated H_2 and He lines in line 1 and 2, NH_3 in line 3 (for corrosive gases) and O_2 in line 4 (for non-corrosive gases). The corrosive gas must be balanced with at least 90% He to protect the ORS^3, and when operating cell line 3, the He line is automatically run at a flow rate of 1 mL/min (Table 10). High purity H_2, He, NH_3, O_2 and Ar were supplied by BOC (UK), with a purity of 99.9999% (N6.0).

Table 9: Agilent 8800 gas modes and flow rates available

Cell line	**Gas used**	**Flow rate range (mL/min)**
Hydrogen	H_2	0-10
Helium	He	0-12
Line 3 (corrosive)	NH_3 (balanced in 90% He)	0-10
Line 4 (non-corrosive)	O_2	0-1

The instrument was tuned each day in single quadrupole (SQ) mode (only Q2 operating) with no cell gas using a 1 ng g^{-1} stable element standard mixture of Be, Ce, Co, Li, Tl and Y in 0.6 M HNO_3, to ensure criteria for sensitivity, measurement uncertainty, interference formation and peak axes alignment were achieved.

3.3 Experimental

3.3.1 Background assessment

A non-active representative concrete analogue was crushed to a fine powder and sub sampled (0.5 g). The concrete samples were individually digested in Teflon pots used 16 mL conc. HCl, conc. HNO_3, aqua regia (3:1 HCl: HNO3) and $LiBO_2$ fusion (0.5 g sample: 2 g $LiBO_2$ flux) followed by HNO_3 digest (8 M, 100 mL). Digests were vacuum filtered through Whatman carbon free filter paper supported on Whatman glass microfiber filters. The supernatant was evaporated to dryness at 90°C in Teflon pots. The residue was then re-dissolved in 20 mL of HNO_3 (0.6 M) for the HNO_3, HCl and aqua regia digests and 50 mL of HNO_3 (0.6M) for the $LiBO_2$ fused samples.

The samples were analysed for all the m/z values associated with the difficult to measure radionuclides, including those that may not necessarily be expected within the active concrete samples (Table 11). This was used as a way to determine overall background in the samples as well as to rule out the radionuclides that would not be measurable under specific acid digest procedures proposed.

Table 10: List of difficult-to-measure (DTM) radionuclides including those expected in active concrete

Radionuclide	Matrix Concrete
^{36}Cl	
^{41}Ca	X
^{59}Ni	
^{79}Se	X
^{90}Sr	X
^{93}Zr	X
^{94}Nb	
^{99}Tc	
^{107}Pd	X
^{126}Sn	X
^{135}Cs	
^{137}Cs	
^{151}Sm	
^{226}Ra	
^{235}U	X
^{236}U	X
^{237}Np	X
^{238}U	X
^{239}Pu	X
^{241}Am	X

3.3.2 Active Concrete analysis

Active concrete samples were selected based on the range of actinides present including bioshield concrete (1433) as well as active constructional concretes (1132-1135) sourced from varying nuclear facilities within the UK. Samples were crushed to a fine powder and sub-sampled (0.5 g). The active concrete samples were individually digested in Teflon pots used 16 mL conc. HCl, conc. HNO_3, aqua regia (3:1 HCl: HNO3) and $LiBO_2$ fusion (0.5 g sample: 2 g $LiBO_2$ flux) followed by HNO_3 digest (8 M, 100 mL). Digests were vacuum filtered through Whatman carbon free filter paper supported on Whatman glass microfiber filters. The supernatant was evaporated to dryness at 90^{o}C in Teflon pots. The residue was then re-dissolved in 20 mL of HNO_3 (0.6 M) for the HNO_3, HCl and aqua regia digests and 50 mL of HNO_3 (0.6M) for the $LiBO_2$ fused samples. Samples were then analysed as dilutions of a factor of 100x, 10x and as concentrates spiked with an internal standard, In and Re (5 ng g^{-1}).

Final sample concentrates were analysed for ^{241}Am using gamma spectrometry. Digest recoveries of ^{241}Am in the unseparated concentrates were compared against those previously measured and analysed through extensive chemical separation and purification with results also compared against ICP-MS/MS analysis.

The sample concentrates along with the dilutions were analysed by ICP-MS/MS analysing for ^{234}U, ^{235}U, ^{236}U, ^{237}Np, ^{238}U, ^{239}Pu, ^{240}Pu and ^{241}Am, under no gas MS/MS mode and He MS/MS mode. Samples were selected with no ^{241}Pu and assumed that the signal at m/z = 241 was explicitly ^{241}Am, however, for other samples the measurement at m/z = 241 would be a combination of ^{241}Pu and ^{241}Am. Detection limits were calculated for the unseparated samples and compared against chemically separated and purified values.

3.4 Results and Discussion

3.4.1 Background assessment

Analysis of non-active concrete samples digested using variable acids showed similarities in background across all the digest procedures and under both no gas MS/MS and He MS/MS modes (Figure 39 and 40), with the highest instrumental backgrounds at m/z = 36, associated with $^{36}Ar^{+}$ in the plasma gas, while m/z = 41 could not be monitored under no gas MS/MS due to the high concentration of $^{40}Ar^{+}$ tailing and $^{40}Ar^{1}H^{+}$ polyatomic interference (Boulyga 2009). The high backgrounds at m/z = 59 and 63 were thoughts to be associated with isobaric $^{63}Cu^{+}$ and polyatomic $^{43}Ca^{16}O^{+}$ and tailing from $^{46}Ca^{16}O^{+}$, $^{48}Ca^{16}O^{+}$ and $^{58}Fe^{1}H^{+}$ (May and Wiedmeyer 1998), present from the concrete matrix itself. The signal at m/z = 79 was an order of magnitude greater in the HCl digest than any other acid, therefore suggesting the presence of Br^{+} as an impurity within the HCl itself. The high background signal at m/z = 90 and 94 was associated with the Zr^{+} present within the concrete itself meaning analysis of ^{90}Sr and ^{94}Nb would be limited without further separation and purification regardless of the acid digest proposed. The Zr^{+} within the concrete digests was also forming a polyatomic interference in m/z = 107 as $^{91}Zr^{16}O^{+}$ due to the favourable enthalpy of reaction (ΔHr = -2.75) (Agilent 2012, Sugiyama, 2012) and the oxygen present. The elevated signal in the HCl containing sample digests at m/z = 93 were thought to be associated with $^{56}Fe^{37}Cl^{+}$, $^{58}Fe^{35}Cl^{+}$ and $^{58}Ni^{35}Cl^{+}$, present as trace elements within the concretes itself. The presence of Ba within the concrete digests resulted in an increased background at m/z = 151 due to the formation of $^{135}Ba^{16}O^{+}$ (ΔHr = -0.50) (Agilent 2012). Isotopes of U in the form of $^{235}U^{+}$ and $^{238}U^{+}$ were both observed in the stable concrete samples however their CPS was <0.004 ng g^{-1}, <3×10^{-7} Bq g^{-1}, and <0.5 ng g^{-1}, <5×10^{-6} Bq g^{-1}, respectively. These values were significantly below the 1 Bq g^{-1} out-of-scope limit for both ^{235}U and ^{238}U (Table 12). The isotopes at m/z = 99, 126 235, 236, 238, 239 and 241 could all be used for sample fingerprint characterisation due to both low background CPS and low activity equivalence concentrations. The active concretes which were chosen for direct digest analysis had previously been characterised as containing isotopes in the actinide series including ^{234}U, ^{235}U, ^{236}U, ^{238}U, ^{239}Pu, ^{240}Pu and ^{241}Am, while the low LoD

measurements in the stable concrete (Table 12) further suggested the capabilities of the technique for such analysis.

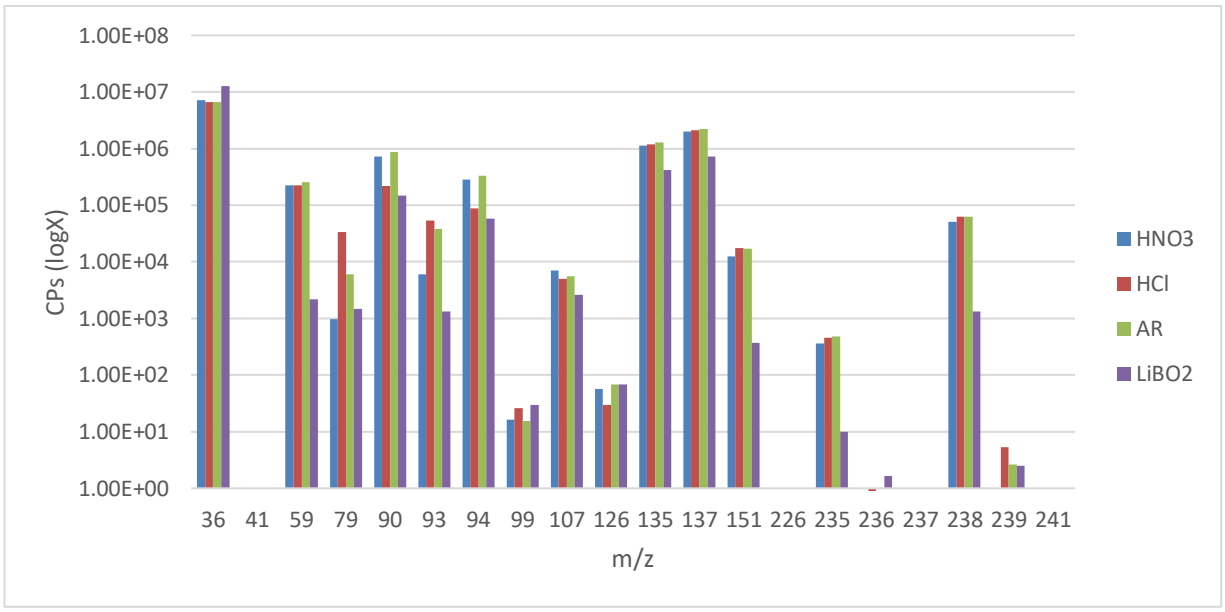

Figure 38: Non-active concrete background assessment under variable acid digests (HNO_3, HCl, aqua regia and $LiBO_2$ fusion) – No gas, MS/MS mode

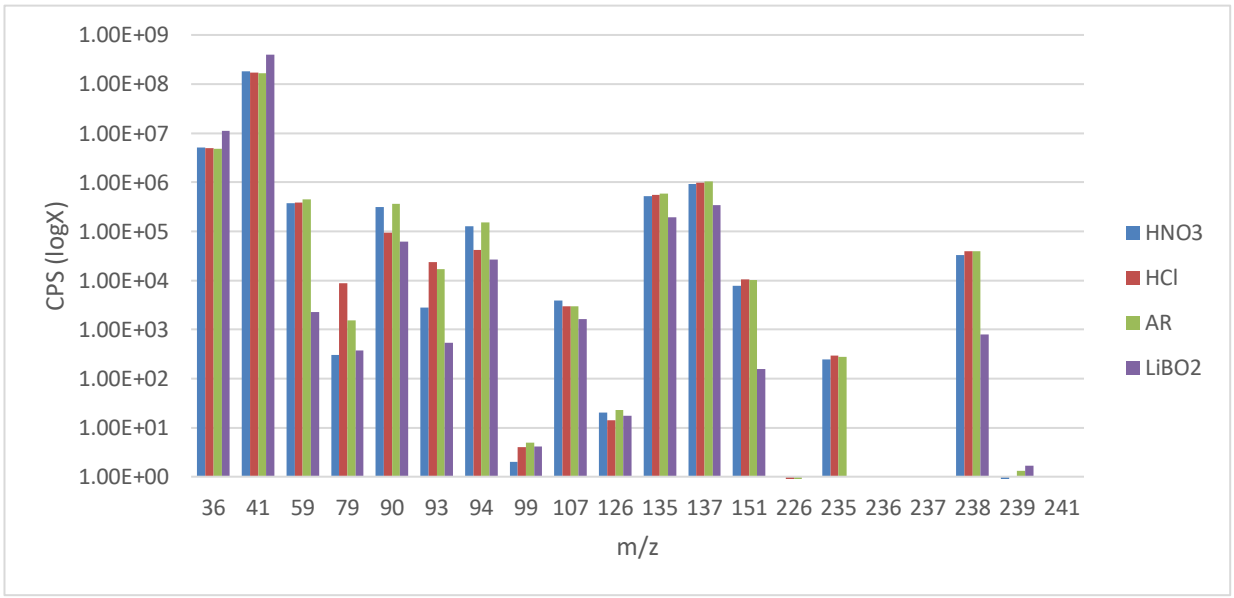

Figure 39: Non-active concrete background assessment under variable acid digests (HNO_3, HCl, aqua regia and $LiBO_2$ fusion) – He (4.3 mL min-1), MS/MS mode

Table 11: Calculated limits of detection for stable concrete samples for the actinides analysed under no gas, MS/MS mode and He (4.3 mL min-1), MS/MS mode

	U-234	U-235	U-236	U-238	Pu-239	Pu-240	Am-241
No Gas MS/MS (Bq g^{-1})	$7x10^{-5}$	$3x10^{-7}$	$9x10^{-8}$	$5x10^{-6}$	$7x10^{-5}$	$3x10^{-3}$	$4x10^{-2}$
He MS/MS (Bq g^{-1})	$1x10^{-11}$	$3x10^{-11}$	$4x10^{-8}$	$3x10^{-6}$	$2x10^{-4}$	$4x10^{-3}$	$5x10^{-3}$
Out-of-scope limit (Bq g^{-1})	1	1	10	1	0.1	0.1	0.1

Analysing all the digests for their impact on internal standard variations further demonstrated how the variable acid digests had no significant variation on the internal standard signal while those containing $LiBO_2$ fused samples reduced this sensitivity due to the presence of the $LiBO_2$ flux in the final digest (Figure 41). However, the internal standard could therefore be used to correct for the plasma suppression and signal dampening caused by the increased TDS in solution.

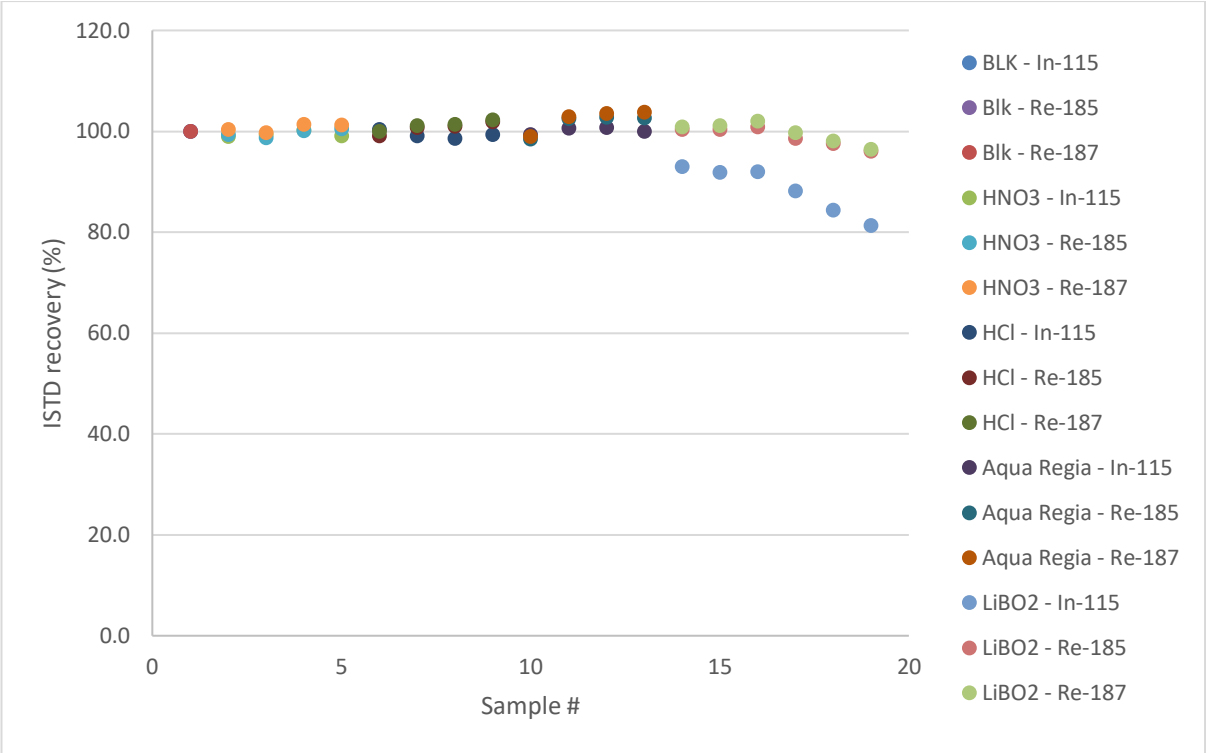

Figure 40: Variations on internal standard (In and Re) recovery dependent on the acid digest or fusion used for non-active concrete processing – No gas MS/MS

3.4.2 Active Concrete analysis

The active concretes selected covered a range of different uses of the concrete within the nuclear facility as well as a range of activities of specific isotopes. The active concretes (1132-1135) were all different concrete samples with variable compositions ranging from grey concrete dusts to sand coloured concretes. The analysis was carried out on concentrates at varying dilutions. The 100x dilutions however showed sensitivities equivalent to background measured values and therefore not taken further for further assessment. Analysis of the 10x dilutions showed the most complete data set as it allowed for $LiBO_2$ fused digests to be analysed without causing any impact on further instrumental measurements or memory effects. The low activity of ^{234}U in all the sample analysed meant that the uncertainty on the measurements was high, resulting in the range of average matrix digest relative to the reference values (Table 13 and 14). However, for the remaining uranium isotopes, ^{235}U, ^{236}U and ^{238}U the average recoveries were ~60-70% for all samples other than 1133, with acid digests and $LiBO_2$ fusion showing equivalent recovery. Sample

1133 had a uranium concentration at least an order of magnitude lower than the other samples suggesting that for samples with trace levels of target analyte the loss from the digest procedures proposed was significantly greater resulting in a larger measurement uncertainty due in part to low measurement sensitivity.

Table 12: Active concrete sample concentrations (Bq g^{-1}) of actinides previously measured following extensive chemical separation and purification used as the reference values

Sample Number	Matrix	U-234	U-235	U-236	U-238	Pu-239	Pu-240	Pu-241	Am-241
1433	Bioshield Concrete	0.01	0.0003	-	0.005	0.39		4.23	0.8271
1132		1.1	0.042	0.013	0.8	19	5.797	-	4.965
1133	Active Concrete	0.11	0.0044	0.0007	0.013	99.99	33.98	-	44.68
1134		0.13	0.0067	0.002	0.16	60.99	20.99	-	27.8
1135		0.62	0.023	0.0042	0.34	55.99	11.99	-	12.91

Table 13: Average measured value across all acid digests relative to reference value of the materials (%) – no gas MS/MS mode

Sample Number	U-234	U-235	U-236	U-238	Pu-239	Pu-240	Am-241
1433	45.5	79.3	-	92.5	80.2		99.5
1132	69.7	66.9	74.5	68.5	56.2	26.0	65.6
1133	34.0	28.1	29.2	46.8	55.4	39.0	37.4
1134	75.5	64.4	72.2	67.7	47.7	36.4	53.0
1135	69.3	60.8	69.9	65.8	36.4	28.7	37.9

Analysing the concrete digests under He MS/MS mode offers the benefit of reducing and removing isobaric interferences that may arise specifically in regard to $^{238}U^{1}H^{+}$ interfering into m/z = 239. However, by analysing the average measured values of the acid digests relative to the reference value there is no significant difference between no gas, MS/MS mode and He, MS/MS mode (Table 14 and 15). When operating in He, MS/MS mode there is however a reduction of ~30 % in overall signal sensitivity resulting in a greater degree of measurement uncertainty. Analysis of the low concentration isotopes, specifically ^{234}U, ^{239}Pu, ^{240}Pu and ^{241}Am had a greater level of loss associated with the significance that sample loss from the digestion procedure would be causing on the measurement.

Table 14: Average measured value across all acid digests relative to reference value of the materials (%) – He (4.3 mL min-1) MS/MS mode

Sample Number	U-234	U-235	U-236	U-238	Pu-239	Pu-240	Am-241
1433	49.0	75.6	-	91.8	66.7		131.6
1132	70.4	66.8	70.6	67.7	52.6	26.6	62.5
1133	41.2	28.6	31.7	46.5	55.0	35.8	43.5
1134	83.3	64.0	63.4	66.7	47.7	36.8	34.8
1135	68.0	61.2	72.9	64.1	36.6	32.4	44.5

The Pu isotopes that were measured showed relatively low sample leaching in the acid digests, with the majority of the Pu isotopes going into solution under $LiBO_2$ fusion followed by HNO_3 digest (Table 16 and 17). This is due to the insoluble compounds that Pu forms, including PuO_2, within the concrete samples meaning concentrated acid digests have limited success in leaching the analyte out of the matrix. Complete matrix break down using $LiBO_2$ fusion enables Pu isotopes to be solubilised and therefore analysed with a lower level of uncertainty. The increased recoveries relative to the reference value for the He, MS/MS analysed samples (Table 16) are due to the suppression of the signal sensitivity resulting in a greater uncertainty on calculation due to the low counts being scaled with this uncertainty. The analysis of these real matrix samples was further complicated by the heterogeneity of the Pu present in the samples, which is especially evident with sample

1133 aqua regia, which showed Pu recoveries relative to the reference value an order of magnitude below that of the individual acid digests that it was composed of. Further replicates may have alleviated this heterogeneity artefact however a more comprehensive digestion procedure such as utilising $LiBO_2$ fusion and a larger initial sample size would also allow for a more representative sample size to be analysed.

Table 15: Measured activity relative to the reference value of the materials (%), separated by acid digests and $LiBO_2$ fusion for ^{239}Pu and ^{240}Pu – No gas, MS/MS

Sample	Pu-239				Pu-240			
	HNO_3	HCl	Aqua Regia	$LiBO_2$ Fusion	HNO_3	HCl	Aqua Regia	$LiBO_2$ Fusion
1433	27.8	33.3	37.5	77.2	40.7	34.8	34.9	20.2
1132	39.7	39.3	36.3	84.6	19.2	22.3	15.4	46.4
1133	25.2	38.9	4.4	144.3	22.5	29.2	3.7	98.9
1134	7.4	79.8	20.5	65.1	7.3	56.1	17.1	62.6
1135	34.1	28.3	19.9	48.8	26.7	25.5	16.2	42.1

Table 16: Measured activity relative to the reference value of the materials (%), separated by acid digests and $LiBO_2$ fusion for ^{239}Pu and ^{240}Pu – He (4.3 mL min-1), MS/MS

Sample	Pu-239				Pu-240			
	HNO_3	HCl	Aqua Regia	$LiBO_2$ Fusion	HNO_3	HCl	Aqua Regia	$LiBO_2$ Fusion
1433	33.4	25.8	40.2	53.7	63.4	105.1	101.4	343.6
1132	18.1	20.4	18.6	46.1	38.2	55.4	41.7	168.6
1133	22.6	25.8	3.7	81.6	24.5	29.5	3.2	111.4
1134	8.1	55.8	17.2	63.5	17.0	51.9	30.6	37.0
1135	25.6	21.8	15.7	34.5	31.8	43.5	25.6	65.3

Analysis and comparison of the ^{241}Am isotopes shows variation in the leachability of the ^{241}Am from the concrete matrix. However, complete matrix digest using $LiBO_2$ fusion showed the best recoveries relative to the reference values of the concrete samples (Table 18 and 19). The variations seen between the variable concrete samples in regards to acid digest recoveries are due to the low counts (<300 cps ± 50) of the measurements, with lower activity samples being significantly more influenced by the uncertainty, making it more difficult to distinguish between significant variations of the procedure, sample heterogeneity and instrumental fluctuations on measurements with <50 cps ± 36. When analysing under He, MS/MS mode the relative signal sensitivity for ^{241}Am are reduced to <200 cps ± 50. The lower counts further increase the uncertainties and therefore when scaled and compared against the reference values of the samples there appears to be a greater level of recovery (Table 19).

Table 17: ICP-MS/MS (no gas, MS/MS) measured activity relative to the reference value of the materials (%), separated by acid digests and $LiBO_2$ fusion for ^{241}Am, and comparing the measured values against values measured by Gamma spectrometry.

Sample number	ICP-MS/MS				Gamma Spectrometry			
	HNO_3	HCl	Aqua Regia	$LiBO_2$ Fusion	HNO_3	HCl	Aqua Regia	$LiBO_2$ Fusion
1433	89.0	78.3	74.7	259.1	91.9	70.1	89.5	120.9
1132	55.3	59.0	48.1	63.2	74.1	79.8	75.3	76.5
1133	27.4	21.5	5.7	84.5	38.0	35.6	6.8	131.2
1134	17.2	57.6	25.5	89.7	23.3	75.4	40.8	95.5
1135	38.8	34.1	37.0	32.7	60.6	64.5	57.3	70.5

Table 18: ICP-MS/MS (He (4.3 mL min-1), MS/MS) measured activity relative to the reference value of the materials (%), separated by acid digests and $LiBO_2$ fusion for ^{241}Am, and comparing the measured values against values measured by Gamma spectrometry

Sample number	ICP-MS/MS				Gamma Spectrometry			
	HNO_3	HCl	Aqua Regia	$LiBO_2$ Fusion	HNO_3	HCl	Aqua Regia	$LiBO_2$ Fusion
1433	63.4	105.1	101.4	343.6	91.9	70.1	89.5	120.9
1132	31.5	20.2	29.8	168.6	74.1	79.8	75.3	76.5
1133	24.5	29.5	3.2	111.4	38.0	35.6	6.8	131.2
1134	17.0	51.9	30.6	37.0	23.3	75.4	40.8	95.5
1135	31.8	43.5	25.6	65.3	60.6	64.5	57.3	70.5

When comparing the ICP-MS/MS measurement to gamma spectrometric measurement of the digest solutions a linear correlation can be seen suggesting that it is possible to compare direct digested samples by ICP-MS/MS and gamma spectrometry for ^{241}Am (Figure 42). However, the low sensitivity must be considered for determining if the samples fall below the out-of-scope limits for ^{241}Am characterisation, as well as the potential presence of ^{241}Pu in the samples and its contribution onto the overall signal at m/z = 241. When analysing real samples, it is important to consider the heterogeneity of the samples and the need to have a complete sample digest, such as $LiBO_2$ fusion and digest, rather than an acid leach to ensure a more representative sample solution to analyse

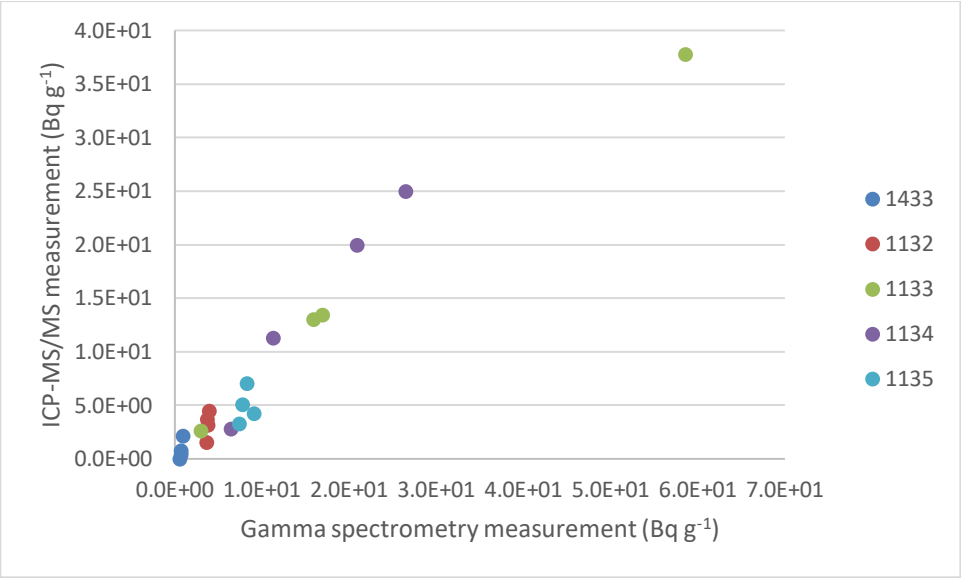

Figure 41: Activity of ^{241}Am measured by Gamma spectrometry compared against ICP-MS/MS for all concrete digests and fusions

The measurement variations between each of the different concrete digest techniques becomes more difficult to determine if the variations are due to the acid digests themselves or if there is a non-homogeneous nature to the samples themselves due to them being true active samples from nuclear facilities. However, from the analysis it is clear to see that analysis of actinides in unseparated matrix digests is possible and can be used for fingerprint characterisation of decommissioning samples below the out-of-scope limits for each of the actinide radionuclides monitored. Utilising the ICP-MS/MS for multiple radionuclide analysis has reduced the time and cost associated with separating the uranium, plutonium and americium isotopes from each other while still able to measure each of the radionuclides to a suitable detection limit for determining the presence of the isotopes themselves.

Analysis of the variable acid digests has shown that across the range of isotopes measured there was minimal discrepancy in the isolation of particular isotopes with reduced backgrounds, suggesting that to ensure complete sample digestion specifically for the actinides utilising $LiBO_2$ is recommended. Samples produced in this way can then be diluted by a factor of 10 and measured without any implications on memory effects.

3.5 Conclusion

Stable concrete digests suggested that the isotopes of ^{234}U, ^{235}U, ^{236}U, ^{238}U, ^{239}Pu, ^{240}Pu and ^{241}Am could be measured well below their out of scope limits as demonstrated by the low background signal measured in the samples. The analysis of variable digest procedures utilising variable acid digests showed that in most cases acid attack in the form of concentrated HNO_3, HCl or a combination of (aqua regia) was not sufficient in liberating the majority of the target analytes from the concrete matrixes investigated. This was thought to be due to insoluble complexes forming specifically in the case of Pu species, which required more extensive chemical attack in the form of a $LiBO_2$ fusion followed by HNO_3 (8M) digest. This greatly improved the recovery of the target analyte. Analysis of each of the acid digests on internal standards of In and Re demonstrated the lack of signal variation when utilising acid digests. However, $LiBO_2$ fused and digested samples introduced a greater level of total dissolved solid in solution and therefore required dilution by a factor of 10 to allow for direct measurement on the ICP-MS/MS without causing any signal suppression on the internal standards or memory effects between samples. The use of He MS/MS mode was shown to have no inherent benefit for actinide analysis, but rather caused an increase in measurement uncertainty due to causing signal suppression. Therefore, no gas, MS/MS mode is the suggested mode of analysis for this particular set of samples allowing for maximum signal sensitivity on low concentration and activity samples for actinide characterisation, while able to measure each of the actinides below the out-of-scope limits proposed by EPR 2018.

Chapter 4 Development of an optimised method for measurement of Iodine-129 in decommissioning wastes using ICP-MS/MS

4.1 Abstract

Iodine-129 is a long-lived radionuclide formed most commonly from anthropogenic activity via nuclear fission, with the majority originating from reprocessing facilities and decommissioning of nuclear sites. The long half-life is theoretically suited to measurement using inductively coupled plasma mass spectrometry (ICP-MS), which offers a rapid alternative to decay counting and AMS techniques. However, previous measurement has been limited by the multiple interferences on m/z = 129. Recent availability of tandem ICP-MS/MS has demonstrated a means to overcoming these interferences using a combination of a collision-reaction cell and tandem mass spectrometer setup. This study builds on previous work with additional improvements in sensitivity (~60% increase) through matrix modification prior to sample introduction and demonstrates the importance of selecting an appropriate internal standard. The method was tested on various decommissioning wastes including silo liquors and slurries, ion exchange resins and graphite, with good agreement between ICP-MS/MS and liquid scintillation counting was observed. A detection limit of 1.05×10^{-4} Bq g^{-1} (0.016 ng g^{-1}) was achieved for ^{129}I, which is two orders of magnitude below the out-of-scope limit of 0.01 Bq g^{-1} (1.53 ng g^{-1}). The results put ICP-MS/MS in a position where routine out-of-scope measurement of ^{129}I is now a possibility, which is beneficial for rapid assessment of materials at decommissioning nuclear sites, and for long term waste storage and disposal with potential development into environmental monitoring.

4.2 Introduction

The decommissioning of nuclear reactor and reprocessing facilities represents a major challenge to the global nuclear industry. Estimated costs are £124 billion over the next 120 years in the UK alone (gov.uk). There are currently 19 nuclear licensed sites, with 11 historic sites undergoing shut down, defueling or decommissioning (IAEA 2018). Nuclear facility decommissioning and waste repository risk assessment is underpinned by reliable waste characterisation requiring the development of robust, reproducible and efficient radioanalytical procedures for accurate measurement of a range of long-lived radionuclides in varied and complex sample matrices.

One such radionuclide is ^{129}I (half-life 1.57×10^{7} years), which is produced by thermal neutron induced fission of ^{235}U (0.706 % yield), spontaneous fission of ^{238}U, and neutron activation of Te isotopes (Hou et al., 2009). Iodine-129 is also produced naturally by cosmic-ray spallation of Xe isotopes in the atmosphere. Iodine-129 decays to ^{129}Xe via β-decay with a beta E_{max} of 154.4 keV and associated gamma emission at 39.58 keV (7.5 % abundance).

The high mobility and volatility of ^{129}I means it can be present in a range of sample matrices relevant to decommissioning. Advanced gas-cooled reactors (AGRs) transport iodine in the gaseous phase, following the release of elemental iodine from CsI particles formed within nuclear fuel (Devell and Johansson 1994, Hou et al., 2009, Hocking et al., 2001, Honda et al., 2015, Honda et al., 2017). The largest accumulation of gaseous ^{129}I is in reactor construction materials and graphite moderators surrounding the reactor as the gaseous iodine migrates away from the cores, and also in activated carbon air filters which filter the cooling gases of any volatile radionuclides. In light water reactors (LWRs) the metal iodides dissolve in water and are carried around the cooling water circuit. The aqueous iodine can further partition into the gas phase as either elemental iodine, or as organic iodide, allowing migration through the cooling circuits, where the dissolved ions are removed using ion-exchange resins (Neeb, 1997, IAEA 1999).

Filters and ion exchangers are used to trap and filter suspended solids within the various reactor cooling circuits. The filter materials used can include high purity cellulose and powdered anion and cation exchange resins, activated charcoal, as well as zeolite materials such as clinoptilolite, which are used for effluent treatment of $^{134/137}Cs$ and ^{90}Sr at nuclear reprocessing sites (Dyer et al., 2018). In the UK, cooling ponds and reprocessing facilities also produce a sludge or slurry and silo liquors from decaying nuclear fuel and cladding rich in Mg-Al alloy from Magnox reactor sites which then formed $Mg(OH)_2$, (Westall and Tawton, 2012, Walling et al., 2015, Radioactive waste management 2018) along with natural growing algae on the surface of the pools and other debris, increasing the range of materials and matrices that the ^{129}I may be trapped in on site (IAEA 1999) and which will ultimately require characterisation prior to disposal.

Accurate characterisation of the waste materials is required to demonstrate that activity concentrations are below the out-of-scope limit, which for ^{129}I is 0.01 Bq g^{-1} (1.53 ng g^{-1}) (EPR 2018), or to correctly assign the waste to the appropriate radioactive waste stream. Previous work has focused on a range of environmental matrices including soil, plant and milk used for environmental monitoring (Takaku et al., 1995, Moran et al., 2002, Shah et al., 2005, Fritz et al., 2006, Reid et al., 2008, Li et al., 2009, Snyder et al., 2010, Shelor and Dasgupta, 2011, Michel et al., 2012, Shikamori et al., 2012, Suzuki et al., 2012, Ohno et al., 2013, Wu et al., 2013, Zhang et al., 2015, Shetaya et al., 2016, Hasegawa et al., 2017,Yang et al., 2018, Zhang et al., 2018). For decommissioning matrices,

there is a range of potential sample compositions that must be accurately characterised, for which the sample preparation techniques used must be carefully considered. Due to the high volatility of iodine an extraction procedure using a tube furnace to liberate the iodine via thermal desorption from the matrix and trapping within an alkali media was used, as iodine is unstable and can be easily volatilised in acidic and oxidizing conditions (Hou et al., 2009). The tube furnace can also volatilise other radionuclides including ^{3}H, ^{14}C and ^{36}Cl (Croudace et al., 2017) which may interfere with radiometric measurement while carbon rich matrices also produces CO_2 when heated, which is co-trapped in the basic trapping solution required. These co-trapped ions may cause interferences with both radiometric and ICP-MS measurement. Heating of the samples in the tube furnace also results in certain matrix types such as those rich in $Mg(OH)_2$ forming a glassy solid, which reduces the overall extraction efficiency of ^{129}I which may become trapped in the solid.

Radiometric and mass spectrometric interferences have previously been removed using offline separation techniques, including solvent extraction and back extraction (Brown et al., 2007, Gómez-Guzmán et al., 2011, Hansen et al., 2011, Lehto et al., 2012, Miyake et al., 2012, Yang et al., 2017), carbon column trapping and alkali leaching(Fujiwara et al., 2011), and extraction chromatography using CL-resin (Kaizer et al., 2016). Measurement of ^{129}I has most commonly been carried out by radiometric techniques including low energy gamma spectrometry, radiochemical neutron activation analysis (RNAA), and most commonly liquid scintillation counting (LSC). Detection limits on the order of 10 mBq ^{129}I on LSC (Suarez et al., 1996, Hou et al, 2009, Zulauf et al., 2010) are achievable (Table 20), with multi-stage sample preparation generally required prior to measurement (Hou et al., 2009).

Table 19: Comparison of techniques for 129I analysis

Detection Method	Matrix	Sample Preparation	Detection Limit Bq	Detection Limit $^{129}I/^{127}I$ ratio	Reference
X-ray and γ spectrometry	Tissue Urine Plant material Radioactive waste	Direct measurement Separated iodine (AgI)	100-200 mBq 20 mBq	10^{-4}-10^{-5} 10^{-5}-10^{-6}	Schmidt et al., 1998 Izmer et al., 2003 Fritz et al., 2006 Hou et al., 2009
LSC	Soil Plant material Water Effluent Filter	Separated iodine	10 mBq	10^{-5}-10^{-6}	Suarez et al., 1996 Hou et al., 2009 Zulauf et al., 2010
RNAA	Soil Sediment Plant material Tissue Water samples	Separated MgI_2/I_2 absorbed on charcoal	1 µBq	10^{-6}-10^{-10}	Schmidt et al., 1998 Szidat et al., 2000 Muramatu et al., 2004
AMS	Soil Soil leachate Plant material Thyroid tissue Water samples	AgI	10^{-9} Bq	10^{-10}-10^{-13}	Schmidt et al., 1998 Izmer et al., 2003 Muramatsu et al., 2004 Hau et al., 2009 Sahoo et al., 2009 Suzuki et al., 2012
ICP-MS	Water	Direct measurement	10 - 100 µBq mL^{-1}	10^{-5}-10^{-6}	Becker and Dietze, 1997 Izmer at al., 2003 Brown et al., 2007 Nakano et al., 2011
	Soil Sediments Water Plant material Radioactive waste	Thermal desorption of gaseous iodine	2.5 µBq g^{-1}	10^{-7}	Becker and Dietze, 1997 Izmer et al., 2004 Hou et al., 2009
ICP-MS/MS	Water Soil	Direct measurement and Chemically extracted standards	0.1 µBq g^{-1}	10^{-6}-10^{-8}	Ohno et al., 2012 Shikamori et al., 2012 Yang et al., 2018

The long half-life of ^{129}I, and its correspondingly low specific activity, makes it well suited to measurement by mass spectrometry. Accelerator mass spectrometry (AMS) is the most sensitive mass spectrometric technique for ^{129}I, where the detection limits, 10^{-9} Bq, allow for measurement of environmental $^{129}I/^{127}I$ ratios in the 10^{-13}-10^{-10} range (Schmidt et al., 1998, Izmer et al., 2003,

Muramatsu et al., 2004, Hau et al., 2009, Sahoo et al., 2009, Miyake et al., 2012, Suzuki et al., 2012,). However, access to AMS instrumentation is limited and currently cannot be considered a routine analytical technique for high throughput waste characterisation (Hou et al., 2009).

Although ICP-MS cannot match the sensitivity of AMS, it is a readily available and flexible analytical technique that has been applied to measurement of a range of radionuclides in decommissioning wastes (Croudace et al., 2017), including ^{129}I (Beals and Hayes, 1995, Kerl et al., 1996, Becker and Dietze, 1997, Lariviere, 2006, Brown et al., 2007, Fehn et al., 2007, Hou et al. 2008, Oliveira et al., 2010). However, accurate measurement of ^{129}I by ICP-MS has been complicated by isobaric interferences from ^{129}Xe (26.4 % abundance) (Beal and Hayes, 1995, Kerl at al., 1996, Becker and Dietze, 1997) present as an impurity in the argon plasma gas, multiple plasma and cell derived polyatomic interferences including $^{127}I^{1}H_2$, $^{97}Mo^{16}O_2$, $^{113}Cd^{16}O$, $^{115}In^{14}N$ and $^{89}Y^{40}Ar$ (Bienvenu et al., 2004, Ohno et al., 2013), and tailing from high concentrations of stable ^{127}I (100% abundance) which cannot be chemically separated and is often present at significantly higher concentrations than ^{129}I. For nuclear decommissioning samples the expected $^{129}I/^{127}I$ ratio is in the order of 10^{-6}-10^{-3} (Hou et al., 2009), compared with ratios as low as 10^{-13} for pre-nuclear environmental samples. The requirement to measure ^{129}I in the presence of significantly higher ^{127}I concentrations has limited analysis by traditional ICP-MS instrumentation, which struggle to resolve $^{127}I^{+}$ tailing and polyatomic $^{127}I^{1}H_2^{+}$(Izmer et al., 2003, Sahoo et al., 2009, Ohno et al., 2013), as well as instrument and matrix based interferences including $^{129}Xe^{+}$ and MoO_2^{+} respectively. Previously methods have resorted to background subtracting to account for isobaric $^{129}Xe^{+}$ interference, as well as offline chemical separation and online reaction/ collision cell separation at high gas flow rates. However, high gas flow rates result in greater signal sensitivity suppression, while single quadrupole instruments also having limited control of the reaction chemistry and the formation of matrix based polyatomic interferences such as Mo, which are allowed through to the cell forming MoO_2^{+}.

Instrumental advances have led to the development of the tandem ICP-MS/MS (Figure 43), which has shown improved interference removal compared to alternative instrument configurations for a number of radionuclides, including ^{90}Sr (Russell et al., 2017), $^{135}Cs/^{137}Cs$ (Zheng et al., 2014) and ^{129}I (Shikamori et al., 2012, Ohno et al., 2013), with a publication of all radionuclides measured and potentially measurable by ICP-MS/MS produced elsewhere for decommissioning (Warwick et al., 2019) and post-accident assessment (Bu et al., 2018).

The ICP-MS/MS configuration consists of two quadrupole mass filters separated by a collision/ reaction cell (Figure 43). The quadrupole prior to the cell entrance improves abundance sensitivity compared to single quadrupole designs from ~10^{-7} to <10^{-10} (Shikamori et al., 2012, Ohno et al., 2013), which is beneficial for ^{127}I tailing removal and low-level sample analysis. The first quadrupole

also filters the ion beam prior to the cell entrance, giving a greater control and selectivity of reaction / collision cell chemistry, and minimising the formation of cell-based polyatomic interferences (Shikamori et al., 2012, Ohno et al., 2013, Yang et al., 2018). Isobaric and polyatomic interferences formed in the plasma can be removed using the collision-reaction cell through the use of variable collision (e.g. H_2 and He) and/or reactive (e.g. O_2 and NH_3) gases (Shikamori et al., 2012, Ohno et al., 2013, Yang et al., 2018). Additionally, the use of a negative voltage gap (termed energy discrimination) between the cell and the quadrupole allows for the suppression of $^{129}Xe^+$ by O_2 gas without significant impact on the iodine signal, confirmed through the use of isotope ratio measurements of $^{129}I/^{127}I$ using certified reference materials (CRMs) (Shikamori et al., 2012, Ohno et al., 2013) and Fukushima soil analysis (Ohno et al., 2013). These developments have put ICP-MS/MS in a position to support or even replace much of the offline chemical separation procedures, increasing the sample throughput and potentially allowing direct analysis of samples.

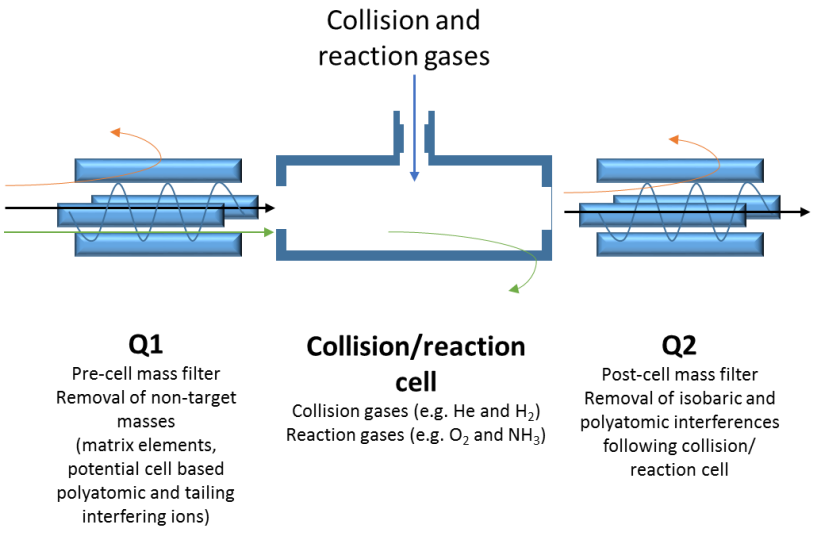

Figure 42: ICP-MS/MS layout and potential benefits of the tandem mass spectrometry configuration

Measurement sensitivity for ^{129}I is low compared to the average sensitivity of ~10^5 cps μg^{-1} (Warwick et al., 2019), due to a high first ionisation energy of 10.45 eV, (Izmer et al., 2003, Todorov and Gray, 2016, Jerše et al., 2018). Improvements in sensitivity have previously been investigated for a range of hard-to-ionise elements, including B, Be, P, S, Zn, As, Se, Pd, Cd, Sb, I, Te, Os, Ir, Pt, Au and Hg, using various carbon modifiers (Grindlay et al., 2013). The carbon rich modifier allows a charge transfer reaction to occur from argon to carbon species in the sample, with further charge transfers to the hard-to-ionise elements, increasing the signal sensitivity (Grindlay et al., 2013). Initially, the carbon species (first ionisation energy 11.26 eV) are ionized in the plasma, followed by a charge transfer to the analyte, in this case iodine. This increases the ionization efficiency of the iodine and improves the signal sensitivity.

Analysis by ICP-MS requires an internal standard to accurately correct for non-spectral interferences associated with changes in the plasma over the course of a run (Vanhaecke et al., 1992). For iodine, this is not straight forward as the internal standard has to have a similar mass and first ionization energy, not be present in the matrix being analysed, and also be interference free in the presence of reaction gases and matrix ions. Additionally, iodine is introduced in alkaline media because of its volatility, which the internal standard must also be soluble in. Previous studies have used In, Re, Cs and Te (Szidat et al., 2000, Sahoo et al., 2009, Fujiwara et al., 2011, Guzman et al., 2011, Hansen et al., 2011, Lehto et al., 2012, Qiao et al., 2012, Zheng et al., 2012, Hou et al., 2013, Ohno et al., 2013, Ežerinskis et al., 2014, Qiao et al., 2014, Yang et al., 2017), however, there is no consensus as to which one is the most suitable candidate for an optimised method of analysis. Previously used internal standards were each assessed for their suitability for ^{129}I measurement (Table 21). Internal standards with a low first ionisation energy relative to iodine (as is the case of In (5.7 eV) and Cs (3.8 eV)) are unrepresentative of iodine ionisation in the plasma. An internal standard with significantly different isotopic masses (^{185}Re and ^{187}Re) is also not desirable, as these could impact the ion transfer by displacing the lighter iodine ions within the ion beam, causing defocusing of the extracted beam because of space charge effects, reducing the analyte sensitivity (Olesik and Jiao 2017). Tellurium has isotopes at masses 128 and 130 (31.74 % and 34.08 % isotopic abundance, respectively) and a first ionisation energy similar to iodine (9.01 eV compared to 10.45 eV), whilst being soluble in alkaline media, and was therefore considered to be a good candidate. Previous single quadrupole instrument studies highlighted the potential of Te tailing in m/z = 129 due to the poor abundance sensitivity, as well as $^{128}Te^{1}H^{+}$ formation (Ežerinskis et al., 2014). Tellurium isotopes may also be affected by isobaric interferences from $^{130}Ba^{+}$ (0.11 % abundance), which could be present in the samples, and $^{130}Xe^{+}$ (4.07 % abundance) which is present as an impurity in the plasma gas. However, the instrumental configuration of the ICP-MS/MS offers a means to overcome the issues identified in previous studies.

Table 20: Properties of internal standards considered for ^{129}I

Element	Isotope	First ionisation energy (eV)	Potential interferences
Iodine	127, 129	10.4	
Indium	113, 115	5.7	$^{115}In^{14}N^{+}$
			$^{113}Cd^{+}$ (12.22)
			$^{115}Sn^{+}$ (0.34%)
Rhenium	185, 187	7.8	$^{187}Os^{+}$ (1.96%)
Caesium	133	3.8	
Tellurium	128, 130	9.0	$^{128}Te^{1}H^{+}$
			$^{130}Ba^{+}$ (0.11%)
			$^{130}Xe^{+}$ (4.07 %)

This paper presents a systematic study to assess the capability of ICP-MS/MS for routine ^{129}I measurements for nuclear decommissioning waste assay, utilising the instruments capability for interference removal. A range of instrumental parameters were investigated for isobaric, polyatomic and tailing removal. Additionally, the use of matrix modification through the introduction of carbon-rich species was investigated for the first time for ^{129}I analysis as a method to improve ^{129}I measurement sensitivity. The study also evaluates internal standard suitability for ^{129}I analysis, given the range of internal standards used in previous studies. The results from these investigations were used to develop an optimised ICPMS/MS method for ^{129}I measurement which was applied to a range of nuclear waste matrices with results compared against radiometric counting using LSC.

4.3 Methodology

4.3.1 Reagents and Materials

Tetra methyl ammonium hydroxide pentahydrate (TMAH, ≥97 %), glycerine (≥99.5 %), NaI (≥99 %), NH_4I (≥99%), single element standard solutions (10 mg g^{-1}) of Te, In, Mo, Cd, Cs, Ce, Co, Li, Tl and a single element standard solution (1 mg g^{-1}) of Y were sourced from Sigma Aldrich, UK. Methanol (99.99 %) was obtained from Fisher Scientific, UK. Iodine-129 standard solution (as NaI) (ISZ44) was obtained from Isotrak Amersham Laboratories, UK. Dilutions were prepared using deionised water (>18.2 MΩ·cm), produced from a Q-Pod Millipore System (Merck, York, UK).

4.3.2 Instrumentation

The samples were put through a Pyrolizer tube furnace where they were combusted in a silica work tube using air/O_2 combustion / carrier gas to 900°C. The combustion products were passed over a crushed quartz and heated to 800°C. The ^{129}I was trapped in a 3 % TMAH bubbler. The ^{129}I collected in the bubblers was then measured using a Quantulus ultra-low level liquid scintillation counter as well as an ICP-MS/MS (Warwick et al., 2019)

All ICP-MS measurements were performed using an Agilent 8800 ICP-MS/MS. The instrument is equipped with a collision-reaction cell (termed an Octopole Reaction System, ORS^3) positioned between two quadrupole mass filters (termed Q1 and Q2). The instrument was fitted with a Scott double pass spray chamber, Micromist nebuliser, quartz torch and nickel sample and skimmer cones. The instrument was fitted with four cell gas lines (Table 22) - dedicated H_2 and He lines in line 1 and 2, NH_3 in line 3 (for corrosive gases) and O_2 in line 4 (for non-corrosive gases). The corrosive gas must be balanced with at least 90% He to protect the ORS^3, and when operating cell line 3, the He line is automatically run at a flow rate of 1 mL/min (Table 22). High purity H_2, He, NH_3, O_2 and Ar were supplied by BOC (UK), with a purity of 99.9999% (N6.0).

Table 21: Agilent 8800 gas modes and flow rates investigated

Cell line	Gas used	Flow rate range (mL/min)
Hydrogen	H_2	0-10
Helium	He	0-12
Line 3 (corrosive)	NH_3 (balanced in 90% He)	0-10
Line 4 (non-corrosive)	O_2	0-1

The instrument was tuned each day in single quadrupole (SQ) mode (only Q2 operating) with no cell gas using a 1 ng g^{-1} stable element standard mixture of Ce, Co, Li, Tl and Y in 0.6 M HNO_3, to ensure criteria for sensitivity, measurement uncertainty, interference formation and peak axes alignment were achieved. Following set-up, the instrument was conditioned with deionised water for approximately 20 minutes to remove HNO_3, before transitioning to 0.5 % TMAH for iodine measurement. All samples were prepared in TMAH (0.5 %) unless otherwise stated to stabilise the iodine in an alkali solution while also ensuring matrix consistency relative to the extraction procedure.

4.4 Experimental

4.4.1 Interference assessment

Abundance sensitivity and hydride formation were monitored under both SQ and MS/MS modes, with no cell gas, by introducing stable ^{127}I (NaI) in TMAH at concentrations ranging from 0.01 ng g^{-1} to 100 µg g^{-1} and monitoring m/z = 125, 126, 128 and 129. A simultaneous analysis of Xe isotopes was carried out monitoring at m/z = 128, 129 and 131 both in blank solutions of TMAH (0.5 %) and those containing varying concentrations of stable ^{127}I.

Polyatomic interference formation was assessed by introducing solutions of TMAH (0.5 %) containing various concentrations (0.001-10 µg g^{-1}) of Mo, In, Cd and Y under both SQ and MS/MS mode operating under no cell gas mode with both Q1 and Q2 set to m/z = 129.

The effect of matrix composition on signal suppression was investigated. The high iodine-127 concentration relative to ^{129}I was assessed for $^{129}I/^{127}I$ ranging from 10^{-2} to 10^{-8}, exceeding the concentrations expected for decommissioning to demonstrate the capabilities of the technique with high plasma loading of the matrix.

Co-extraction of potential polyatomic interference precursors were assessed, under the same combustion conditions used for iodine extraction (Warwick et al., 2019), using a 1 μg g^{-1} solution of Y, Mo, Cd, In, Sn and Ba and trapped in TMAH (3 %) and HNO_3 (0.6 M). Sample measurement was done under MS/MS mode operating under no cell gas mode, operating under each element's most favourable peaks (highest abundance and fewest interference), 89, 95, 111, 115, 118 and 137 respectively.

The carbon content in the form of CO_2 co-trapped through the extraction procedure was investigated on its impact on sample introduction, signal stability and sensitivity on the ICP-MS/MS through the formation of a carbamate in TMAH. A range of CO_2 concentrations ranging from 0.001 g to 1 g were used. A comprehensive assessment of the tube furnace extraction published elsewhere (Warwick et al., 2019).

4.4.2 Sensitivity assessment

An assessment of instrument sensitivity for iodine was undertaken using a 10 ng g^{-1} stable ^{127}I solution prepared in 0.5 % TMAH. Operating the instrument under single quadrupole mode (only Q2 operational at m/z = 127) and MS/MS mode (both Q1 and Q2 operating at m/z = 127) with no cell gases used allows the instrumental configuration to be assessed and demonstrate the abundance sensitivity and tailing removal capabilities. Further assessment was done with collision (H_2 and He) and reaction gases (NH_3 and O_2), using the instrumental auto tune for each gas mode. Each gas flow rate was scanned across the range outlined in Table 22, in 1 mL min^{-1} increments for H_2, He and NH_3, and 0.1 mL min^{-1} increments for O_2 measuring the signal both on m/z = 127 and 129 and on the shifted signals +16 m/z units. Custom tuning was further investigated by starting with the auto-tune parameters and then adjusting each lens, quadrupole and cell parameter to optimize for sensitivity of iodine signal and suppression of background signal on m/z = 129.

4.4.3 Matrix modification

The impact of introducing the sample in a carbon-rich solution on measurement sensitivity was investigated using TMAH, glycerol and methanol as carbon sources. Stable ^{127}I standards from 0.001 ng g^{-1} to 0.025 μg g^{-1} and blank were prepared in TMAH with concentrations ranging from 0.5-3 %, and in methanol and glycerol with concentrations ranging from 0-3 % and a constant 0.5 % of TMAH. The signals at m/z = 127 and m/z = 129 were monitored to assess the impact of varying sample

matrix on the blank background signal on m/z = 129 and stable iodine background and sensitivity on m/z = 127.

4.4.4 Internal standard assessment

Indium, Re, Cs and Te were evaluated as internal standards. The suitability of the internal standard was assessed considering their similarity in mass and ionisation energy to ^{129}I, solubility in basic media, the potential to form polyatomic interferences, and the additional contribution of the element inherent in the sample being measured.

The internal standards were assessed for their ability to match and correct for the changes occurring within the ICP, following high matrix loading of stable ^{127}I, including plasma instability and matrix suppression on signal sensitivity. Varying $^{129}I/^{127}I$ ratios were analysed, ranging from 10^{-3} to 10^{-8}. The target analyte, ^{129}I (1 ng g^{-1} and 10 ng g^{-1}), was measured in the presence of up to 10,000 µg g^{-1} ^{127}I. The capability of the internal standards to correct against this change in plasma ionisation efficiency was evaluated using a custom tuned instrument with a matrix modification of 3 % TMAH solution.

4.4.5 Measurement of decommissioning samples

Representative nuclear waste simulant samples, including graphite moderators, ion exchange resins, silo liquors and $Mg(OH)_2$ based slurries, as well as clinoptilolite used as a filtration material were assessed. A sample containing 1 g simulant was spiked with a known activity of ^{129}I (target activity 23 Bq) and thoroughly mixed until homogenised to be as representative of actual waste samples, where by the iodine would have migrated throughout the materials, before being put through the tube furnace for iodine separation. Iodine was extracted from 1 g of the sample by combustion in a tube-furnace (Raddec Pyrolyser Trio™) at 900°C in a flow of air. The liberated iodine was trapped and measured without dilution. Samples were measured without dilution, and also following dilution by a factor of 10 and 100. Samples were spiked with an internal standard to monitor for plasma variability. The dilutions ranged from 1.21 Bq g^{-1} to 0.01 Bq g^{-1} of ^{129}I, to show the capabilities of the technique and measurement of ^{129}I an order of magnitude below the required out-of-scope limits (0.1 Bq g^{-1}). The instrument was conditioned with TMAH as previously described, and samples were analysed under the optimal instrument conditions (Table 26). Sample

concentrations were calculated by using calibration standards ranging from 1 to 200 ng g^{-1} ^{129}I, prepared from a ^{129}I standard (ISZ44) and measuring the blank acid spiked with internal standard to assess the background signals on m/z = 129 and 130. The ICP-MS/MS values were compared against LSC measurements, with the tube-furnace extraction recovery calculated using LSC.

4.4.6 Comparison to previous methods

An assessment of the performance of previously published ICP-MS/MS methods was performed based on the work of Shikamori et al., 2012 and Ohno et al., 2013. The instrumental parameters used in these studies were assessed using ^{127}I calibration standards and assessing signal sensitivity at m/z = 127, measured background at m/z = 129 and signal stability with further custom tuning carried out using a 0.01 µg g^{-1} ^{127}I standard in 0.5 % TMAH. An assessment of signal-to-noise ratio was performed for the previous published methods and the optimised technique developed in this study.

4.5 Results and Discussions

4.5.1 Interference removal

Iodine-127 tailing was initially assessed, as this cannot be removed by offline chemical separation, and is reliant on the abundance sensitivity of the instrument. Tailing into m/z = -1 and -2 for SQ mode was 3×10^{-7} and $<7\times10^{-9}$ relative to the signal on m/z = 127, respectively, and for MS/MS mode was $<1\times10^{-8}$ and $<1\times10^{-8}$, respectively. Operating under MS/MS mode reduced the tailing into m/z = 125 and 126 to background (<10 CPS). A signal increase into m/z = +1 of ~$6x10^{-5}$ relative to the signal on m/z = 127 was observed for both SQ and MS/MS mode associated with $^{127}I^{1}H^{+}$ formation. The 129/127 ratio as a result of $^{127}I^{1}H_2^{+}$ formation was reduced from 1×10^{-6} in SQ mode to 6×10^{-8} in MS/MS mode (Figure 44).

An improved ^{127}I concentration tolerance in MS/MS mode, 10^{2} µg g^{-1}, over SQ mode, lends itself to low level ^{129}I analysis in the presence of higher ^{127}I, covering the range of expected concentration ratios for decommissioning samples. The use of collision and/ or reaction gases are required to removed further interferences on m/z = 129 associated with the isobaric $^{129}Xe^{+}$, equivalent to ~0.1 µg g^{-1} or ~1×10^{-3} Bq g^{-1}, as well as potential cell derived polyatomic interferences.

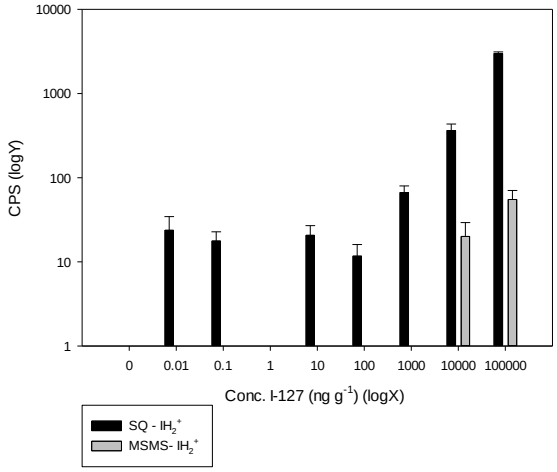

Figure 43: Signal on m/z = 129 with increasing concentrations of ^{127}I under SQ and MS/MS modes

Operating under no gas MS/MS achieved a sensitivity of ~20,000 CPS for ^{127}I (1 ng g^{-1}), with a background at m/z=129 of ~2,000 ± 1300 CPS from isobaric ^{129}Xe. This interference cannot be chemically removed offline as it is introduced as a plasma gas impurity. The use of He (8 mL min^{-1}) removed the ^{129}Xe background but also reduced the ^{127}I signal to 300 CPS, whilst H_2 was relatively ineffective, with a maximum background signal suppression of ~50 % at 8 mL min^{-1}, with a sensitivity of ~600 CPS on mass. Ammonia removed the ^{129}Xe background at a flow rate of 3 mL min^{-1}, however, the iodine signal was reduced to <3 CPS, and no significant cell products were formed, suggesting NH_3 is not effective as a reaction gas.

In agreement with previous studies, the use of O_2 effectively reduced the ^{129}Xe contribution to the signal at m/z = 129 (Shikamori et al., 2012, Ohno et al., 2013, Yang et al., 2017). The ^{127}I signal increased with increasing O_2 up to a flow rate of 0.4 mL min^{-1}, with a sensitivity of ~15,500 CPS for 1 ng g^{-1} ^{127}I. The signal increase is a result of collisional focusing, which reduces the translational energy and concentrates the ion beam to the centre of the quadrupole. Above 0.4 mL min^{-1}, collisional energy damping results in a reduced signal sensitivity (Tanner et al., 2002). Increasing the flow rate to 0.5 mL min^{-1} slightly reduced the iodine sensitivity to ~14,000 CPS per ng g^{-1}, but improved the background reduction on m/z = 129 to >97 %, compared to >95 % at 0.4 mL min^{-1} (Figure 45), resulting in an improved signal-to-noise ratio. There was limited formation and loss of sensitivity as a result of $^{127}I^{16}O^+$ formation (<9 % of the total iodine signal), at 0.5 mL min^{-1} O_2, due to unfavourable thermodynamics (ΔH_r = +2.08). At the maximum O_2 flow rate (1 mL min^{-1}) the analyte signal was suppressed by >65 % to ~4,000 CPS per ng g^{-1}, and the background removal at m/z = 129 was >99 % (~15 CPS), resulting in an overall reduction of figure of merit (Figure 45). To further minimise the contribution of the background, a baseline-subtraction was applied, which

monitors m/z = 129 before and after a sample, and then subtracts the average blank signal intensity. The background signal at m/z = 129 was 40±5 CPS (~0.003 ng g^{-1}, ~$2x10^{-5}$ Bq g^{-1})at a flow rate of 0.5 mL min^{-1} O_2, allowing for significant removal of ^{129}Xe to be accounted for by combining with the baseline-subtraction without the need for high gas flow rates and analyte suppression or oxide formation.

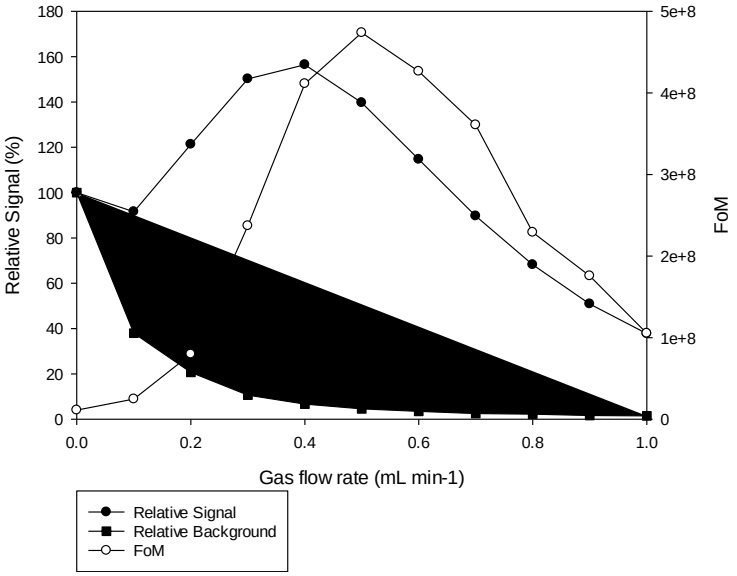

Figure 44: Change in background signal and iodine sensitivity at varying oxygen flow rates relative to MS/MS no gas mode, and figure of merit (FoM) to determine optimal gas flow rate

Polyatomic interference formation was initially assessed by introducing solutions containing up to 100 µg mL^{-1} of Y, In, Cd and Mo under both SQ and MS/MS modes with no cell gas. An initial assessment of sensitivity on mass of interferences was assessed at m/z = 89, 95, 111, 115, respectively, under both SQ and MS/MS no gas mode. In both modes, there was no increase in background at m/z=129 for any of the elements tested. Under SQ O_2 (0.5 mL min^{-1}) there was also no increase in background for both In and Y. However, both Cd and Mo showed a contribution on m/z = 129 with a relative signal ratio (129/expected signal on mass) of 10^{-4}, associated with $^{113}Cd^{16}O^+$ and $^{97}Mo^{16}O_2^+$, respectively. Operating the instrument under MS/MS O_2 (0.5 mL min^{-1}) the signal associated with $^{113}Cd^{16}O^+$ was reduced to $<1.0\times10^{-9}$, suggesting that there is limited $^{113}Cd^{16}O^+$ formation in the plasma, and the removal of $^{113}Cd^+$ by the first quadrupole prevents the formation of $^{113}Cd^{16}O^+$ in the reaction cell. The formation of $^{97}Mo^{16}O_2^+$ was reduced by 10^2 in MS/MS compared to SQ mode, suggesting formation of MoO_2^+ in the plasma (which would then pass through Q1 at m/z = 129) as well as in the reaction cell. In SQ mode, Mo^+ and MoO^+ in the plasma pass through Q1 and react with O_2 in the cell to form MoO_2^+. Further assessment of Mo standards ranging from 0.001 µg g^{-1} to 100 µg g^{-1} showed concentrations of 0.5 µg mL^{-1} and above will interfere with the signal at m/z = 129 under MS/MS O_2 mode, whilst an increase in signal was observed at 0.001 µg g^{-}

[1] in SQ O_2 mode (Figure 46). The use of MS/MS mode therefore increased the Mo tolerance, which may prevent or restrict the extent of offline separation required prior to measurement.

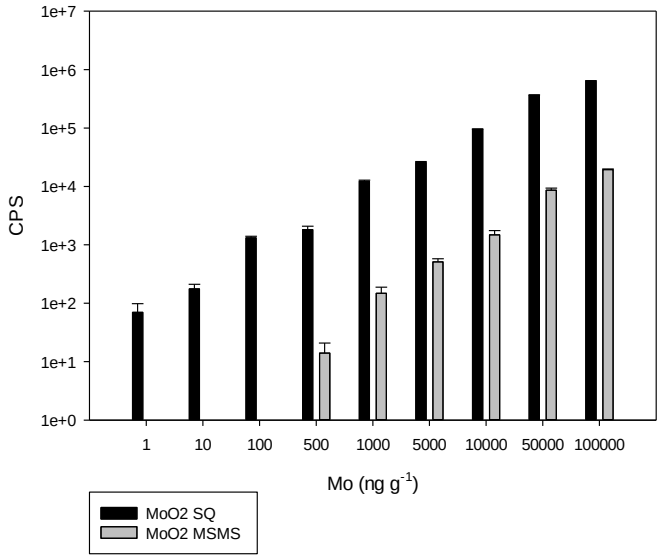

Figure 45: Impact of MS/MS mode on MoO_2^+ formation compared against SQ mode

To assess interference removal using the tube furnace extraction technique, a mixed solution containing Mo, Cd, In, Y, Sn and Ba (0.5 µg of each) was run, with a TMAH trapping solution and a HNO_3 trapping solution in sequence, allowing for samples to be trapped either in a basic or acid media depending on their specific stability and solubility in either. Of the elements tested the recovery of Y, Cd and In was <1 % in the TMAH fraction. The secondary trap of HNO_3 was also able to trap ~1 % of the analytes, suggesting that in total <2 % of the total sample was recovered. The most significant interfering ion, Mo, was found to trap 1.35 % of the 1 µg g^{-1} of sample volatilised in TMAH and <1 % in the HNO_3 fraction (Table 23). The extraction technique reduced the concentration of potential polyatomic interferences. An assessment of Sn and Ba was performed as both contain isotopes which would act as potential isobaric interferences for In and Te internal standards being considered in this study, respectively. It was found that Ba was not co-extracted with the iodine (Table 23) with the TMAH fraction containing <0.01 %, compared to <2% in the HNO_3 secondary trap. This low volatilisation meant that the technique would be able to tolerate a high Ba concentration with no significant impact on the final separated solution, allowing for an interference free Te signal to be monitored at m/z = 130. However, the Sn was found to partially volatilise with ~21 % trapped in the TMAH fraction, which must be considered if ^{115}In is used as an internal standard.

Table 22: Recoveries of 1 µg g-1 solutions of 129I interferences in TMAH (3 %) and HNO3 (0.6 M) following tube furnace extraction

Element	Volatilisation through the tube furnace %	
	TMAH (3 %)	HNO_3 (0.6 M)
^{89}Y	0.0015	1.04
^{95}Mo	1.35	0.82
^{111}Cd	0.00076	0.01
^{115}In	0.22	0.02
^{118}Sn	21.06	0.73
^{137}Ba	0.0096	1.69

Due to the thermal desorption separation technique used on solid samples in this study, carbon rich samples are volatilised as CO_2 and co-trapped in TMAH. An assessment was done over a range of CO_2 concentrations (0.001 g to 1 g) with a fixed activity of ^{129}I (~1.2 Bq g^{-1}) to determine if the increased CO_2 in solution would reduce the performance of the plasma and affect stability due to an increased matrix loading. It was found that there was no significant signal suppression across the range of carbon concentrations measured (Table 24). Results were comparable to those measured on the LSC with recoveries ranged from 93-97 %, which was within the standard method uncertainty of the TMAH extraction (~9 %) showing the robustness of the technique and a tolerance to CO_2 levels up to 1 g, with no impact on signal sensitivity or measurement uncertainty on the ICP-MS/MS. The high carbon tolerance offers a potential to investigate samples rich in carbon including graphite moderators, cellulose filters and organic samples.

Table 23: Changes in ^{129}I recovery and measurement with increasing concentrations of CO_2 present using a fixed concentration of ^{129}I (~1.2 Bq g-1) (Warwick et al., 2019)

CO_2 present	**Reference Value Bq g^{-1} ± 2SD)**	**LSC measured Bq g^{-1} ± 2SD**	**MS measured Bq g^{-1} ± 2SD**	**LSC vs ICP measured ratio**
0.001 g	1.18 ± 0.11	1.14 ± 0.13	1.09 ± 0.11	0.97
0.01 g	1.21 ± 0.12	1.14 ± 0.13	1.14 ± 0.11	0.96
0.1 g	1.14 ± 0.11	1.07 ± 0.12	1.10 ± 0.11	0.93
1 g	1.16 ± 0.11	1.06 ± 0.12	1.07 ± 0.10	0.97

4.5.2 Sensitivity assessment

Custom tuning (manual adjustment of instrument settings) potentially allows the sensitivity and/or interference removal efficiency to be optimised. All lenses and Q1 parameters were assessed, with the majority showing no significant change compared to the auto tune values. However, an improvement in sensitivity of ~20 % was achieved by shifting from a negative to a positive lens deflect voltage (-1 to 2.5 V), with further increases in the lens deflect reducing the signal sensitivity and the signal-to-noise ratio.

The cell parameters were the most significant with regards to impact on sensitivity and interference removal. The octopole bias affects the energy of ions in the cell. In MS/MS O_2 mode (0.5 mL min^{-1}) at the auto tune value of -10 V, the instrument background from $^{129}Xe^+$ was ~500 CPS. Increasing the octopole bias to -5 V increased this value to ~600 CPS, with an increase in iodine sensitivity from ~15,000 CPS to ~25,500 CPS for 1 ng g^{-1} ^{127}I, improving the signal-to-noise ratio from 4.78×10^5 to 1.09×10^6, and decreasing the $^{129}Xe/^{127}I$ ratio from 0.031 to 0.015. Xenon reacts $>10^4$ times faster with O_2 then I^+ (Izmer, 2003), allowing for a less negative octopole bias to be used to achieve a near complete charge transfer for Xe^+ with O_2 while also producing an improved signal for I^+. Further increases or decreases of the octopole bias resulted in a decrease in signal sensitivity.

Kinetic energy discrimination (KED) is a means of controlling cell-forming interferences within the collision/reaction cell by attenuating them based on their size, as well as the energy of the cell

products formed (Rousis et al., 2014). This is especially useful for polyatomic interferences, however, due to the difference in ionic radius of ^{129}Xe (216 pm) and ^{129}I (198 pm) ions and therefore the collisional cross section being greater for ^{129}Xe, it is possible to improve Xe separation further (Yamada et al., 2015). A KED of -7 V gave the best signal-to-noise ratio and the highest overall analyte sensitivity. As the KED tended towards zero the overall signal sensitivity dropped by >85 %, with negative values required to account for the energy loss of ions within the cell when operating with reaction gases. However, further decreasing the KED below -7 V also resulted in a decrease in signal sensitivity.

4.5.3 Matrix Modification

An improvement in iodine sensitivity of ~60 % was observed by increasing TMAH concentrations from 0.5 % to 3 %, compared to ~80 % for the same increase in methanol and glycerol (Figure 47). However, the TMAH contained trace iodine as an impurity ($<5\times10^{-4}$ µg g^{-1}), which resulted in the increase of >300 % in background at m/z = 127 under no gas, MS/MS mode compared to 0.5 % TMAH. The increase in background at m/z = 127 with methanol and glycerol modification was proportional to the signal improvements associated with increased matrix modification, meaning the signal from any trace iodine present in the original 0.5 % TMAH solution prior to matrix modification would be further enhanced. No significant changes in background at m/z = 129 were observed under all matrix modifications for no gas and MS/MS O_2 modes, meaning the double charge transfer process is not occurring for Xe isotopes. The improved iodine sensitivity with no change in background interference on m/z = 129 further improves the figure of merit in MS/MS O_2 mode (0.5 mL min^{-1}) by an order of magnitude from 10^8 to 10^9.

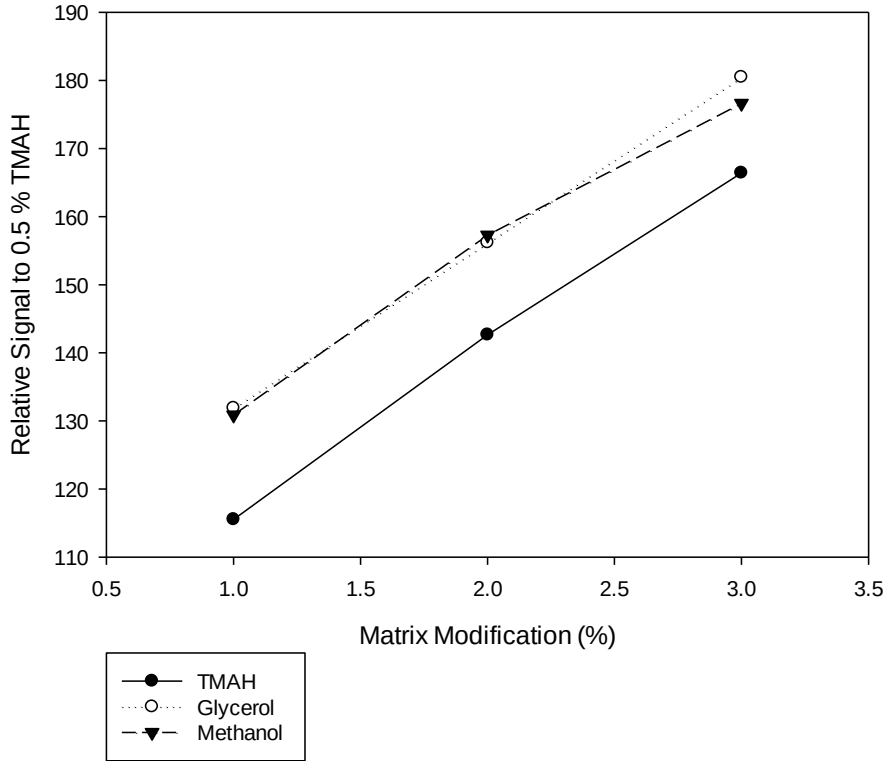

Figure 46: Impact of matrix modification on relative signal sensitivity compared to 0.5% TMAH solution

TMAH can be used as a matrix modifier for analysis of ^{129}I, but the stable ^{127}I contamination would have implications for $^{127}I/^{129}I$ ratio measurements, which could potentially be resolved using a higher purity of TMAH. Methanol matrix modification is favourable for isotopic ratio analysis because of its lack of stable ^{127}I contamination, and the ease of handling for routine analysis relative to more viscous glycerol. In this study, 3 % TMAH was an effective trapping solution for iodine after thermal desorption using a tube furnace, which then can then be directly analysed on the ICP-MS/MS to facilitate a higher sample throughput. A maximum organic content of 3 % is recommended, as further increases lead to an increase in plasma instability, resulting in higher measurement uncertainty.

4.5.4 Internal Standard

Te was assessed for its performance as an internal standard with a similar first ionization energy (9.01 eV) to iodine as well as being within the same mass region. Using the optimised instrument setup, a solution containing 1 ng g^{-1} Te produced a signal of ~200,000 CPS in 3 % TMAH solution at both m/z = 128 and 130, with no increase in background at m/z = 129, suggesting no impact from tailing or hydride formation. However, the $^{127}I^{1}H^{+}$ formation rate of ~4×10^{-5} means concentrations of ^{127}I above 1 µg g^{-1} (within the expected range in real samples) contribute to the signal at m/z = 128, limiting the application of ^{128}Te as an internal standard. For ^{130}Te, the relatively low concentrations of ^{129}I expected (1 - 200 ng g^{-1}, equivalent to 0.0064 - 1.27 Bq g^{-1}) meant that overlapping $^{129}I^{1}H^{+}$ was not significant, with a concentration of ~100 µg g^{-1} of ^{129}I required to produce a 10 % increase of signal on m/z = 130. Isobaric ^{130}Xe was supressed to background levels (<10 CPS) through charge transfer with O_2, however, isobaric ^{130}Ba increased the signal on m/z =130 by ~10% at concentrations of ~10 µg g^{-1} (Figure 48). The presence of Ba must therefore be monitored for an alternative isotope (m/z = 137) when using Te as an internal standard.

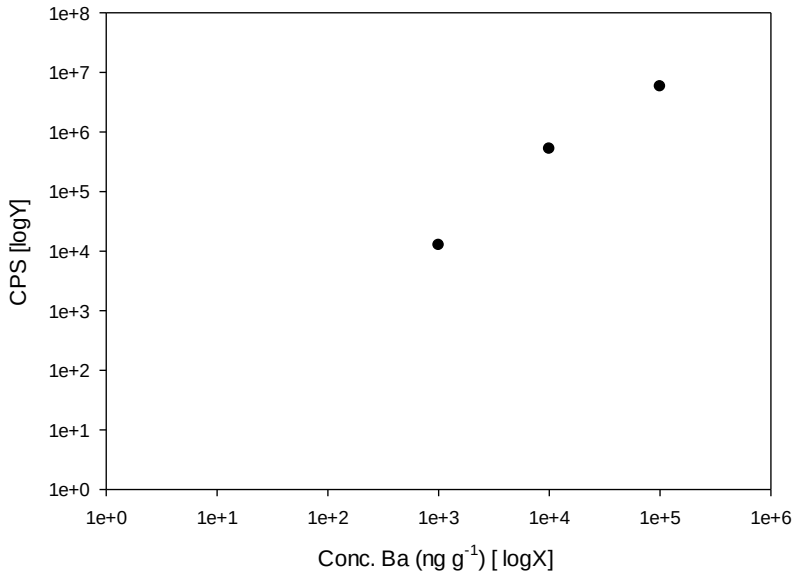

Figure 47: Impact of Ba concentration on signal on m/z = 130.

Indium-115 was assessed for its performance as an internal standard with a significantly lower first ionization energy (5.79 eV) compared to the analyte. No contribution to m/z = 129 from polyatomic $^{115}In^{14}N^{+}$ was detected at concentrations up to 10 µg g^{-1}. However, for real samples, an isobaric interference from $^{115}Sn^{+}$ must be considered given that >20% was volatized through the tube furnace into the TMAH fraction (Table 25), with monitoring of a major isotope of Sn (m/z = 118) when using ^{115}In as an internal standard.

When comparing the total correction factor of both In and Te (5 ng g^{-1}) across a range of matrix loading concentrations the ionisation difference between the iodine and the internal standards

starts to become more evident, with ^{130}Te able to account for 100.2 % of the ^{129}I compared to ~77.0 % using ^{115}In (Figure 49). The difference in ionization efficiency in the plasma at 7000 K between iodine (~10 %) and indium (~98 %) means that changes in plasma energy (e.g. due to high matrix loading) would not be accurately represented using an indium internal standards (Houk 1986). By comparison, the tellurium ionization efficiency is lower than the other candidate internal standards (~40 %) and is more representative of iodine (Table 25). The difference in ionization potential plays a greater role at higher concentrations of matrix loading (as expected in decommissioning samples) as only the lower ionization energy ions are still ionized when the overall plasma energy is reduced through high plasma loading. Therefore a Te (5 ng g^{-1}) internal standard is recommended, monitoring at m/z = 130, as this prevents any interference from the internal standard on the target analyte at m/z = 129 as well as being able to most accurately correct for the changes occurring within the plasma relative to the iodine.

Table 24: Impact of plasma temperature (K) on ionization potential for candidate 129I internal standards (adapted from Jacobs 2015)

Element	**Ionization potential**		
	6500 K	**7000 K**	**7500 K**
Iodine	~3 %	~10 %	~29 %
Indium	~95 %	~98 %	~99 %
Tellurium	~15 %	~40 %	~ 66 %

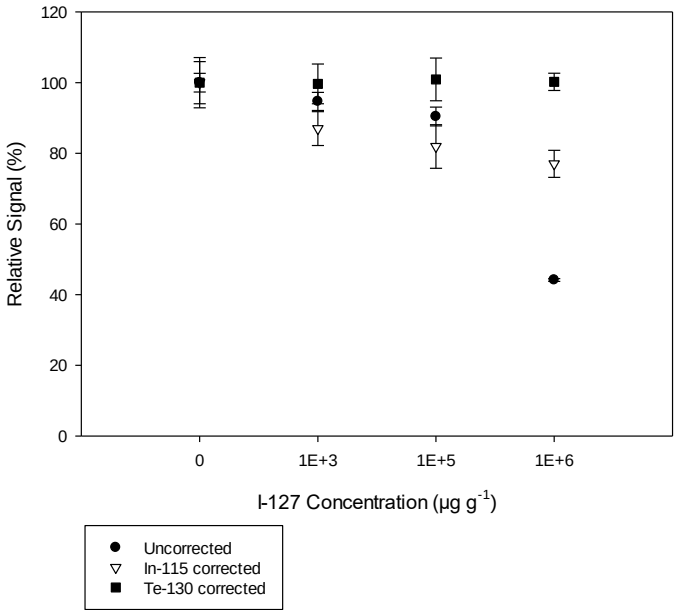

Figure 48: Comparison of internal standard correction on 1 µg g^{-1} ^{129}I with increasing concentrations of ^{127}I

4.5.5 Measurement of decommissioning samples

The optimised instrument setup (Table 26) achieved a ^{129}I instrument detection limit of 1.05×10^{-4} Bq g^{-1} (0.016 ng g^{-1}), when applied to ^{129}I standards prepared in TMAH and analysed under the optimised instrumental parameters and calculated using 3SD, which is comparable to previously published techniques by Shikamori et al. 2012 (1.83×10^{-4} Bq g^{-1}, 0.029 ng g^{-1}) and Ohno et al., 2012 (1.96×10^{-4} Bq g^{-1}, 0.031 ng g^{-1}) (Table 27). The signal-to-noise ratio of ~10^8 is comparable across all three methods, which is 3 orders of magnitude above the SQ no gas and MS/MS no gas method, further supporting the use of O_2 as a reaction gas to remove the isobaric ^{129}Xe interference. However, the improved signal sensitivity provided by operating with matrix modification increases the counts of even low concentration measurements above the background noise providing an improved LOD and LOQ over the other two methods. The use of an internal standard, ^{130}Te, which has similar first ionization energy iodine has also been demonstrated as a robust way to correct for changes within the plasma even at high plasma loading. Of the other techniques Shikamori et al., 2012 used no internal standard and Ohno et al., 2013 used ^{133}Cs which has a lower first ionization energy (3.89 eV) than In (5.79 eV), suggesting that at high plasma loading the effective correction would not be suitable. The sample types analysed across the methods ranged from NIST SRM purified solutions diluted and directly analysed by Shikamori et al., 2012; Fukushima soil samples

which underwent pyrohydrolysis and solvent-extraction by Ohno et al., 2013, as well as a range of decommissioning materials which were put through the tube furnace and directly analysed in this method. Sample handling and preparation of real samples was significantly lower for this method as it is a two-step process with no further purification or separation steps required, allowing for faster sample throughput with strong agreement with radiometric measurements (LSC).

Table 25: Optimised instrumental parameters for ^{129}I analysis

Instrument parameter	**Value**
Sample introduction media	3 % TMAH (^{129}I)
Internal standard	5 ng g^{-1} Te (monitored at ^{130}Te)
Q1/Q2	129/129 (I) and 130/130 (Te)
RF power	1550 W
Scan mode	MS/MS
Plasma mode	Low Matrix
Extraction lens 1,2	0 V, -190 V
Omega lens	8.2 V
Lens Deflect	2.5 V
Octopole Bias	-5.0 V
Energy discrimination	-7.0 V
O_2 gas flow rate	0.5 mL min^{-1}

Table 26: Comparison of ICP-MS/MS methods for ^{129}I measurement

Method of analysis	**Gas (flow rate, mL min^{-1})**	**Sensitivity (1 ng g^{-1}, CPS)**	**Background (CPS)**	**Detection limit (Bq g^{-1})**		**Signal-to-Noise ratio**
				LoD (3*SD)	**LoQ (10*SD)**	**mean$_{cps}^2$/ blank$_{cps}$**
This study (MS/MS)	O_2 (0.5)	75,000	40	1.1×10^{-4}	1.3×10^{-4}	1.5×10^8
Replicated Shikamori (MS/MS)	O_2 (0.7)	18,000	4	1.8×10^{-4}	5.2×10^{-4}	1.6×10^8
Replicated Ohno (MS/MS)	O_2 (0.9)	11,000	2	2.0×10^{-4}	6.5×10^{-4}	1.1×10^8

The use of offline tube furnace extraction of iodine into TMAH (Warwick 2019), followed by direct measurement by ICP-MS/MS reduces sample handing and increases throughput, allowing samples to be processed within ~8 hours. This compares favourably to procedures that use subsequent separation prior to measurement using alternative techniques including X-ray and γ spectrometry, LSC, RNAA and AMS, which can take ~3 days (Yiou et al., 2004, Hou et al., 2009).

The highest uncertainty associated with ICP-MS/MS and LSC was sample preparation, with the determination of furnace recovery (9.1 %), calculated by LSC measurement of a reference solution put through the tube furnace, making up the majority of the 11.2 % overall method uncertainty. The measurement uncertainties for ICP-MS/MS across 3 orders of magnitude of ^{129}I (0.01 - 1.21 Bq g^{-1}, 1.57 - 189.96 ng g^{-1}) were ~1 %, helped by the improvement in instrumental sensitivity using matrix modification.

A range of nuclear waste samples were analysed by both LSC and ICP-MS/MS and results compared against the reference values (Table 28). The proposed method showed good agreement between LSC and ICP-MS/MS, with <7 % variation between reference values and measured values. The $Mg(OH)_2$ sludge samples showed a lower recovery of ~74 %, probably due to the $Mg(OH)_2$ forming a glassy solid upon heating in the tube furnace, resulting in the iodine being trapped within the lattice structure rather than being released completely (Warwick et al., 2019). Samples rich in $Mg(OH)_2$ need an improved extraction procedure to further improve the recovery (Warwick et al., 2019). Excluding the $Mg(OH)_2$ samples improved the agreement between LSC and ICP-MS/MS to <3 %, showing good reproducibility, including for high carbon containing samples (0.5 g) such as the ion exchange resin and graphite as well as for zeolite minerals of clinoptilolite and aqueous standards. The standards and sample dilutions were measured below the Out-of-Scope limit of 0.01 Bq g^{-1} (1.53 ng g^{-1}) (EPR, 2018). Analysis of all the matrix types at 10% of the Out-of-Scope limit (0.001 Bq g^{-1}) was able to achieve measurement variation of <0.8%.

Table 27: Representative matrix sample measurements compared to radiometric analysis (LSC), recovery of extraction, and discrepancy of LSC measurement

Sample Type	Details	Reference Value Bq g^{-1}	LSC measured Bq g^{-1}	MS measured Bq g^{-1}	LSC vs MS variation true recoveries %
Acid-washed sand		1.27 ±0.12	1.25 ± 0.17	1.27 ± 0.045	98.46
Silo liquor	$Mg(OH)_2$ (saturated solution)	1.19 ± 0.12	1.14 ± 0.15	1.25 ± 0.27	92.30
		1.20 ± 0.12	1.15 ± 0.15	1.18 ± 0.032	97.69
Sludge / slurry	$Mg(OH)_2$ (~50%)	1.24 ± 0.12	0.85 ± 0.11	0.86 ± 0.0015	98.96
		1.20 ± 0.12	0.94 ± 0.13	0.93 ± 0.055	101.12
Ion exchange resin		0.67 ± 0.07	0.58 ± 0.08	0.57 ± 0.043	102.13
		0.62 ± 0.06	0.62 ± 0.08	0.61 ± 0.072	102.02
Mineral (zeolite)	Clinoptilolite	1.26 ± 0.12	1.20 ± 0.16	1.23 ± 0.057	97.15
		1.23 ± 0.12	1.14 ± 0.15	1.15 ± 0.033	98.90
Graphite		1.24 ± 0.12	1.21 ± 0.16	1.22 ± 0.12	99.87
		1.25 ± 0.12	1.09 ± 0.15	1.09 ± 0.14	100.23
Aqueous Standard	MAPEP (XAW29) Reference Standard	0.0038	<0.05	0.0012 ± 0.0013	N/A
				0.0012 ± 0.0008	
				0.0022 ± 0.0012	
Aqueous standard			1.15	1.14 ± 0.07	100.48

4.6 Conclusion

An optimised method has been developed for ^{129}I measurement in various nuclear waste assays by ICP-MS/MS. The thermal desorption technique successfully extracted iodine from a range of matrices, whilst also removing potential polyatomic interferences (>98 % Y, In, Cd, Mo and Ba) prior to sample introduction. The ICP-MS/MS design also further reduced interferences present, with the first quadrupole able to filter the potential cell-based polyatomics before they reached the cell, in particular MoO_2^+ with an increased tolerance of $5x10^2$ orders of magnitude in MS/MS mode compared to SQ mode. The use of MS/MS mode was also able to improve the tolerance of ^{127}I up to 10^2 µg g^{-1}, over SQ mode, reducing the impact from tailing and dihydride formation. The use of O_2 (0.5 mL min^{-1}) as a reaction gas is able to remove the isobaric $^{129}Xe^+$ interference by >97 %. The use of matrix modification in the form of an increased TMAH concentration, allows for an improved signal sensitivity for the hard to ionize iodine analyte, improving the overall signal stability and signal-to-noise ratio, and is also a selective extractant for iodine from the tube furnace procedure. After assessing all previously used internal standards, the use of ^{130}Te has been shown to be most effective in correcting for instrument drift and signal suppression associated with the high matrix loading of ^{127}I in real samples, relative to ^{115}In. This supports the notion that an internal standard should be representative of the analyte in terms of atomic mass, ionization energy and stability within the sample introduction media. Representative samples were run through the complete extraction and analysis procedure with the Iodine trapped in 3 % TMAH following thermal desorption using a tube furnace, spiked with an internal standard of Te and then measured without additional sample preparation. The method achieved an instrument detection limit of 1.05×10^{-4} Bq g^{-1} (0.016 ng g^{-1}) for ^{129}I, which is two orders of magnitude below the out-of-scope limit, providing a means for characterisation of nuclear waste materials with minimal procedural stages prior to measurement. A high throughput technique that is able to cope with a range of decommissioning matrices will contribute to reducing the procedural time and consequently the cost of analysis and decommissioning overall.

Chapter 5 Assessment of isotope ratio measurement capabilities by ICP-MS/MS

5.1 Abstract

Advances in inductively coupled plasma mass spectrometry (ICP-MS) have led to the development of the tandem mass spectrometer (ICP-MS/MS), which offers capabilities in overcoming both isobaric and polyatomic interferences for a range of different matrices. The interferences present have limited isotope ratio measurement by traditional instruments such as the multi-collector ICP-MS require extensive offline chemical separation and purification to be carried out, to reduce but not remove the interference. The ICP-MS/MS offers the capabilities of doing direct digest analysis of samples while still being able to accurately measure isotope ratios. Lead isotope ratios were selected as a representative stable element system which is well understood for the anthropogenic source terms with results compared against MC-ICP-MS data. The technique was able to achieve measurement uncertainties <0.2% for the single quadrupole configuration and <0.6 % for $^{206}Pb/^{204}Pb$ and ~0.25 % for $^{206}Pb/^{207}Pb$ under MS/MS mode, self-aspirated and using NIST SRM 981 Pb standard sample bracketing. The use of MS/MS was shown to increase uncertainty however, for radiometric isotopic systems where interfering ions associated with isobars and neighbouring isotope tailing into the m/z = ±1 and ±2, as well as polyatomic interferences, utilising the MS/MS, mass filtering capabilities of Q1 it is possible to reduce this impact and potentially allow for isotope ratios to be measured with results comparable to those achievable by MC-ICP-MS without the need for extensive sample preparation.

5.2 Introduction

The ICP-MS allows for accurate measurement of individual isotopes by their mass to charge (m/z), allowing for concentration to be determined. However, to determine the source terms of elements, isotope ratio comparison becomes essential. For many radionuclides isotope ratio is calculated between the low concentration or short half-life active isotope

and the stable or high fission yield, long half-life, high concentration isotope, with variations as high as 10^{-13} for $^{129}I/^{127}I$ (Hou et al., 2009, Hou et al., 2010) and as low as 10^{-1} for $^{240}Pu/^{239}Pu$ (Smith et al., 2002). Many radionuclides are measured using radiometric analysis however for certain isotopes this is not possible due to decay energies interfering and masking the signals meaning only total radionuclide activities and concentrations can be determines, as in the case of $^{240}Pu/^{239}Pu$ (Xu et el., 2014). To achieve accurate measurement with potential interferences present, offline chemical separation of matrix ions, online reaction cell separation or high instrumental resolution is necessary. However, unlike stable isotope ratios where isotope ratios tend to follow the relative abundance ratios which are distinct but often prevent major tailing, radionuclide ratios differ greatly dependent on the formation pathway of the radionuclide and what parent radionuclide concentrations are. Measurement of isotope ratio analysis has traditionally been carried out using multi-collector instrumentation or accelerator mass spectrometry (AMS) combined with ICP-MS analysis to accurately measure the ultra-low concentration of radionuclides in high concentration stable isotope matrixes (Kutschera 2005). However, developments in ICP-MS technology for interference removal and improved abundance sensitivity suggest that an improved isotope ratio capability may be possible with the ICP-MS/MS. The ICP-MS/MS has been utilised for multiple radionuclide measurements including ^{90}Sr (Russell et al., 2017), ^{93}Zr (Petrov et al., 2018), ^{129}I (Shikamoi et al., 2012, Ohno et al., 2013, Yang et al., 2018), ^{151}Sm (García-Miranda et al., 2017) and ^{226}Ra (van Es et al., 2017) as well as isotope ratio measurements of $^{135}Cs/^{137}Cs$ in environmental samples (Yang et al., 2016), $^{236}U/^{238}U$ in seawater (Bu et al., 2018) and ^{237}Np in the presence of ^{238}U in sediments (Caborn, 2017). Utilising the ICP-MS/MS it is possible to reduce radiometric analysis times and allow for potential emergency response analysis to be carried out as was done for soil samples in the Fukushima region following the release of contaminants by the Fukushima Daiichi nuclear power plant (FDNPP) accident (Ohno et al., 2013, Yang et al., 2017, Matsunaka et al., 2016).

To better understand the capabilities of the ICP-MS/MS for isotope ratio analysis a stable analogue was selected in the form of Pb isotope analysis, as the range in isotopic abundances lends well to demonstrating the relationship between similar yield radionuclides where the ratio is ~1:1 and those where the ratio is greater at ~40:1. Due to the nature of isotopic measurements minor changes in ratio may reflect major changes in

source, mass bias corrections are required to remove the artificial changes that may impact measurement including the range of masses being investigated and the fractionation that may be occurring as well as the variation in signal sensitivity that occur over the course of instrumental analysis. The measurement of Pb isotopes also requires interference removal to account for the potential isobaric interference of ^{204}Hg.

It is well established that the relative abundance of the four stable Pb isotopes, ^{204}Pb (1.4%), ^{206}Pb (24.1%), ^{207}Pb (22.1%) and ^{208}Pb (52.4%) can be used to infer lead pollution source terms from industrial and other anthropogenic processes (e.g. lead ore extraction, lead pipes used for water supplies, lead paint, lead added to gasoline) (Longerich et al., 1987, Sun et al., 2006, O'brien, 2011, Larsen et al., 2012, Martín et al. 2015). The addition of tetraethyl lead to gasoline as an anti-knock agent was introduced in 1923 and was widespread from the 1920s to the 1980s producing a significant environmental impact (Horn et al., 2000, Ellam 2010, Gioia et al., 2017). Regulatory pressures as well as the introduction of catalytic converters, which Pb interfered with, led to reductions and final elimination of leaded gasoline in the USA (1995), Canada (1990) and Europe (2002) driven further by cogent evidence of proven neuro-toxicological effects (Flora et al., 2012, Mason et al., 2014).

Traditionally, high precision Pb isotopic analysis has been carried out using thermal ionisation mass spectrometry (TIMS) and multi-collector (MC-ICP-MS) instruments (Yuan et al., 2016), with stable isotope spiking and double spike having been used to correct for isotopic mass fractionation in which a spiked and un-spiked sample is analysed in tandem with the spiked being used to calculate the mass fractionation at the time of analysis (Taylor et al., 2015). The low abundance of ^{204}Pb isotope limits analysis of samples containing small quantities of Pb, while inherently carrying an interference on m/z=204 from ^{204}Hg. The use of MC-ICP-MS was only able to reduce and not completely remove the isobaric interference presented by ^{204}Hg through rigorous cleaning and offline chemical separation and purification of the Pb fractions as well as utilising a large Pb ion beam (Taylor et al., 2015). The use of TIMS and MC-ICP-MS instrumentation were able to achieve a precision down to ±0.0027 % and ±0.0022 % 2SD respectively for ^{206}Pb/^{204}Pb isotope ratios.

With the most common sample matrix analysed being sediment cores in which Pb profiles can be accurately mapped out with anthropogenic and industrial activities of an area. Any

potential interferences, Table 29, would initially be eliminated through extensive chemical separation.

Table 28: Interference list on m/z values for Pb isotopes

	204	206	207	208
Isobaric	^{204}Hg			
Polyatomic	$^{203}Tl^{1}H$	$^{205}Tl^{1}H$	$^{191}Ir^{16}O$	$^{192}Os^{16}O$
	$^{188}Os^{16}O$	$^{190}Os^{16}O$		$^{192}Pt^{16}O$
		$^{190}Pt^{16}O$		

Previous research has suggested the use of a reaction gas, NH_3, as charge transfer agent for the removal of $^{204}Hg^+$ isobaric interference on $^{204}Pb^+$ (Woods, 2014), Equation 1, focusing on high purity single element standard analysis spiked with increasing concentrations of Hg, to demonstrate a proof of concept for the use of NH_3 as a reaction gas. However, for this work the Hg signal was monitored at m/z = 198, 199, 200, 201 and 202 and no presence above background was found to be potentially impacting the signal at m/z = 204.

Equation 5.1: Charge transfer reaction between Hg^+ and NH_3 gas

$Hg^+ + NH_3 \rightarrow Hg^0 + \text{“}NH_3^+\text{”}$

A set of sediment core samples collected from UK saltmarshes and lakes were chosen to study temporal variations in Pb isotopes with true sample matrix present. The use of UK samples was particularly beneficial for Pb isotope analysis due to the alkyl lead additives originating from Australian and Canadian ores, which have a significantly different isotopic signature than the natural UK lead background (Bollhöfer and Rosman, 2001). This meant that a very distinct change could be observed in the sediment core profiles when assessing the contribution of Pb following the introduction of alkyl lead in the 1920’s followed by the reversion of the isotopic signature to the natural Pb isotopic ratio as alkyl lead additives were phased out from petrol in the 1970’s. Lake Windermere samples were chosen as they

were collected within a national park which experienced the direct effects of anthropogenic activities as it became a popular tourist destination from the late 19th century (Miller et al., 2014). Hythe saltmarsh samples were selected as the waters around Southampton have been used as an industrial port since the Victorian era, with further naval activity occurring during world war two prior to the D-day operations (Cundy & Croudace, 2017). Results were compared against MC-ICP-MS.

5.3 Methodology

5.3.1 Reagents and Materials

Sub-boiled reagents of Primer Plus HNO_3 (68 %) and ARISTAR grade HCl (37 %) were obtained from Fisher Scientific, UK. A solution of HBr (0.5 M) was prepared from concentrated HBr (47 %) obtained from Sigma Aldrich, UK. Dilutions were prepared using deionised water (>18.2 MΩ·cm), produced from a Q-Pod Millipore System (Merck, York, UK). A working solution of NIST® SRM® 981 Pb isotopic standard (10 ng g^{-1}) was prepared from a NIST® SRM® 981 high purity Pb metal wire, dissolved in HNO_3. Dowex AG1-X8 resins produced by Bip-Rad were used for Pb separation. Piston or hand driven cores were collected at both the Lake Windermere basin in 2012 by Miller, Croudace, Bull, Cotterill, Dix and Taylor, Southampton and the Hythe saltmarsh (2016) by Cundy and Croudace, Southampton.

5.3.2 Sample preparation

All sample handling and chemical processing was carried out in HEPA filtered workstations to limit any environmental contamination. Samples were first leached with *aqua regia* for 8 hours then centrifuged. Small aliquots of leachate were evaporated and converted to bromides using sub-boiled HBr before separating the Pb using an HBr-anion exchange

procedure (Taylor et al., 2015). Temporal variations in Pb isotopic composition were determined for sequences of dated sediment cores. The profiles from Southampton, Hythe saltmarshes and Lake Windermere (English Lake District) reveal distinct variations relating to major historical events and known changes in source terms. An age vs depth model was calculated based on ^{210}Pb (t ½ = 22.3 years) to calculate accumulation rate of sediment and a combination of ^{137}Cs, WDXRF and Itrax to link the changes in elemental composition to events occurring within the region and environment, (BOSCORF, National Oceanography Centre, UK, Miller et al., 2015, Croudace et al., 2012, Croudace 2017), and supplied for this assessment, producing age depth profiles such as those for Windermere in Figure 50.

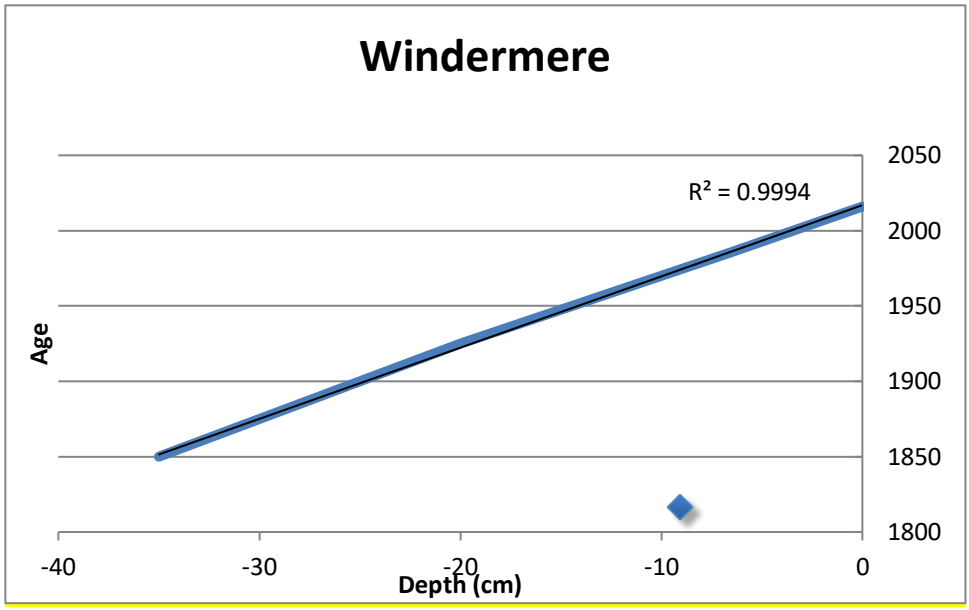

Figure 49: Age / Depth profile for the Lake Windermere sediment core using ^{210}Pb and ^{137}Cs

Core samples of lake sediment were collected from Lake Windermere in 2012 and the saltmarsh at Hythe in 2016. Two depths were sampled at both locations, with a 50 mm overlap to ensure chemical signal continuity. Major and trace element analysis was then undertaken to establish chemical distributions and chronologies.

Samples were then divided into sub-samples for subsequent analysis techniques. Using data from historic cores collected by Croudace and Cundy (University of Southampton) in 2014, an estimate of 5 mm/yr was attained. Samples were divided to gain the highest resolution for the region of highest interest (1940-1950): 10 mm segments from 0 mm – 250 mm depth, 5 mm segments from 250 mm – 400 mm depth and 10 mm from 400 mm to 550 mm depth, to get better resolution for the specific depths of interest. Samples were

freeze dried, milled and turned into pellets before being subject to wavelength dispersive x-ray fluorescence (WDXRF) analysis. A sub sample was analysed using Gamma ray Spectrometry. Finally, Pb isotope analysis was undertaken on an Agilent 8800 ICP-MS/MS. All sample handling and chemical processing was carried out in HEPA filtered workstations to limit any environmental contamination. Sub-boiled reagents were used for all digestions and chemical separations. Separation of lead was carried out using Dowex AG1-X8 anion exchange resins. The sub-samples were each digested in *aqua regia* and converted to bromide salts, before single stage separation via the hydrochloric acid method as described by Farley et al., 2016. Dilutions of the separated Pb solutions were initially diluted 100x and analysed for their total concentrations of Pb before being prepared to approximately 10 ng g^{-1} (in 0.6 M HNO_3) and run on an ICP-MS/MS, Agilent 8800 to obtain Pb isotope fractions (Figure 51).

Unseparated samples were prepared by digesting with *aqua regia* for 8 hours then centrifuged. The supernatant was the removed and diluted to approximately 10 ng g^{-1} (in 0.6 M HNO_3), with the dilution factor based on the results from measurement of a 100× dilution by ICP-MS/MS (Figure 51).

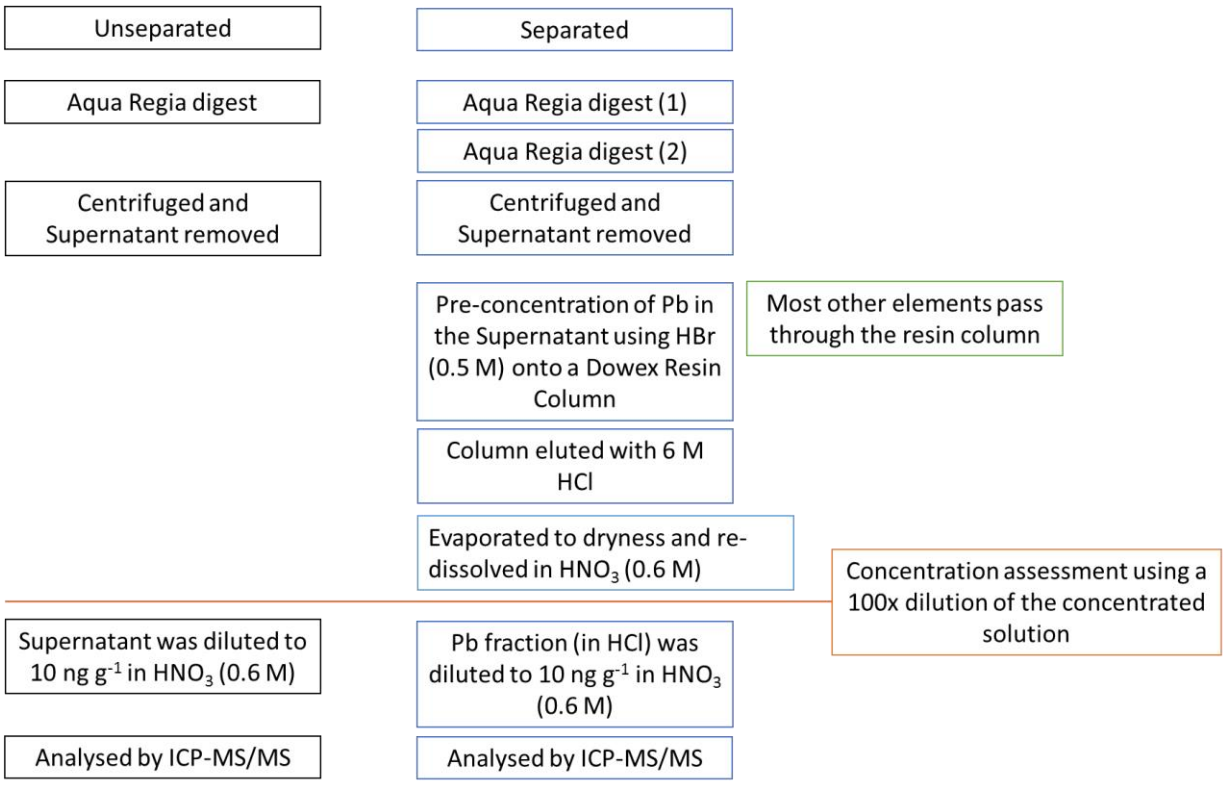

Figure 50: Sample preparation procedure for Unseparated and Separated Pb isotope ratio analysis

5.3.3 Instrumentation

An Itrax micro-XRF core scanner was utilized to produce an elemental profile of the sediment cores collected. This vertically scanned the core using energy dispersive X-ray fluorescence (EDXRF) at an excitation voltage of 30 kV and a measurement increment size of 200 µm over a 15 hours period.

A Philips Magix-PROTM WDXRF Spectrometer PW 2440 was used for analysing the sample pellets. Gamma ray spectrometry was undertaken on selected sub-samples using 30% High Purity Germanium (HPGe) detectors. Each sub-sample was counted for at least 16 hours, differing slightly depending on the activity. The spectra were analysed using FITZPEAKS gamma analysis software.

All ICPMS measurements were performed using an Agilent 8800 ICP-MS/MS. The instrument is equipped with a collision-reaction cell (termed an Octopole Reaction System, ORS^3) positioned between two quadrupole mass filters (termed Q1 and Q2). The instrument was fitted with a Scott double pass spray chamber, Micromist nebuliser, quartz torch and nickel sample and skimmer cones. The instrument was fitted with four cell gas lines (Table 30) - dedicated H_2 and He lines in line 1 and 2, NH_3 in line 3 (for corrosive gases) and O_2 in line 4 (for non-corrosive gases). The corrosive gas must be balanced with at least 90% He to protect the ORS^3, and when operating cell line 3, the He line is automatically run at a flow rate of 1 mL/min (Table 30). High purity H_2, He, NH_3, O_2 and Ar were supplied by BOC (UK), with a purity of 99.9999% (N6.0).

Table 29: Agilent 8800 gas modes and flow rates available

Cell line	Gas used	Flow rate range (mL/min)
Hydrogen	H_2	0-10
Helium	He	0-12
Line 3 (corrosive)	NH_3 (balanced in 90% He)	0-10
Line 4 (non-corrosive)	O_2	0-1

The instrument was tuned each day in single quadrupole (SQ) mode (only Q2 operating) with no cell gas using a 1 ng g^{-1} stable element standard mixture of Ce, Co, Li, Tl and Y in 0.6 M HNO_3, to ensure criteria for sensitivity, measurement uncertainty, interference formation and peak axes alignment were achieved.

ICP-MS/MS data was compared against results collected by Miller et al., 2014 and Cundy and Croudace, 2017. Where by major and trace elements were determined using a Philips PW1400 sequential X-ray fluorescence spectrometer system, and Pb isotopic abundances determined using a Fisons Elemental PQZ inductively coupled plasma mass spectrometer (ICP/MS) following acid leaching and pre-concentration on Dowex AG1-X8 resins (Cundy and Croudace, 2017). High precision lead isotopic abundances were also determined to yield information on geochemical origin. Isotopic data were acquired using a Thermo Scientific NEPTUNE multi collector ICP-MS. Instrumental mass bias was corrected using the SBL74 ^{207}Pb–^{204}Pb double spike developed at the University of Southampton (Miller et al., 2014).

5.4 Experimental

5.4.1 Optimising instrumental parameters

5.4.1.1 Gas modes

An assessment of signal sensitivity with variable gas modes was carried out using a NIST SRM 981 standard (1 ng g^{-1}) with variable gas modes, including no gas SQ and MS/MS, as well as He, H_2 O_2 and NH_3 MS/MS monitoring on mass and mass shifted. Signal were measured on mass at m/z = 208 for all the gas modes, and O_2 and NH_3 MS/MS were mass shifted to m/z = 208 → 224 (PbO^+), m/z = 208 →225 ($PbNH_3^+$) and m/z = 208 → 242 $Pb(NH_3)_2^+$. Mass shifts were analysed to determine if it was possible to improve the signal-to-noise ratio by reducing the overall background signal.

The use of NIST SRM 981 was monitored for mass bias correction, assessing the change in isotope ratio measurement over the course of a day and replicate sample analysis in the gas modes that showed the best signal sensitivity and signal-to-noise ratio.

5.4.1.2 Sample introduction

The impact of the peristaltic pump on isotope ratio analysis was assessed by comparing the uncertainty of the measurements for both pumped and self-aspiration of an isotopic standard (NIST SRM 981) (1 ng g^{-1}) under SQ and MS/MS.

5.4.1.3 Integration time

Integration time or dwell time is the time that the instrument spends acquiring the data at each of the channels which make up a peak on the mass spectrum. This will have an impact on isotope ratio precision due to the influence of various noise on analytical measurement. Adjusting the integration time of specific ions can increase the time allocated for its measurement which increases the sensitivity of detection, which is particularly beneficial for low abundance ions such as ^{204}Pb (1.4 %).

The impact of integration time on measurement uncertainty was assessed based on varying integration times for each isotope. Integration times were increased proportionally to the isotope of 206, which was used as the reference isotope for the isotope ratios, 206/X, where X is the other Pb isotopes (204, 207 and 208), due to ^{206}Pb being the final decay product of ^{238}U and being well established for isotope ratio analysis. Integration times were increased to the instrumental limit of 25 seconds for the lowest abundance isotope, ^{204}Pb, while also setting integration times proportional to isotopic abundance for the remaining Pb isotopes, ^{206}Pb (5 seconds), ^{207}Pb (5.1 seconds) and ^{208}Pb (1 second).

5.4.1.4 Replicates vs Sweeps

Replicates are the number of times a sample is analysed, while the number of sweeps is the number of times the signal pulse passing through the quadrupole passes across the mass spectrum of the selected m/z values, in this case 204, 206, 207 and 208.

Analysis of operational conditions was carried out to assess the effects of increasing the number of replicates (1, 10, 25, 50 and 100) independently of sweeps/replicate (10, 100, 500 and 1000) and vice versa. As well as assessing the impact that the variable point analysis modes, including single-point, 3 point, 6 point and 20 point peak analysis, had on the analysis time of samples. This was to allow for the maximum number of isotopic measurements while achieving the lowest measurement uncertainties.

5.4.1.5 Analysis mode

An assessment was done to determine if adjusted the preferential mass range would have an impact on both signal sensitivity and measurement uncertainty, as the isotope ratio analysis was focused specifically on the high mass range. A NIST SRM 981 standard (1 ng g^{-1}) was analysed under the full range of preferential mass range tunes, 0 – 100% (low to high mass). Signal sensitivity and RSD was monitored and optimised for maximum signal sensitivity and minimal signal variation, RSD.

Mass bias corrections were compared using both an internal standard, Tl (5 ng g^{-1}), and sample bracketing using NIST SRM 981 (10 ng g^{-1}). The RSD was compared for both correction factors to determine which approach would be best suited for isotope ratio analysis.

Real sample analysis was done under self-aspirated, SQ, no gas mode for maximum signal sensitivity due to the potential interferences having been removed through the chemical separation procedure which has been well established (Korkish and Sorio 1975).

All samples were first dip tested at 100x dilutions to allow for final dilutions to be set at ~10 ng g^{-1}. Sample bracketing with NIST SRM 981 (10 ng g^{-1}) was used for isotope ratio analysis.

5.4.2 Measurement of real samples

5.4.2.1 Separated

Samples (0.1 g) were digested in aqua regia (3:1, HCl:HNO_3) (10 mL). Samples were centrifuged and the supernatant was taken. Samples were then converted to bromide salts using HBr (0.5 M) and passed through a Dowex AG1-X8 resin. Only the Pb was retained by the column allowing for a single stage hydrochloric acid elution (6 M) of the column to be used to obtain the separated Pb fraction. The HCl was then evaporated to dryness and re-dissolved in HNO_3 (0.6 M) (5 mL). A 100x dilution of the concentrate was measured on the ICP-MS/MS to determine the concentration of Pb present, followed by further dilution of the separated Pb concentrate to approximately 10 ng g^{-1} (in 0.6 M HNO_3) and analysed on an ICP-MS/MS, Agilent 8800, with sample bracketing using NIST SRM 981 (10 ng g^{-1}) to obtain Pb isotope fractions. Results were compared against MC measured values

Sample bracketing using NIST SRM 981 was utilised to account for the mass bias correction within the instrument.

5.4.2.2 Unseparated

Samples (0.1 g) were digested in aqua regia (3:1 HCl:HNO_3) (10 mL). Samples were centrifuged and the supernatant was taken. A 100x dilution of the supernatant (0.1 mL) was prepared in HNO_3 (0.6 M HNO_3). Samples were dip tested to assess concentration before diluting down to approximately 10 ng g^{-1} in HNO_3 (0.6 M HNO_3). Samples were then analysed with sample bracketing using NIST 981 (10 ng g^{-1}). Results were compared against ICP-MS/MS separated and MC measured values

5.5 Results and Discussions

5.5.1 Optimised instrument parameters

5.5.1.1 Gas modes

Polyatomic interferences require the use of collisional gases such as H_2 and He to break up the interference. Isobaric interferences require a means to either mass shift the target analyte off mass or the interference off mass. This can be achieved through the use of reaction gases such as O_2 and NH_3. Another potential benefit of reaction gases is their ability to cause charge transfer reactions which turn ions into neutral species preventing them from passing through the system and hence, removing them as an interfering ion.

Signal sensitivity favoured No gas, SQ as well as NH_3, MS/MS mode (Figure 52). However, Pb isotopes only have an interference from isobaric ^{204}Hg (204) as well as polyatomic $^{203}Tl^{1}H$ (204) and $^{205}Tl^{1}H$ (206). Using MS/MS would be beneficial if there were interferences within the matrix, however, due to the sample preparation and Pb separation few matrix interferences are expected to be present. Using MS/MS mode reduces signal sensitivity due to the use of two mass filters (Q1 and Q2). The use of NH_3 has been reported for removal of Hg (Glenn Woods, 2014) from the samples however, due to the separation procedure used the interference was not present in the final fractions. The lack of matrix interferences meant that polyatomic interferences were also unlikely to be present meaning the use of a collisional gas such as He or H_2 would not be necessary as the potential benefit would be greatly outweighed by the loss of signal sensitivity. The use of reaction gases to mass shift the Pb signal was not observed to a significant degree for either O_2 or NH_3 mode, which in turn meant that a very low signal sensitivity was measured at the mass shifted values. With sensitivity being the main factor for achieving the greatest isotope ratio measurement with the lowest uncertainty no gas, SQ mode was selected for the final isotope ratio measurements.

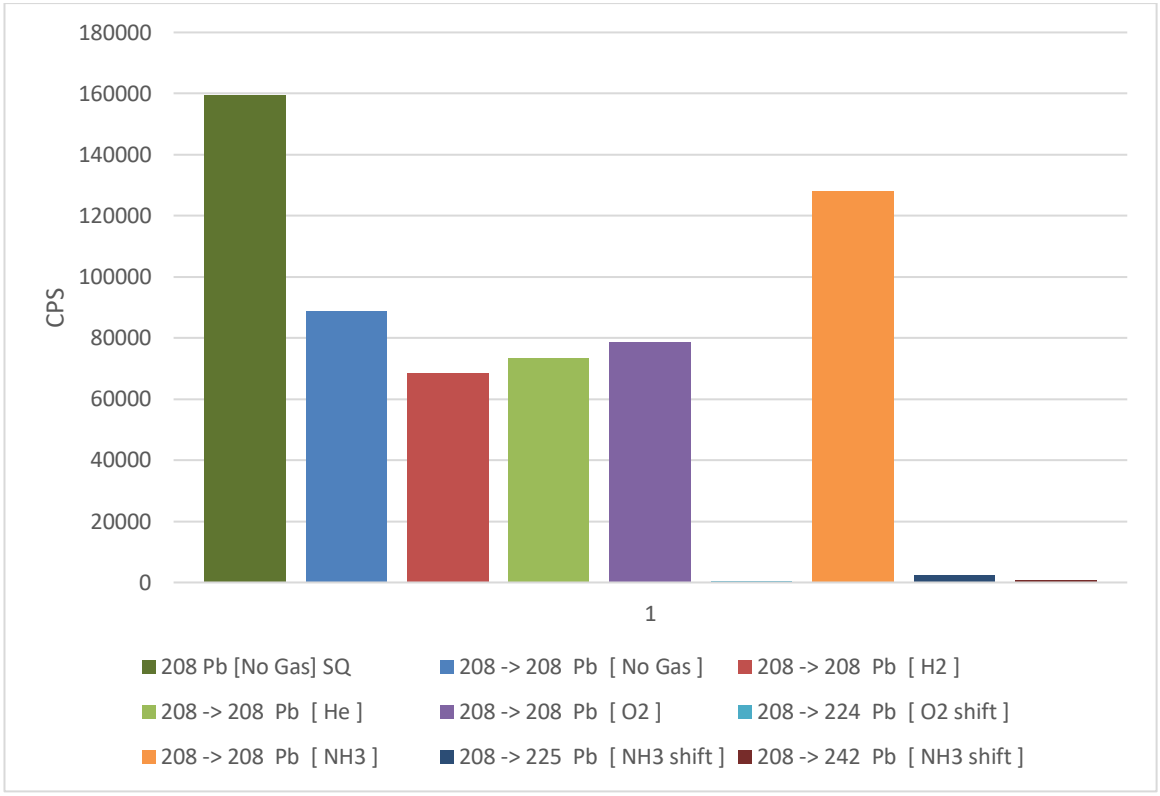

Figure 51: Analysis of ^{208}Pb sensitivity using NIST STD 981 (1 ng g-1) under all standard gas modes, analysing on mass and mass shifted

5.5.1.2 Pumped vs self-aspirated

Assessment of SQ and MS/MS, no gas mode was utilised for comparing the variation in isotope ratio uncertainties. It was fond the SQ mode produced a smaller measurement uncertainty than MS/MS mode (Table 31 and 32), across all the Pb isotope ratios, associated with a greater signal sensitivity in SQ mode. However, it was determined that the peristaltic pump that is used for standard sample introduction could be impacting the overall measurement uncertainty. The use of self-aspiration was investigated by creating a direct link to the nebulizer, bypassing the peristaltic pump. It was determined that self-aspirated SQ, no gas mode was able to achieve the lowest uncertainties and greatest accuracy for isotope ratio measurement, while also achieving a greater signal sensitivity than MS/MS mode.

Table 30: Isotope ratio uncertainty assessment between pumped and self-aspirated, SQ and MS/MS, no gas mode

	Isotope Ratio RSD		
	206/204	206/207	206/208
Peristaltic pumped SQ	0.1189	0.1540	0.2008
Self-aspirated SQ	0.1140	0.1301	0.2085
Peristaltic pumped MS/MS	0.2649	0.2811	0.3829
Self-aspirated MS/MS	0.2412	0.1814	0.1545

Table 31: Comparison of instrument configurations RSD variations

	206/204	206/207	206/208
Peristaltic pumped SQ vs MS/MS	0.45	0.55	0.52
Self-aspirated SQ vs MS/MS	0.47	0.72	1.35
SQ self-aspirated vs peristaltic pumped	0.96	0.84	1.04
MS/MS self-aspirated vs peristaltic pumped	0.91	0.65	0.40

5.5.1.3 Integration time

Improvements in measurement uncertainty were achieved for all isotopic ratios by increasing the integration time to instrumental limits. This was due to increasing the signal

sensitivity of the lower abundance isotopes, ^{204}Pb, ^{206}Pb and ^{207}Pb, relative to the most abundant isotope ^{208}Pb. The improvement in isotope uncertainty was reduced from >5.5 % to <0.5 % for $^{206}Pb/^{204}Pb$ which is the most challenging isotope ratio to accurately measure, as well as reducing uncertainty from ~2.3 % to ~0.2 % for $^{206}Pb/^{207}Pb$ and <1.5 % to ~0.2 % for $^{206}Pb/^{208}Pb$ (Figure 53). Integration time was increased from 0.1 seconds for all Pb isotopes to 0.1 seconds for ^{206}Pb and ^{207}Pb keeping ^{208}Pb at 1 second. This integration time was increased in increments for ^{206}Pb and ^{207}Pb up to 5 seconds while setting the ^{204}Pb at the maximum instrumental integration time of 25 seconds. An even better isotope ratio RSD may have been achieved if the integration time could have been increased to 50 seconds for ^{204}Pb to better reflect the ratios of the Pb isotopes.

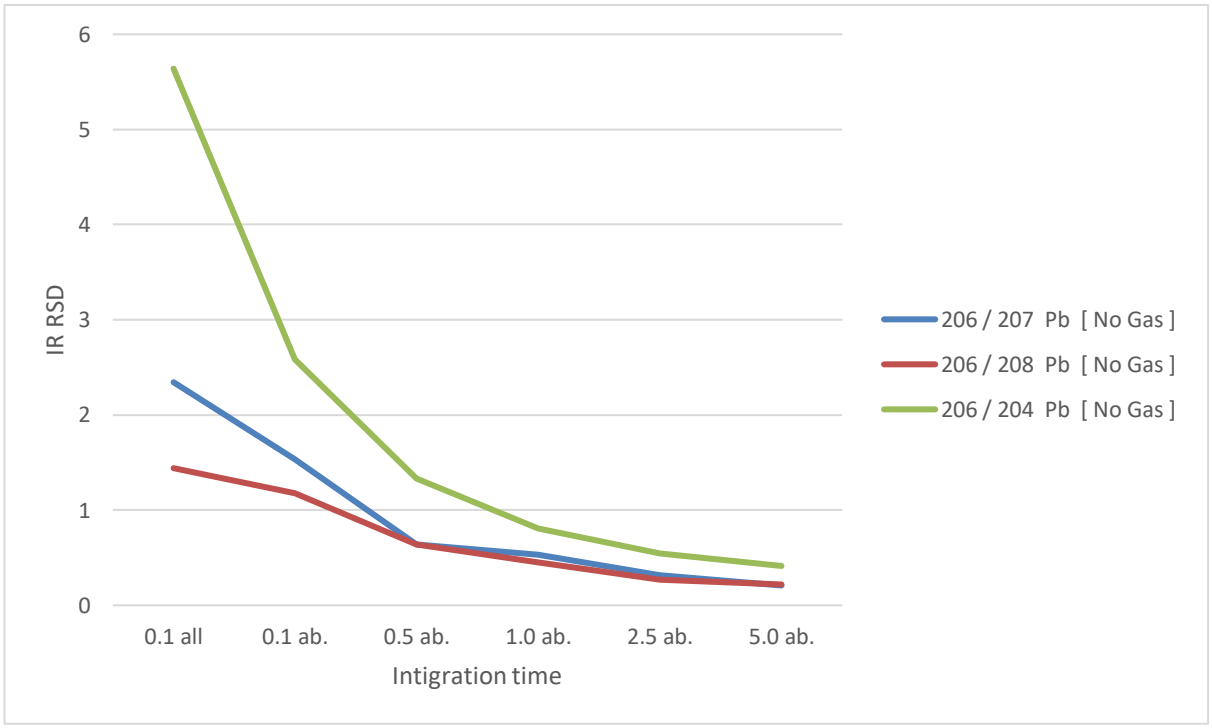

Figure 52: Impact of varying integration times on isotope ratio RSD

Table 32: Optimised integration times for all Pb isotopes based on relative abundances

Element	Isotope	Integration time (s)
Pb	204	25.0
	206	5.0
	207	5.1
	208	1

5.5.1.4 Replicates vs sweeps

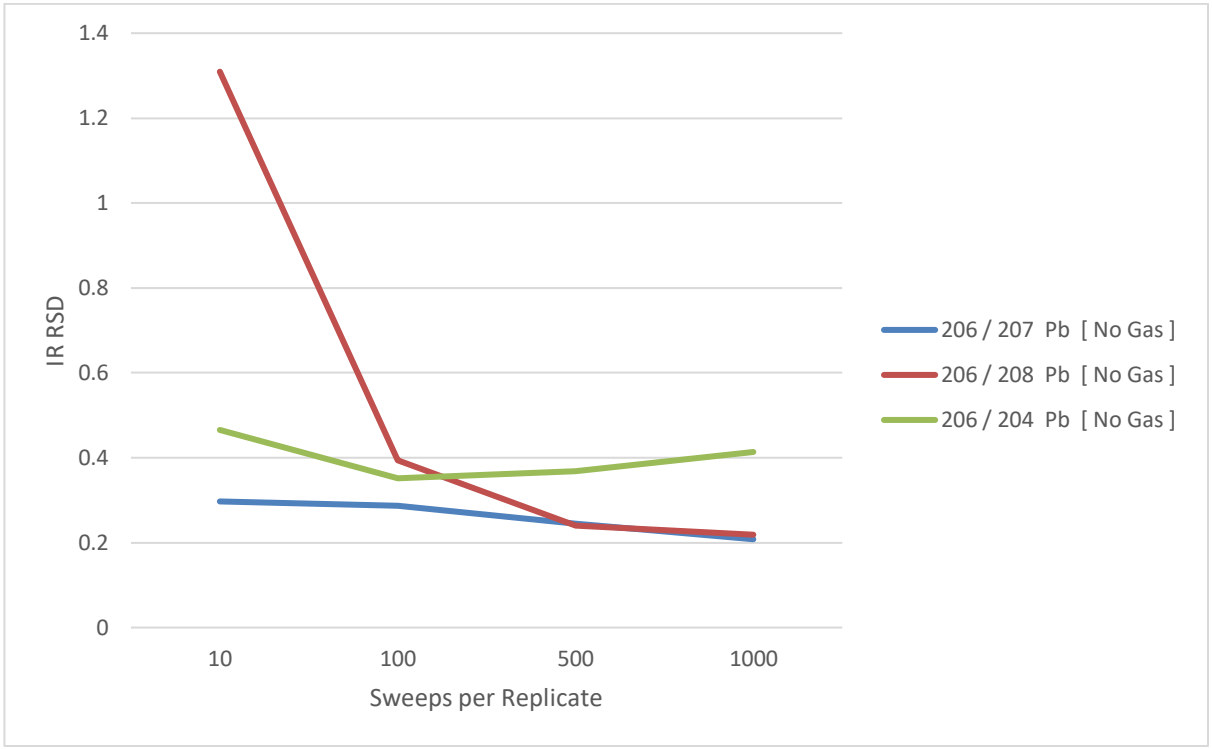

Figure 53: Impact of increasing the number of sweeps/ replicate on measurement uncertainty

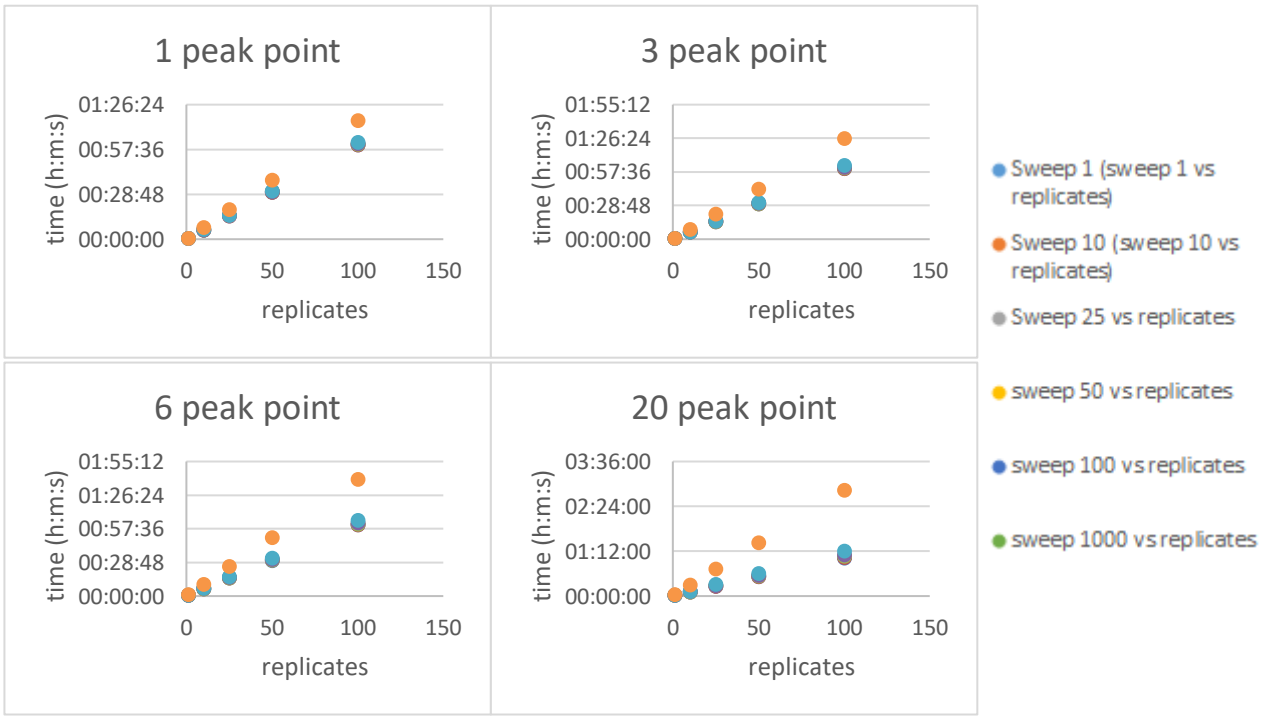

Figure 54: An assessment of sample analysis time with varying peak point analysis and increasing replicate measurements

A linear increase is observed as the number of replicates increased, so did the analysis time for a sample (Figure 55). The variation of peak point modes also increased time of analysis. However, 3 and 6 peak point analysis varying by the smallest amount suggesting that for better accuracy of data for minimal sample consumption increase 6 peak point analysis is favoured. For limited sample volumes or for immediate response 1 peak point analysis is optimal. If peak shape analysis is wanted 20 peak point analysis can be used however, it must consider that the sample volume needed will greatly increase.

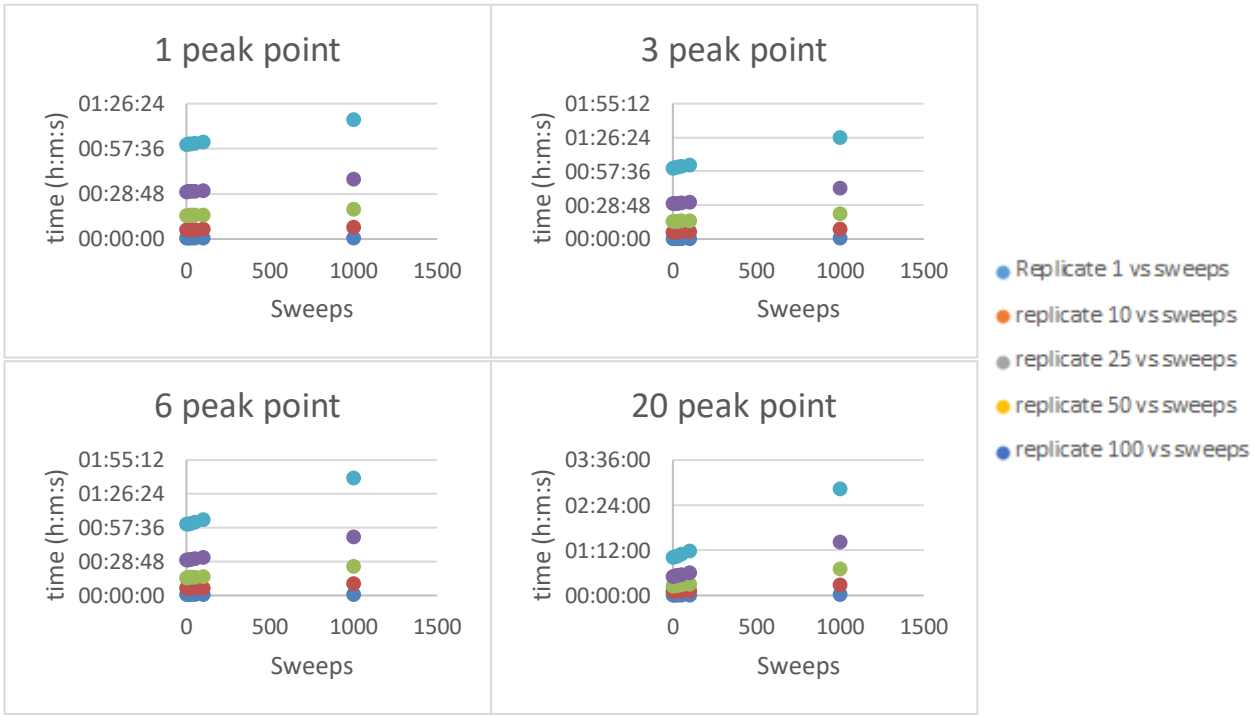

Figure 55: Impact on sampling time between increasing replicates vs sweeps

The increase in sweeps from 1 to 1000 showed that there was an increase in time however, the increase was not as great as the effect from the number of replicates. This is because the number of sweeps is represented as sweeps/replicate, i.e. 1000 sweeps within a replicate, sweeping from low too high in the allocated integration time (Figure 56 and 57). There is a small settle time from mass to mass, so a sweep is one complete multi-element measurement cycle.

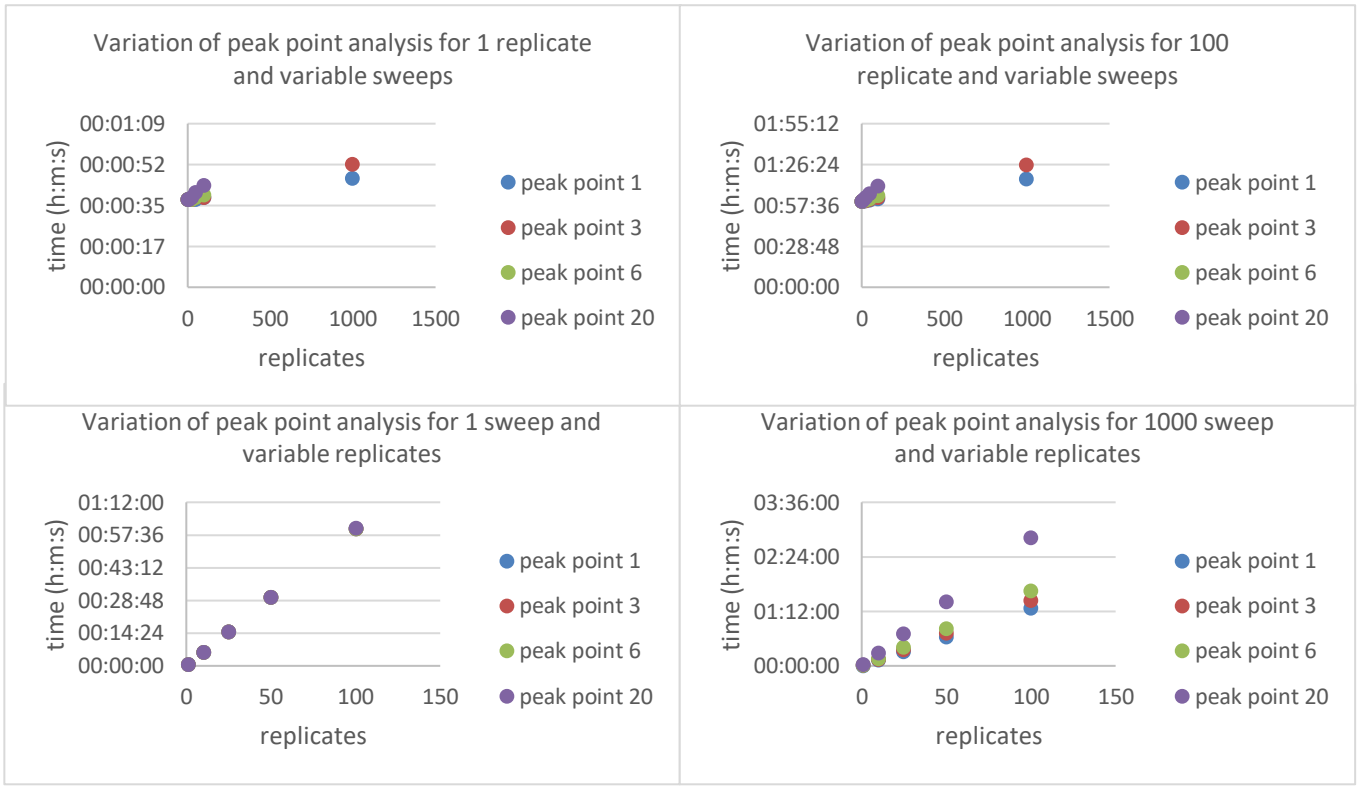

Figure 56: Variation in sample analysis time in relation to peak point analysis across varying replicate times

The variation of sweeps to replicates demonstrates that as the sweeps increase there is very little change in overall analysis time, however the increase in replicate measurements results is a steady increase in the analysis time meaning a compromise in overall replicates must be selected in which a statistically significant number of sample replicate measurements can be carried out without the waste of sample and measurement time.

For final sample analysis the Sweeps were set to 1000 per replicate allowing for more transitions between the measured ion peaks, improving the measurement uncertainty. Integration times were set to 25.0s 204, 5.0s 206, 5.1s 207, 1.0s 208. The ratio of the integration time is the maximum of the instrumental settings (25s). Ideally, it would be 50.0s on the 204 integration however, the reduction on the 208, 207 and 206 integrations would reduce the signal sensitivity on those isotopes resulting in a greater RSD and reduced accuracy and precision for isotope ratio analysis.

The replicates were capped at 5, due to the large increase in the analysis time and sample usage if the replicates are increased. The ability to access more replicates can be overcome by running samples in parallel to achieve the best isotope ratio average and hence further reduce the RSD. Sweeps however cannot be reduced as the impact on RSD is substantial.

5.5.1.5 Analysis mode

Tuning the instrument for high masses (Pb-204->208) means that it is possible to increase the sensitivity for the higher mass. Pb-208 has a 92,000 CPS for a 1 ppb solution of Pb at 0% sensitivity, which is increased to 109,000 CPS at 100% sensitivity tune. Pb-204 has an increase in sensitivity from 2,500 at 0% sensitivity tune, to 3,000 CPS at 100% sensitivity tune. Preferential mass tuning to the high mass range (100 %) improves the RSD for all the ratio analysis and shows a notable improvement due to the reduced impact of signal variability (Table 34).

Table 33: Impact on uncertainty of isotope ratio measurement with varying preferential mass tune using a 1.14 ng g-1 NIST SRM 981

Tune	206/207 RSD	206/208 RSD	206/204 RSD
0 %	0.555 %	0.453 %	0.594 %
100 %	0.285 %	0.347 %	0.534 %

To optimise the signal sensitivity and minimise the uncertainty in isotope ratios operating the instrument self-aspirated and in no gas, SQ mode it is possible to remove the peristaltic pump noise and increase the signal sensitivity by removing the signal suppression introduced by using both quads. The increased signal also results in an improvement in measurement uncertainty.

Optimal sample concentrations for the analysis of Pb isotopic ratios was shown to be ~10 ppb. This was determined by analysing the NIST SRM 981 at varying concentration over

multiple replicates and monitoring the measurement signal and uncertainty (Figure 58) as well as the ease with which it would washout of the instrument and therefore prevent carry over or memory effects.

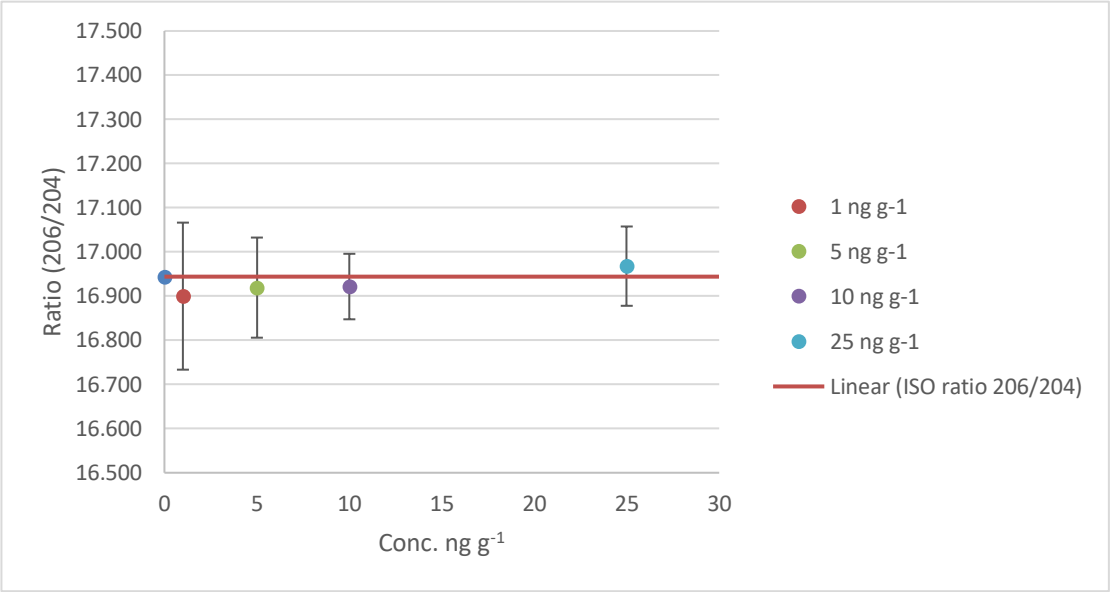

Figure 57: Variation in measurement uncertainty (2SD) of isotope ratio measurements ($^{206}Pb/^{204}Pb$) with increasing concentrations of a single element solution of Pb

Table 34: Variation in uncertainty with varying concentrations of a single element solution of Pb

Concentration	206/204 RSD
1 ppb	0.381 %
10 ppb	0.217 %
25 ppb	0.242 %

Initial sensitivity analysis was carried out using a single element solution of Pb to establish a concentration range where the lowest uncertainty was measured. This was then compared to the NIST SRM 981 isotopic standard with comparable results observed. This suggests that ~10 ng g^{-1} solution is the optimal concentration to analyse the samples at

while also allowing for an optimal mass bias correction to be established (Table 35 and Figure 59).

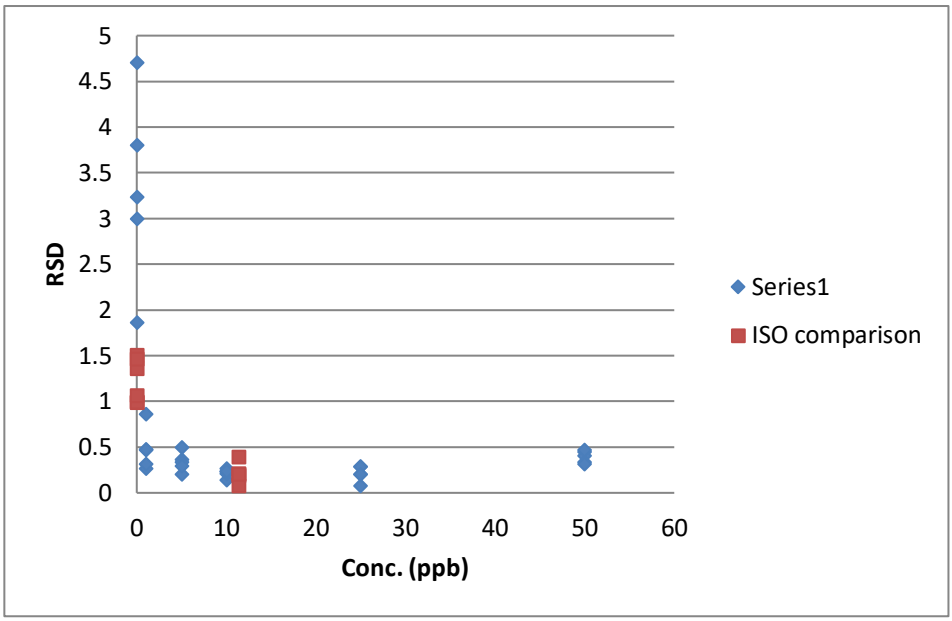

Figure 58: Variation in measurement uncertainty of isotope ratio measurements ($^{206}Pb/^{204}Pb$) with increasing concentrations of a single element solution of Pb compared with the NIST SRM 981

Tl correction and sample bracketing.

The Tl correction factor applied to the samples made a significant increase in uncertainty and RSD compared to not correcting the samples (Table 36). This may have been due to the integration time being set at 0.1s for the Tl measurement. However, an increase in the integration time would result in a decrease in signal sensitivity for the Pb isotopes and a significant increase in sample usage and an overall increase in isotope ratio uncertainty therefore a higher Tl integration time is not suitable.

Table 35: Impact on measurement uncertainty for isotope ratio analysis when applying a Tl mass bias correction

Tune	206/207 RSD	206/208 RSD	206/204 RSD
No Tl correction	0.182 %	0.156 %	0.268 %
Tl correction	0.815 %	0.899 %	0.861 %

Sample bracketing

Does not affect the measurement uncertainty of the samples due to applying a factor to the isotopic ratios already measured. However, the correction does, improve the accuracy of the isotope ratio measurement bringing them closer to the true values calculated on both the MC-ICP-MS and the certified values given for the NIST SRM 981 isotopic Pb standard.

Samples analysis involved analysing unknown samples in batches of 3 bracketed between two NIST981 standards (Table 37). A complete wash sequence was implemented between samples to ensure no memory effects were being carried through and impacting the isotope ratio measurement. This is specifically important for systems in which the target analyte is particularly “sticky” such as in the case of Th, in which even more robust cleaning procedures much be implemented to prevent the background signals from increasing due to an accumulation of the analyte passing through the introductory systems and tubing.

Table 36: Order of sample analysis for NIST SRM 981 Pb standard bracketing

Sample blank wash – 0.6 M HNO_3
NIST SRM 981 - Standard
Sample 1
Sample 2
Sample 3
NIST SRM 981 – Standard
Sample blank wash – 0.6 M HNO_3

Analysing all samples at ~10 ng g^{-1}, followed by using a NIST SRM 981 (11.4 ng g^{-1}) as the mass bias correction by bracketing the samples in batches of three, allowed isotope ratio measurement within error to be comparable to those collected utilising the MC-ICP-MS.

An improvement in signal sensitivity could be further improved by tuning the instrument to a higher mass preference, with minimal impact on isotope ratio uncertainty, Figure 60 and 11. An assessment of uncertainty was investigated for $^{204}Pb/^{208}Pb$ ratios, as this would give an understanding of how increasing the preferential mass tune would impact the relationship between isotopes 4 mass units apart, Figure 61 and 62. It was found that there was no significant change to isotope uncertainty which was already relatively low, ~0.5 %, however an improvement in signal sensitivity may prove beneficial for systems in which the isotopic ratios are more varied than those for Pb, in which the lowest abundance isotope will have an improvement in its signal sensitivity and therefore be less impacted by the variations in the background signal.

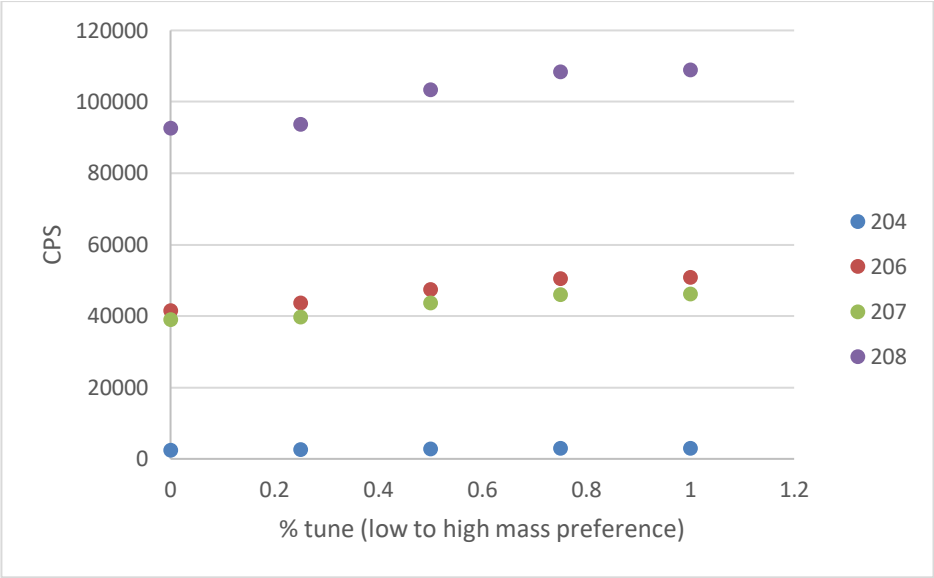

Figure 59: The impact on signal sensitivity of adjusting the mass preference from low to high, while monitoring a 1.14 ng g^{-1} Pb isotopic standard (NIST981)

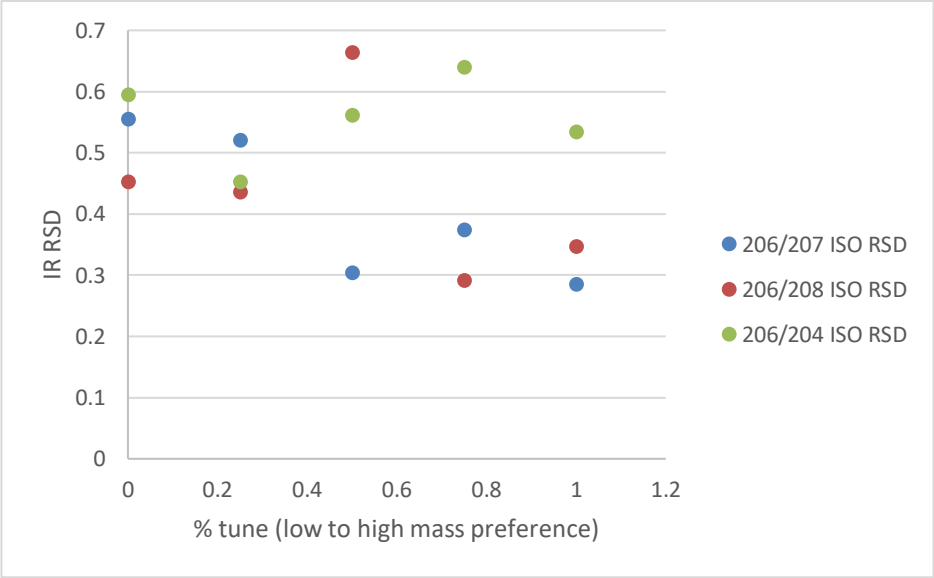

Figure 60: Impact on isotope ratio RSD across the range of mass preference

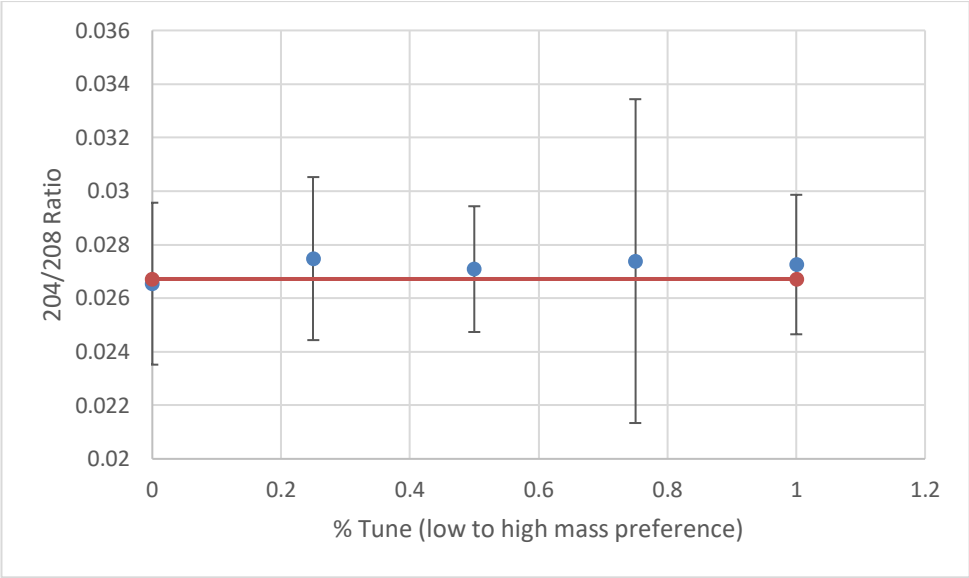

Figure 61: Impact of pass preference tuning on isotope ratio uncertainty of $^{204}Pb/^{208}Pb$ analysis

5.5.2 Real samples – separated

Analysis of samples processed and separated from the matrix for both Hythe's saltmarsh and Lake Windermere, sediment cores showed good agreement between the ICP-MS/MS and the MC-ICP-MS. This is due to the purified fractions being free from any potential isobaric ^{204}Hg as well as other matrix ions, with further measurement uncertainties being reduced through the use of free-aspiration and heightened signal sensitivity by operating the instrument under no gas, SQ mode.

Initial analysis showed good agreement between the $^{206}Pb/^{204}Pb$ and $^{206}Pb/^{207}Pb$ isotope ratios (Figure 63 and Figure 64). However, a discrepancy between the $^{206}Pb/^{208}Pb$ ratios was observed. This was determined to be due to an increase in background signal of the instrument, which when used to background correct samples, produced an offset of the isotope ratios throughout the core. This therefore highlights the importance of ensuring the lowest possible background signal for all isotopes when attempting to carry out isotope ratio analysis, as minor changes in one isotope may drastically alter the relationship between them and therefore artificially influence measured ratio and potentially the source term.

5.5.2.1 Hythe – Saltmarsh

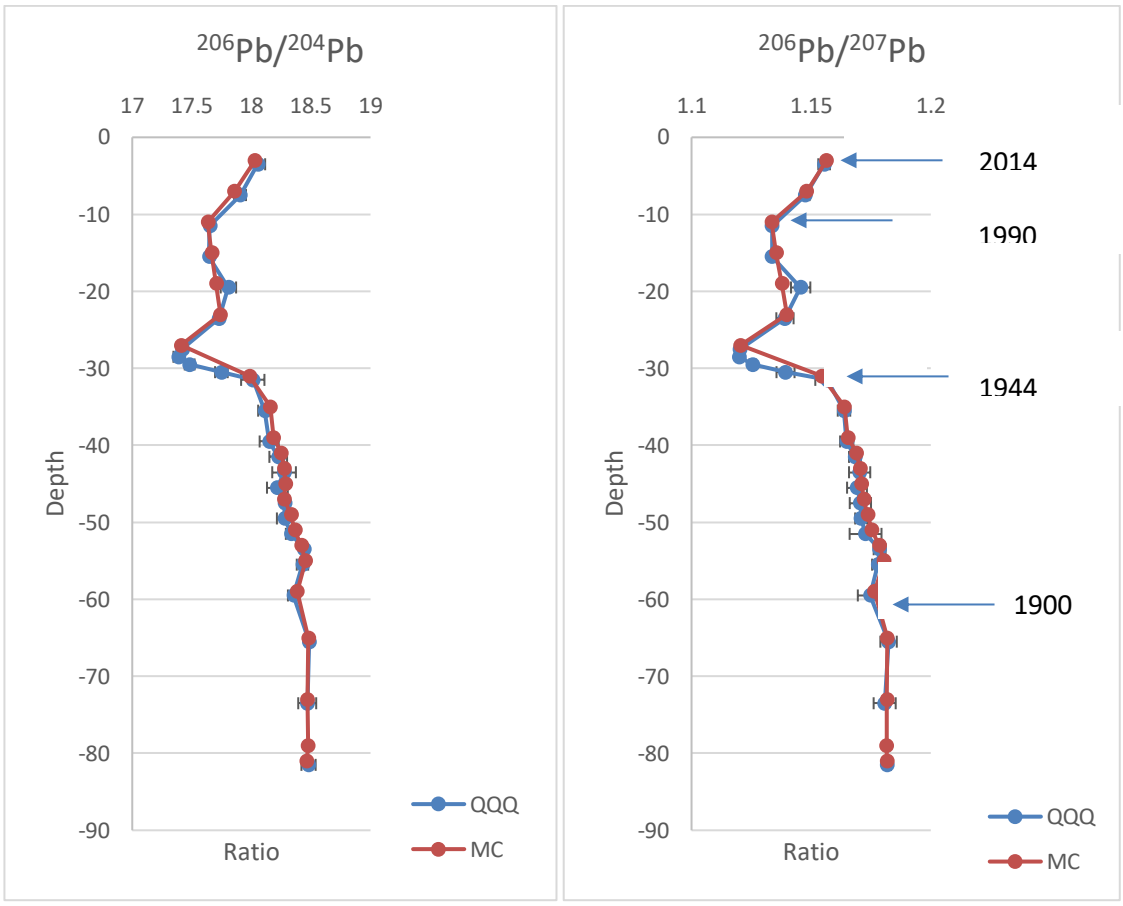

Figure 62: Hythe Saltmarsh sediment core analysis. Comparison of $^{206}Pb/^{204}Pb$ and $^{206}Pb/^{207}Pb$ isotopic signatures measured on the MS/MS Agilent 8800 against the multi-collector measurements taken on the Thermo-Fisher Neptune, plotting up 2sd error bars for the MS/MS

5.5.2.2 Windermere – Lake

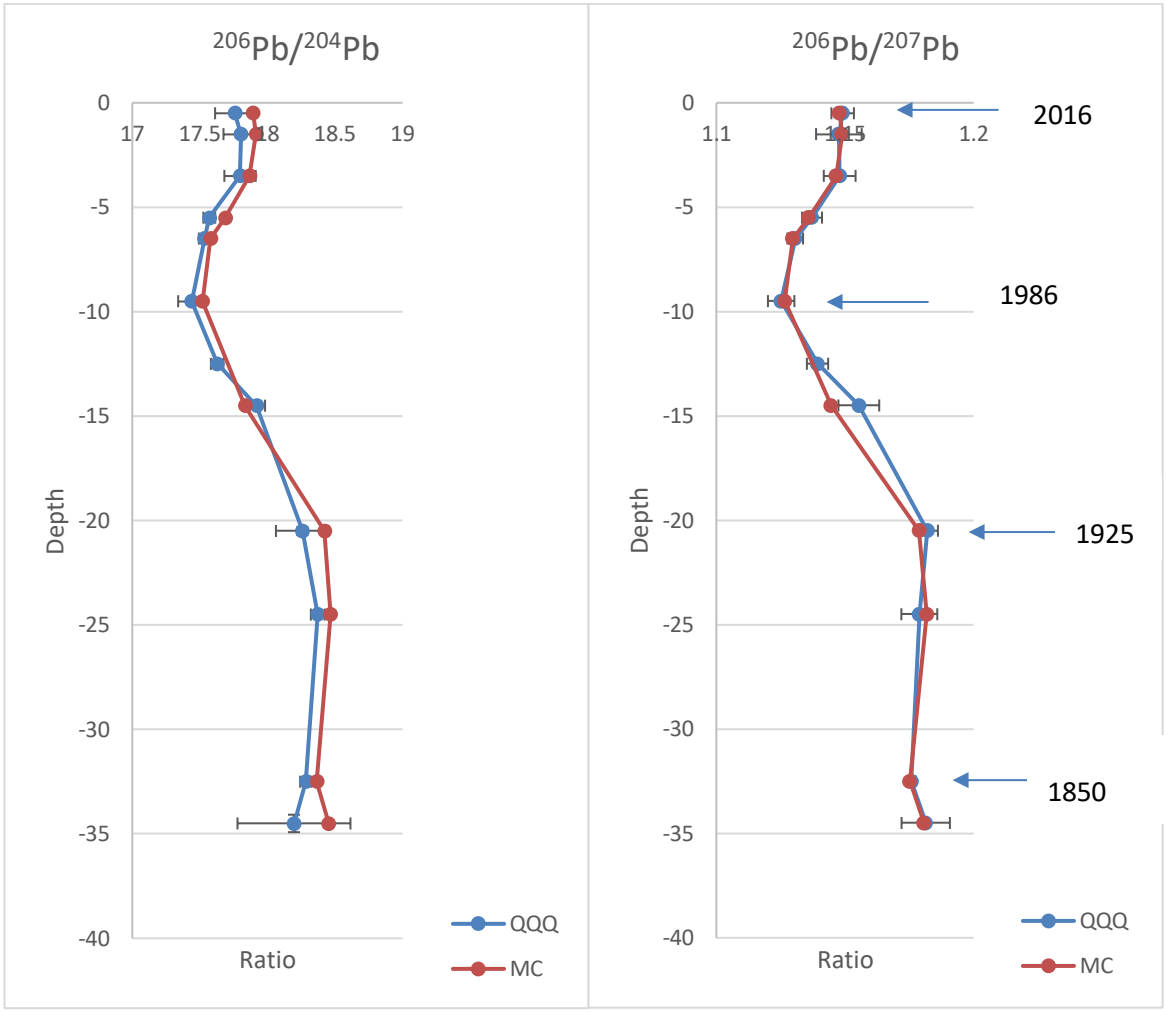

Figure 63: Windermere sediment core analysis. Comparison of $^{206}Pb/^{204}Pb$ and $^{206}Pb/^{207}Pb$ isotopic signatures measured on the MS/MS, Agilent 8800 and the multi-collector measurements taken on the Thermo-Fisher Neptune, plotting up 2sd error bars for the MS/MS

5.5.3 Real samples – unseparated

Samples which were digested in aqua regia, diluted to 10 ng g^{-1} in HNO_3 (0.6 M) and measured on the ICP-MS/MS also achieved results comparable to those that underwent extensive chemical separation and were measured on both the MC-ICP-MS and ICP-MS/MS. The samples were monitored for a range of Hg isotopes including ^{196}Hg, ^{198}Hg, ^{199}Hg, ^{200}Hg, ^{201}Hg and ^{202}Hg with no significant change in counts above background (<100 CPS) determining that there was no Hg present meaning that no reaction gases (NH_3) needed to be used to charge transfer the isobaric interference away.

Samples were analysed as separated and purified solutions on the MC-ICP-MS as well as two runs on the ICP-MS/MS. An unseparated solution was also analysed on the ICP-MS/MS for direct comparison between the techniques (Figure 65, 66 and 67). It was found that when analysing in MS/MS mode the impact of an increased background signal has a major impact on isotope ratio analysis. The separated MS/MS – 2 analysis showed a large disparity specifically for the 206/208 isotope ratio measurement due to a background of ~3000 CPS at m/z = 208 rather than the optimal <1000 CPS measured in both the separated MS/MS – 1 and unseparated MS/MS samples. However, the low background in 204, 206 and 207 meant that the impact on isotope ratio measurements for 206/204 and 206/207 still showed good agreement with the MC-ICP-MS data. The isotope ratio measurement agreement between the separated MC-ICP-MS and the unseparated MS/MS showed that isotope ratio analysis could be performed on direct digest solutions, improving the sample processing times without impeding the isotope ratio measurement.

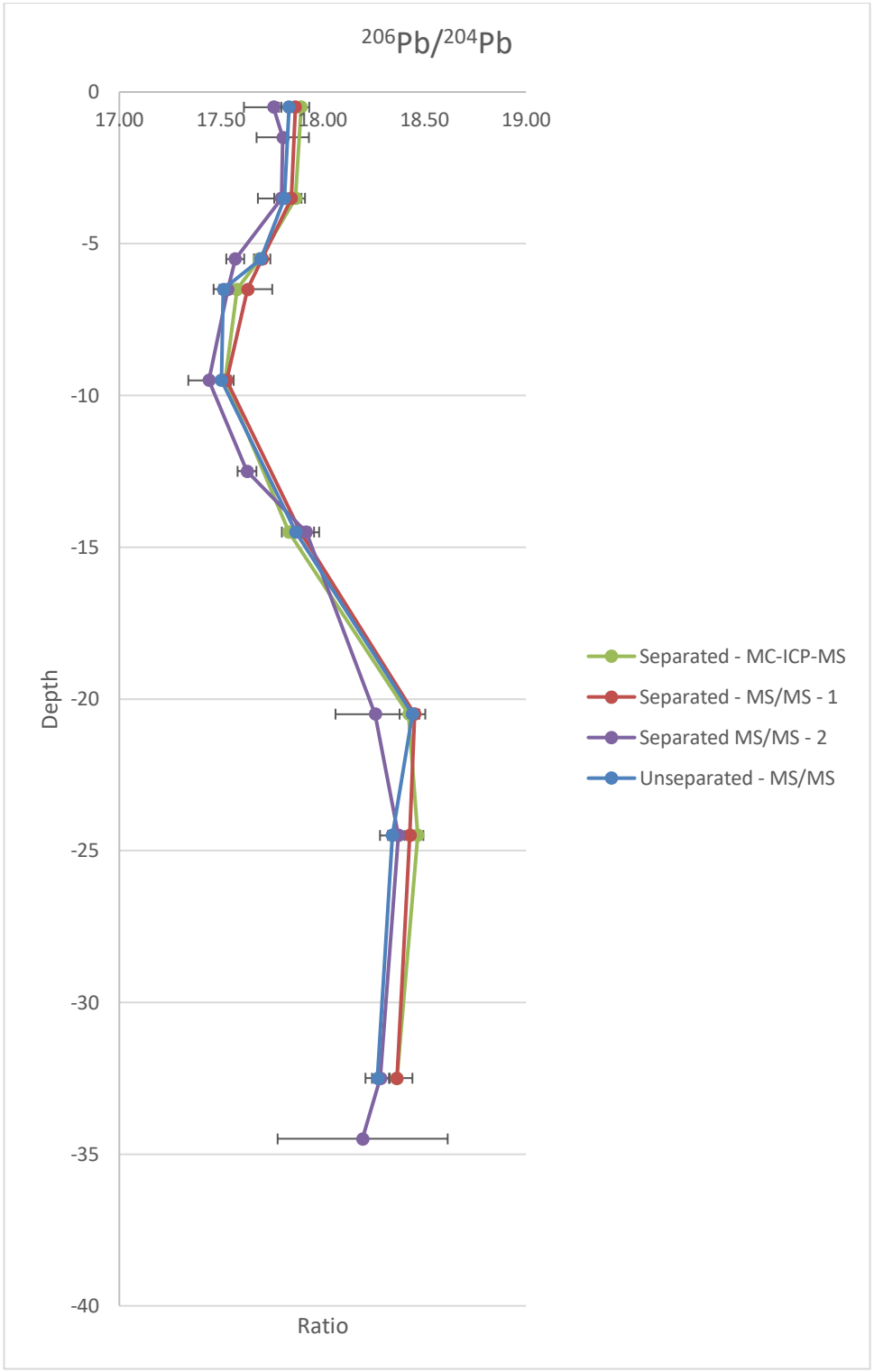

Figure 64: Windermere $^{206}Pb/^{204}Pb$ ratio measurement for Separated - MC-ICP-MS, MS/MS - 1, MS/MS - 2, and Unseparated MS/MS

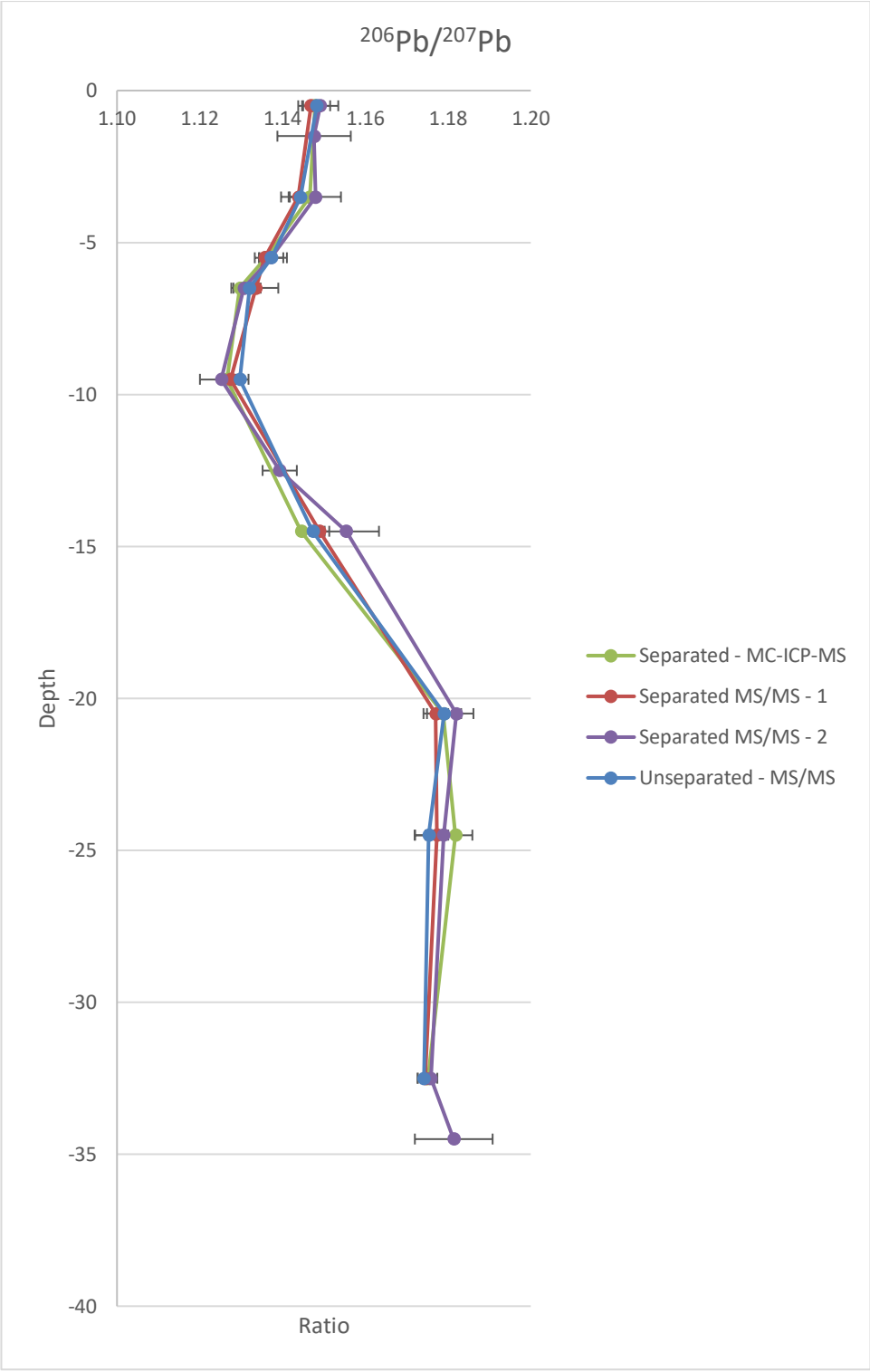

Figure 65: Windermere $^{206}Pb/^{207}Pb$ ratio measurement for Separated - MC-ICP-MS, MS/MS - 1, MS/MS - 2, and Unseparated MS/MS

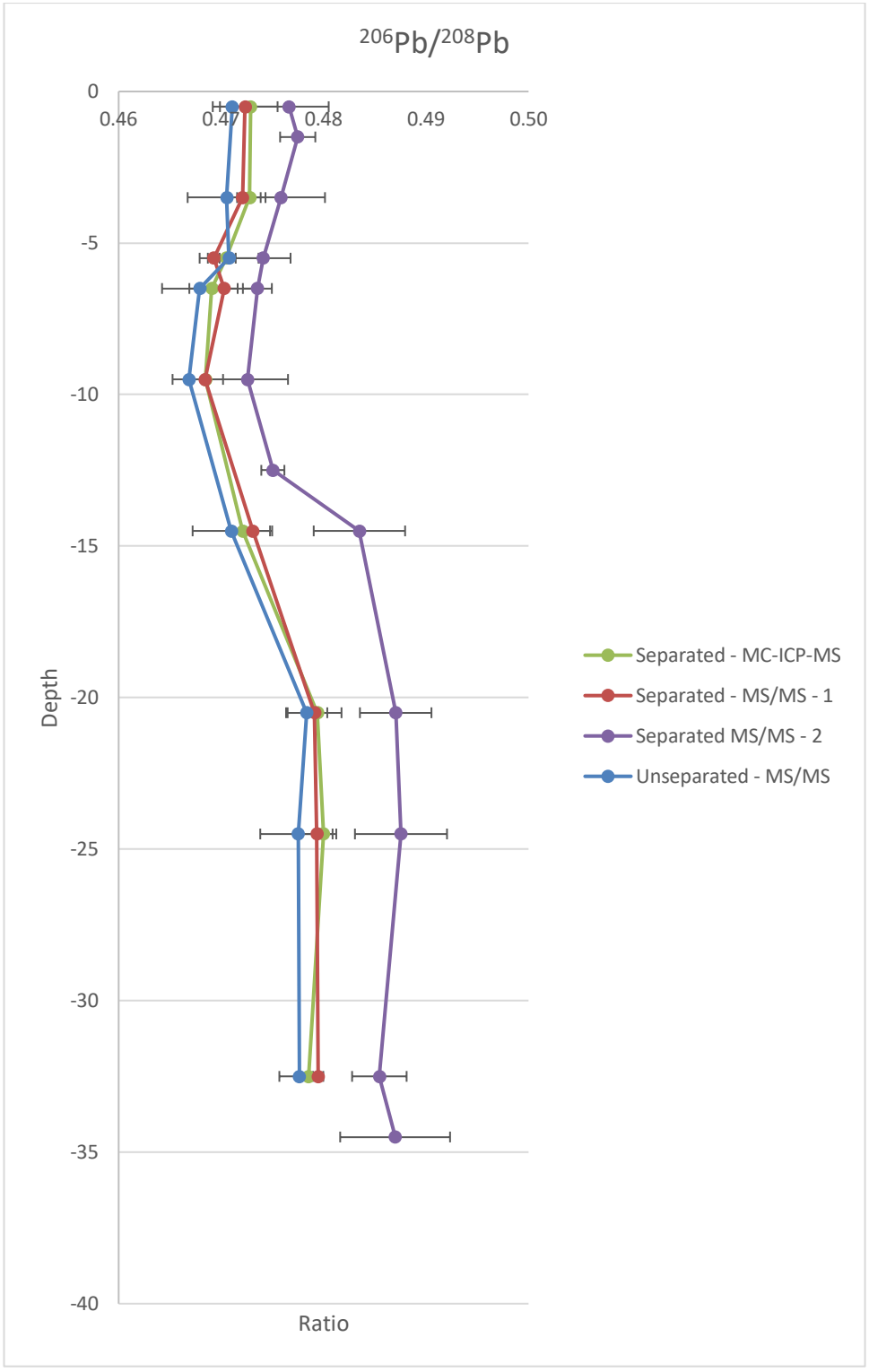

Figure 66: Windermere $^{206}Pb/^{208}Pb$ ratio measurement for Separated - MC-ICP-MS, MS/MS - 1, MS/MS - 2, and Unseparated MS/MS

5.6 Optimised instrument set up:

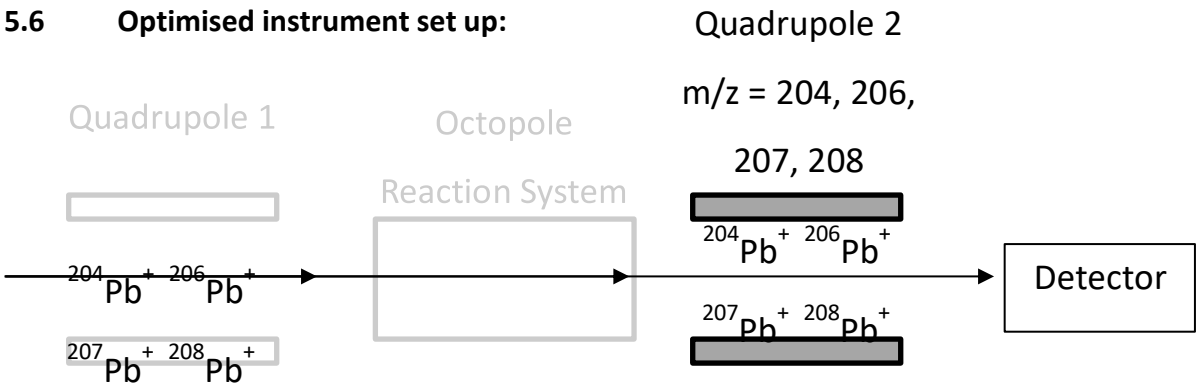

Figure 67: Optimised instrument set up for Pb isotope ratio analysis

Table 37: Optimised instrumental conditions for Pb isotope analysis

Instrument parameter	Value
Sample introduction media	2 % HNO_3
RF power	1550 W
Scan mode	Single Quad (SQ)
Plasma mode	Low Matrix
Extraction lens 1	0.0 V
Extraction lens 2	-180.0 V
Octopole bias	-8.0 V
Omega lens	10.0 V
Energy discrimination	5.0 V
Gas mode	No gas
Q2	204, 206, 207, 208

Table 38: Optimised integration times for each Pb isotope

Element	Isotope	Integration time (s)
Pb	204	25.0
	206	5.0
	207	5.1
	208	1

Using the optimised set up, Table 38 and 39, as well as a NIST981 (10 ng g^{-1}) sample-standard bracketing, it was possible to account for mass bias fractionation. All samples were initially dip tested and then diluted down to 10 ng g^{-1} to ensure the consistency of signal sensitivity between the sample and the bracketing solution.

The method has been shown to be effective for Pb isotope analysis for anthropogenic environmental changes whereby the isotopic ratio variation occurs on the second or third decimal place. However, to achieve the absolute isotope ratio measurement for variations on the fourth decimal place with minimal measurement uncertainty a multi-collector instrument is required (Taylor et al., 2014), which can be used to determine geological changes and variations in isotope ratios.

Table 40 shows the potentially achievable % RSDs for the variable lead isotopic ratios on different instruments.

Table 39: Comparison of varying instruments for Pb isotope analysis % RSD

Mode	Instrument Precision (% RSD) 206/207	Instrument Precision (% RSD) 206/204	References
SQ	1-2	~2-4	Walder and Furuta 1993, Mukal et al., 1993,
TIMS	0.009	0.0260	Galer and Abouchami 1998, Thirlwall 2002, Kuritani and Nakamura 2003, Amelin and Davis 2006, Hoernle et al., 2011
MC	0.003	0.007	Thirlwall 2002, Baker et al., 2004, Makishima et al., 2008, Makishima and Nakamura 2010
TOF	0.099	0.854	Tian et al., 2000, Baker et al., 2004
MS/MS (SQ mode)	0.185	0.134	This study
MS/MS (MS/MS mode)	0.254	0.563	This study

5.7 Conclusion

Analysis of Pb isotope ratios using the ICP-MS/MS was able to achieve instrumental uncertainty of <0.2 % when operating under no gas, SQ mode and self-aspirating the samples. This level of accuracy is perfectly suited for monitoring large changes in source terms related to anthropogenic activities, such as those related to the introduction and eventual removal of tetraethyl lead in petrol. However, when utilising the MS/MS capabilities this uncertainty increased to <0.6 % for $^{206}Pb/^{204}Pb$ and ~0.25 % for $^{206}Pb/^{207}Pb$.

It has however also been demonstrated that samples could undergo acid digest followed by a single step dilution and produce equivalent isotope ratio measurements without the need for extensive chemical separation and purification. This highlights the tolerance of the ICP-MS/MS for high matrix samples while also offering a means for reduced sample preparation and rapid analysis in the case of emergency responses following contamination and fallout such as those experienced in Fukushima. The importance of low background for isotope ratio analysis and characterisation is highlighted by the repeat analysis of the separated Windermere samples, whereby a small increase in the background (~2000 CPS) can result in a significant shift in isotope ratio measurement. The use of MS/MS mode increases this tolerance for variable matrix inferences by filtering them out through the use of Q1. For isotope ratio systems whereby the interferences present require separation or removal and an increased abundance sensitivity would benefit measurement the increased measurement uncertainty when operating under MS/MS mode would need to be considered for the improvement in instrumental capabilities. The use of the collision and reaction gases further expand the range of isotope ratios that can be measured for example those including $^{135}Cs/^{137}Cs$ whereby there is an isobaric Ba interference on both m/z = 135 and 137 can be resolved using N_2O as a collision gas to remove the Ba signal(Zheng et al., 2014), $^{129}I/^{127}I$ where an isobaric ^{129}Xe cannot be chemically removed offline as well as the high ^{127}I signal causing polyatomic and tailing issues which can both be resolved by operating under MS/MS mode and using a collision gas, O_2 (Ohno et al., 2013) and $^{236}U/^{238}U$ (Tanimiziu et al., 2013) in which the isobaric and polyatomic interferences cannot be resolved on a multi-collector instrument where spectral resolution needed greatly exceed the capabilities of the instrument.

Chapter 6 Conclusions and future work

The use of the ICP-MS/MS has been used to demonstrate its capabilities for not only analysing a selection of representative waste matrixes, including ground waters, stainless steels, air filters and concretes, to determine the potential radionuclides that may be measurable without complex multi stage separation but taking the work further and demonstrating the capabilities for active concrete characterisation following variable acid digests and $LiBO_2$ fusion. Assessment of all the non-active and active representative matrixes highlights the benefits that the ICP-MS/MS offers to the nuclear decommissioning industries as a means to carry out rapid waste material screening and finger print characterisation for actinide species including ^{234}U, ^{235}U, ^{236}U, ^{238}U, ^{239}Pu, ^{240}Pu and ^{241}Am, below the out-of-scope limits as proposed by EPR 2018, while simultaneously showing the tolerance of the instrument to high matrix loading associated with complete digest analysis. Sample analysis also demonstrated the potential capabilities of the ICP-MS/MS for rapid analysis, within the same run, of other radionuclides specifically ^{59}Ni, ^{93}Zr, ^{99}Tc, ^{126}Sn, ^{135}Cs and ^{151}Sm bellow their EPR 2018 out-of-scope limits when operating under no gas, MS/MS, demonstrates the potential for further fingerprint analysis as well as emergency response analysis for a range of radionuclides across the mass range, allowing for minimal sample handling and preparation which further helps reduce sample turn around, and improves response times. Potential future work would assess the impact of heterogeneity within the concrete samples and how best to overcome this, be that with a larger sample volume or multiple sample analysis, as well as extending the range of radionuclides analysed beyond the actinides analysed in this study with further matrix assessment expanding beyond that of concrete for screening and waste characterisation purposes. By utilising the collision (He and H_2) and specifically the reaction gases (O_2 and NH_3) it may also be possible to increase the list of measurable radionuclides within the unseparated matrix digests. Utilising the range of alternative reaction gases such as N_2O, CO and CO_2 more controlled oxidation reaction may benefit specific radionuclide reactions.

An optimised method was development into ^{129}I, utilising the tube furnace extraction into TMAH, whilst also removing potential polyatomic interferences (>98 % Y, In, Cd, Mo and Ba), followed by analysis using optimised instrumental parameters including O_2 reaction gas (0.5 ml min^{-1}) to remove the isobaric ^{129}Xe interference (>97 %) and MS/MS mode to

remove the potential tailing associated with the high concentrations of stable ^{127}I. Signal sensitivity was further enhanced through matrix modification of the trapping solution, increasing the counts from <20,000 to ~75,000 counts per ng g^{-1}, and fluctuations within the instrumental measurement where accounted and corrected for utilising a suitable internal standard (^{130}Te) which has been demonstrated to be stable in basic media (TMAH) and also behave in a representative manor to the ^{129}I in solution. A robust method for ^{129}I has been demonstrated across a range of representative and complex nuclear waste matrixes including sands and aqueous standards, as well as silo liquors, sludge's and slurries rich in $Mg(OH)_2$, ion exchange resins, mineral zeolites (clinoptilolite) and graphite further expanding the application of the technique to the nuclear decommissioning industries. All results were compared with LSC analysis and achieved an agreement of >97 % with exception of $Mg(OH)_2$ samples had a 74 % recovery, due to the $Mg(OH)_2$ forming a glassy solid upon heating in the tube furnace, resulting in the iodine being trapped within the lattice structure rather than being released completely and volatilised into the trapping solution. Samples rich in $Mg(OH)_2$ need an improved extraction procedure to further improve the recovery. The method achieved an instrument detection limit of 1.05×10^{-4} Bq g^{-1} (0.016 ng g^{-1}) for ^{129}I, which is two orders of magnitude below the out-of-scope limit, providing a means for characterisation of nuclear waste materials with minimal procedural stages prior to measurement. Further development and optimisation of existing techniques for difficult to measure (DTM) radionuclides with specific focus to real and representative waste material for the nuclear decommissioning industry is of great importance so as to overcome challenges that may not be recognised if only carrying out method development on ideal solutions. The ICP-MS/MS offers many possibilities for instrumental optimisation using the techniques gained from method development of the ^{129}I, specifically custom tuning and parameter optimisation, matrix modification and representative internal standard determination.

Finally, instrumental capabilities were investigated through isotope ratio analysis utilising a single collector instrument, with the ICP-MS/MS capable of producing comparable data to that of the Neptune MC-ICP-MS for Pb isotope systems with distinct anthropogenic source terms, for core samples collected from both lake and saltmarshes within the UK. The technique demonstrated the tolerance of the ICP-MS/MS not only for purified Pb solutions but also direct digests which would not be possible on MC-ICP-MS instruments. The instrument offers a means for more extensive isotope ratio analysis to be carried out

on radionuclides which may have interferences, both isobaric and polyatomic that are not currently resolvable by traditional single quadrupole ICP-MS instrumentation or MC-ICP-MS. The improvements in abundance sensitivity resolution, 10^{-7} to 10^{-10}, through the use of the MS/MS capabilities also offer a means to overcome specific tailing interferences from stable isotopes on activation product radionuclides. The use of direct digest analysis for isotope ratio analysis offers a means for the ICP-MS/MS to be utilised in emergency response scenarios where by sample turn around, determination of source and activity measurements below the out-of-scope limits become necessary to reduce the impact on the exposed communities and sites.

The work has focused on nuclear decommissioning samples however environmental sample analysis could also be investigated to further demonstrate the capabilities of the ICP-MS/MS in not only dealing with environmental matrixes, such as soils, plant matter and tissue, but also developing methods more suitable to emergency response analysis where by isotope ratio analysis would be necessary to distinguish natural background ratios from contamination sources and also to measure samples that the general public would be most likely to be exposed to.

Appendix A Evaluation of Inductively coupled plasma tandem mass spectrometry for radionuclide assay in nuclear waste characterisation

P.E. Warwick, B.C. Russell, I.W. Croudace, Ž. Zacharauskas

J. Anal. At. Spectrom., 2019, DOI: 10.1039/C8JA00411K

Contribution from Ž. Zacharauskas included instrument background, sensitivity, abundance sensitivity and hydride formation assessment, as well as case studies of Stronium-90, Iodine-129 and Neptunium-237. Further corrections and drafts where completed as part of a group effort by everyone involved.

List of References

Abouchami, W., 2014. Practical Application of Lead Triple Spiking for Correction of Instrumental Mass Discrimination.

Aïtcin, P. C., 2015. Portland cement. In: *Science and Technology of Concrete Admixtures.* s.l.:Elsevier Inc., pp. 27-51.

Amelin, Y. & Davis, W. J., 2006. Isotopic analysis of lead in sub-nanogram quantities by TIMS using a 202 Pb-205 Pb spikew.

Amr, M. A., Helal, A. F. I., Al-Kinani, A. T. & Balakrishnan, P., 2016. Ultra-trace determination of 90Sr, 137Cs, 238Pu, 239Pu, and 240Pu by triple quadruple collision/reaction cell-ICP-MS/MS: Establishing a baseline for global fallout in Qatar soil and sediments. *Journal of Environmental Radioactivity,* 1 3, Volume 153, pp. 73-87.

NDA., 2013. *2013 UK Radioactive Waste Inventory: Radioactive Waste Composition NDA and DECC February 2014,*

SDF, 2017. *The UK Nuclear Industry Guide To: Clearance and Radiological Sentencing: Principles, Process and Practices*

NDA, 2018. *Integrated Waste Management Radioactive Waste Strategy,*

Radioactive Waste Management., 2018. *Inventory for geological disposal Method Report,*.

EPR, 2018. *SCOPE OF AND EXEMPTIONS FROM THE RADIOACTIVE SUBSTANCES LEGISLATION IN ENGLAND, WALES AND NORTHERN IRELAND Guidance document*.

NDA., 2019. *Business Plan*

Agilent, 2015. *AGILENT 8800 ICP-QQQ APPLICATION HANDBOOK 2ND EDITION Agilent 8800 ICP-QQQ Application Handbook,*

Agilent .2012,. *Agilent 8800 Triple Quadrupole ICP-MS: Understanding oxygen reaction mode in ICP-MS/MS*

IAEA, 2007. *Basic Principles Objectives IAEA Nuclear Energy Series Determination and Use of Scaling Factors for Waste Characterization in Nuclear Power Plants*.

NEA.,2011. *Decontamination and Dismantling of Radioactive Concrete Structures A Report of the NEA Co-operative Programme on Decommissioning (CPD) Decontamination and Dismantling of Radioactive Concrete Structures,*.

ThermoFinnigan,2001, *ELEMENT2 Operating Manual,*

Miyake, Y., Matsuzaki, H., Fujiwara, T., Saito, T., Yamagata, T., Honda, M., Muramatsu, Y., 2012. Isotopic ratio of radioactive iodine ($^{129}I/^{131}I$) released from Fukushima Daiichi NPP accident,Geochemical Journal,46, 327-333

NDA 2016, gov.uk., n.d. nda inventory - https://ukinventory.nda.gov.uk/the-2016-inventory/2016-uk-data.

RAENG 2012,The Royal Academy of Engineering, 2012, *Nuclear Construction Lessons Learned Guidance on best practice: concrete Engineering the Future,*

Nuclear Decommissioning: Decommission nuclear facilities - World Nuclear Association. [Online] Available at: https://www.world-nuclear.org/information-library/nuclear-fuel-cycle/nuclear-wastes/decommissioning-nuclear-facilities.aspx

gov.uk, *Nuclear Provision: the cost of cleaning up Britain's historic nuclear sites - GOV.UK.* [Online] Available at: https://www.gov.uk/government/publications/nuclear-provision-explaining-the-cost-of-cleaning-up-britains-nuclear-legacy/nuclear-provision-explaining-the-cost-of-cleaning-up-britains-nuclear-legacy

Nucleonica. [Online]
Available at: https://nucleonica.com/

Ohno, T, Muramatsu, Y., Toyama, C., Nakano, K., Kakuta, S., Matsuzaki., 2013, Determination of ^{129}I in Fukushima Soil Samples by ICP-MS with an Octopole Reaction System.,Analytical Sciences, 29, 271-274

IAEA, 1998. Radiological Characterization of Shut Down Nuclear Reactors for Decommissioning Purposes.

Thermo Finnigan ELEMENT2 Operating Manual | Calibration | Regression Analysis. [Online] Available at: https://www.scribd.com/document/240504469/Thermo-Finnigan-ELEMENT2-Operating-Manual

NDA, 2010. *Understanding activities that produce radioactive wastes in the UK*.

Baker, J., Peate, D., Waight, T. & Meyzen, C., 2004. Pb isotopic analysis of standards and samples using a 207Pb-204Pb double spike and thallium to correct for mass bias with a double-focusing MC-ICP-MS. *Chemical Geology,* 15 11, 211(3-4), pp. 275-303.

Bandura, D. R., Baranov, V. I., Litherland, A. E. & Tanner, S. D., 2006. Gas-phase ion-molecule reactions for resolution of atomic isobars: AMS and ICP-MS perspectives. *International Journal of Mass Spectrometry,* 1 9, 255-256(1-3), pp. 312-327.

Beals, D. & Hayes, D., 1995. Technetium-99, iodine-129 and tritium in the waters of the Savannah River Site. *Science of The Total Environment,* 1 12, Volume 173-174, pp. 101-115.

Becker, J. S., 2002. *State-of-the-art and progress in precise and accurate isotope ratio measurements by ICP-MS and LA-ICP-MS., Journal of Analytical Atomic Spectrometry, 17,* 1172-1185.

Becker, J. S., 2005. *Inductively coupled plasma mass spectrometry (ICP-MS) and laser ablation ICP-MS for isotope analysis of long-lived radionuclides, International Journal of Mass Spectrometry, Volume 232, Issue 2-3, pp. 183-195*

Becker, J. S. & Dietze, H.-J., 1997, double-focusing Sector Field Inductively coupled Plasma MAss Spectrometry for Highly Sensitive Multi-element and Isotopic Analysis, Journal of analytical Atomic Spectrometry.Volume 12, pp. 881-889.

Becker, J. S., Matusch, A., Palm, C., Salber, D., Morton, K.A., Becker, J.S., 2010. Bioimaging of metals by laser ablation inductively coupled plasma mass spectrometry (LA-ICP-MS). Metallomics, Volume 2, pp. 104-111.

Bienvenu, P., Brochard, E., Excoffier, E. & Piccione, M., 2004. *Determination of Iodine 129 by ICP-QMS in environmental samples.*, pp. 423-428.

Boomer, D. W. & Powell, M. J., 1987. *Determination of Uranium in Environmental Samples Using Inductively Coupled Plasma Mass Spectrometry, Analytical Chemistry, pp. 2810-2813*

Boulyga, S. F., 2009. CALCIUM ISOTOPE ANALYSIS BY MASS SPECTROMETRY, Mass Spectrometry Reviews, 29, pp. 685-716.

Boulyga, S. F. & Becker, J. S., 2002, Improvement of abundance sensitivity in a quadrupole-based ICP-MS instrument with a hexapole collision cell, J. Anal. At. Spectrom., 17, 1202-1206

Boulyga, S. F., Testa, C., Desideri, D. & Becker, J. S., 2001. Optimisation and application of ICP-MS and alpha-spectrometry for determination of isotopic ratios of depleted uranium and plutonium

in samples collected in Kosovo, Journal of Analytical Atomic Spectrometry, Volume 16, pp. 1283-1289

Braysher, E., Russell, B., Woods, S., García-Miranda, M., Ivanoc, P., Bouchard, B., Read, D., 2019. Complete dissolution of solid matrices using automated borate fusion in support of nuclear decommissioning and production of reference materials. *Journal of Radioanalytical and Nuclear Chemistry,* Volume 321, pp. 183-196.

Brown, C. F., Geiszler, K. N. & Lindberg, M. J., 2007. Analysis of 129I in groundwater samples: Direct and quantitative results below the drinking water standard. *Applied Geochemistry,* 3, 22(3), pp. 648-655.

Brown, R. M., Long, S. E. & Pickford, C. J., 1988. The measurement of long lived radionuclides by non-radiometric methods. *Science of the Total Environment, The,* 70(C), pp. 265-274.

Bryant, C. J., Mcculloch, M. T. & Bennett, V. C.,2002. Impact of matrix effects on the accurate measurement of Li isotope ratios by inductively coupled plasma mass spectrometry (MC-ICP-MS) under ''cold'' plasma conditions, Journal of Analytical Atomic Spectrometry, Volume 18, pp. 734-737

Bu, W., Ni, Y., Steinhouser, G., Zheng, W., Zheng, J., Furuta, N., 2018. *The role of mass spectrometry in radioactive contamination assessment after the Fukushima nuclear accident. Journal of Analytical Atomic Spectrometry, Volume 33, pp. 519-546*

Bu, W., Tang, L., Liu, X., Wang, Z., Fukuda, M., Zheng, J., Aono, T., Hu, S., Wang, X., 2019. Ultra-trace determination of the 135 Cs/ 137 Cs isotopic ratio by thermal ionization mass spectrometry with application to Fukushima marine sediment samples, Journal of Analtical Atomic Spectrometry, Volume 34, pp. 301-309

Caborn, J. A., 2017. *Migration and distribution of 237 Np in saltmarsh sediments,* Phd Thesis.

Cao, L., Zheng, J., Tsukada, H., Pan, S., Wang, Z., Tagami, K., Uchida, S., 2016. Simultaneous determination of radiocesium (135Cs, 137Cs) and plutonium (239Pu, 240Pu) isotopes in river suspended particles by ICP-MS/MS and SF-ICP-MS. *Talanta,* 1 10, Volume 159, pp. 55-63.

Clases, D., Birka, M., Sperling, M., Faust, A., Karst, U., 2017. Isobaric dilution analysis as a calibration tool for long lived radionuclides in ICP-MS. *Journal of Trace Elements in Medicine and Biology,* 1 3, Volume 40, pp. 97-103.

Croudace, I. W., Russell, B. C. & Warwick, P. W., 2017. *Plasma source mass spectrometry for radioactive waste characterisation in support of nuclear decommissioning: A review, Journal of Analytical Atomic Spectrometry, Volume 32, pp. 494-526*

Croudace, I. W., Warwick, P. E. & Marsh, R., 2017. A suite of robust radioanalytical techniques for the determination of tritium and other volatile radionuclides in decommissioning wastes and environmental matrices. *Fusion Science and Technology,* 1 4, 71(3), pp. 290-295.

Croudace, I. W., Warwick, P. E., Reading, D. G. & Russell, B. C., 2016. Recent contributions to the rapid screening of radionuclides in emergency responses and nuclear forensics, TrAC Trends in Analytical Chemistry, Volume 85, pp. 120-129

Cundy, A. B. & Croudace, I. W., 2017. The Fate of Contaminants and Stable Pb Isotopes in a Changing Estuarine Environment: 20 Years On.. *Environmental science & technology,* 5 9, 51(17), pp. 9488-9497.

Dae, J. K., Warwick, P. E. & Croudace, I. W., 2008. Tritium speciation in nuclear reactor bioshield concrete and its impact on accurate analysis. *Analytical Chemistry,* 15 7, 80(14), pp. 5476-5480.

Devell, L. & Johansson, K., 1994. *SKI Report 94:29 NEA/CSNI/R(94)28 Specific Features of Cesium Chemistry and Physics Affecting Reactor Accident Source Term Predictions*

Duckworth, G. and Woods, G., 2016. Introduction Accurate analysis of neptunium 237 in a uranium matrix, using ICP-QQQ with MS/MS Application note. Agilent

Dunne, J. A., MArtin, P.G., Yamashiki, Y., Ang., I.X.Y., Scott, T.B., Richards, D.A.,2018. Spatial pattern of plutonium and radiocaesium contamination released during the Fukushima Daiichi nuclear power plant disaster, Scientific Reports, Volume 8, article number: 16799 (2018)

Dyer, A., Hriljac, J., Evans, N., Stokes, I., Rand, P., Kellet, S., Harjula, R., Moller, T., Maher, Z., Heatlie-Branson, R., Austin, J., Williamson-Owens, S., Higgins-Bos, M., Smith, K., O'Brian, L., Smith, N., Bryan, N., 2018, The use of columns of the zeolite clinoptilolite in the remediation of aqueous nuclear waste streams. *Journal of Radioanalytical and Nuclear Chemistry,* 1 12, 318(3), pp. 2473-2491.

Ellam, R. M., 2010. The graphical presentation of lead isotope data for environmental source apportionment. *Science of the Total Environment,* 7, 408(16), pp. 3490-3492.

Ewing, R. C., 2015. *Long-term storage of spent nuclear fuel, Nature Materials, Volume 14, pp. 252-257.*

Ežerinskis, Ž. Spolaor, A., Kirchgeorg, T., Cozzi, G., Vallelonga, P., Kjær, H.A., Šapolaitė, J., Barbante, C., Kruteikienė, R., 2014. Determination of 129I in Arctic snow by a novel analytical approach using IC-ICP-SFMS. *Journal of Analytical Atomic Spectrometry,* 29(10), pp. 1827-1834.

Fehn, U., Snyder, G. T. & Muramatsu, Y., 2007. Iodine as a tracer of organic material: 129I results from gas hydrate systems and fore arc fluids. *Journal of Geochemical Exploration,* 10, 95(1-3), pp. 66-80.

Field, K. G., Remec, I. & Pape, Y. L., 2015. Radiation effects in concrete for nuclear power plants - Part I: Quantification of radiation exposure and radiation effects. *Nuclear Engineering and Design,* Volume 282, pp. 126-143.

Flora, G., Gupta, D. & Tiwari, A., 2012. *Toxicity of lead: A review with recent pdates. Interdisciplinary Toxicology, Vol. 5(2), pp. 47-58*

Fritz, B. G. & Patton, G. W., 2006. Monitoring iodine-129 in air and milk samples collected near the Hanford Site: An investigation of historical iodine monitoring data. *Journal of Environmental Radioactivity,* 86(1), pp. 64-77.

Fujiwara, H., Kawabata, K., Suzuki, J. & Shikino, O., 2011. Determination of 129I in soil samples by DRC-ICP-MS. *Journal of Analytical Atomic Spectrometry,* 12, 26(12), pp. 2528-2533.

Gioia, S. M., Babinski, M., Weiss, D.J., Spiro, B., Kerr, A.A.F.S., Veríssimo, T.G., Ruiz, I., Prates, J.C.M., 2017. An isotopic study of atmospheric lead in a megacity after phasing out of leaded gasoline. *Atmospheric Environment,* 1 1, Volume 149, pp. 70-83.

Gómez-Guzmán, J. M., Enamorado-Báez, S. M., Pinto-Gómez, A. R. & Abril-Hernández, J. M., 2011. Microwave-based digestion method for extraction of 127I and 129I from solid material for measurements by AMS and ICP-MS. *International Journal of Mass Spectrometry,* 1 6, 303(2-3), pp. 103-108.

Grindlay, G., Mora, J., De Loos-Vollebregt, M. & Vanhaecke, F., 2013. A systematic study on the influence of carbon on the behavior of hard-to-ionize elements in inductively coupled plasma-mass spectrometry. *Spectrochimica Acta - Part B Atomic Spectroscopy,* 1 8, Volume 86, pp. 42-49.

Hansen, V., Roos, P., Aldahan, A., Hou, X., Possnert, G., 2011. Partition of iodine (129I and 127I) isotopes in soils and marine sediments. *Journal of Environmental Radioactivity,* 102(12), pp. 1096-1104.

Hasegawa, H., Kakuichi, H., Akata, N., Ohtsuka, Y., Hasamatsu, S.., 2017. Regional and global contributions of anthropogenic iodine-129 in monthly deposition samples collected in North East

Japan between 2006 and 2015. *Journal of Environmental Radioactivity,* 1 5, Volume 171, pp. 65-73.

Hocking, W. H., Verrall, R. A. & Muir, I. J., 2001. *Migration behaviour of iodine in nuclear fuel,* Journal of Nuclear Materials, Volume 294, pp. 45-52

Hoernle, K., Hauff, F., Werner, R., Bogaard, P.V.D, Gibbons, A.D., Conrad, S., Müller, R.D., 2011. Origin of Indian Ocean Seamount Province by shallow recycling of continental lithosphere. *Nature Geoscience,* 12, 4(12), pp. 883-887.

Honda, M., Matsuzaki, H., Miyake, Y., Maejima, Y., Yamagata, T., Nagai, H., 2015. Depth profile and mobility of 129I and 137Cs in soil originating from the Fukushima Dai-ichi Nuclear Power Plant accident. *Journal of Environmental Radioactivity,* 1 8, Volume 146, pp. 35-43.

Honda, M., Matsuzaki, H., Nagai, H. & Sueki, K., 2017. Depth profiles and mobility of 129I originating from the Fukushima Dai-ichi nuclear power plant disaster under different land uses. *Applied Geochemistry,* 1 10, Volume 85, pp. 169-179.

Horn, I., Rudnick, R. L. & Mcdonough, W. F., 2000. *Precise elemental and isotope ratio determination by simultaneous solution nebulization and laser ablation-ICP-MS: application to U-Pb geochronology,* Chemical Geology, Volume 167, pp. 405-425

Houk, R. S.,1986. *Instrumentation, Mass Spectrometry of Inductively Coupled Plasmas,Analytical Chemistry, Vol. 58*. 97A

Hou, X., 2005. *Radiochemical determination of 41Ca in nuclear reactor concrete.* s.l., R. Oldenbourg Verlag GmbH, pp. 611-617.

Hou, X., 2007. Radiochemical analysis of radionuclides difficult to measure for waste characterization in decommissioning of nuclear facilities. *Journal of Radioanalytical and Nuclear Chemistry,* 273(1), pp. 43-48.

Hou, X., Hansen, V., Aldahan, A., Possnert, G., Lind, O.C., Lujaniene, G., 2009. *A review on speciation of iodine-129 in the environmental and biological samples, Analytica Chemica Acta, Volume 632, pp. 181-196*

Hou, X., Povinec, P.P., Zhang, L., Shi, K., Biddulph, D., Chang, C.C., Fan, Y., Golser, R., Hou, Y., Ješkovský, M., Jull, A.J.T., Liu, Q., Lou, M., Steier, P., Zhou, W., 2013. Iodine-129 in seawater offshore fukushima: Distribution, inorganic speciation, sources, and budget. *Environmental Science and Technology,* 2 4, 47(7), pp. 3091-3098.

Hou, X., Zhou, W., Chen, N., Zhang, L., Liu, Q., Luo, M., Fan, Y., Liang, W., Fu., Y., 2010. Determination of ultralow level 129I/127I in natural samples by separation of microgram carrier free iodine and accelerator mass spectrometry detection. *Analytical Chemistry,* 15 9, 82(18), pp. 7713-7721.

Hu, K. & Houk, R. S., 1993. *Inductively Coupled Plasma Mass Spectrometry with an Enlarged Sampling Orifice and Offset Ion Lens. II. Polyatomic Ion Interferences and Matrix Effects,* Journal of the American Society for Mass Spectrometry, Volume 4, pp. 28-37

Hu, Q. H., Weng, J. Q. & Wang, J. S., 2010. Sources of anthropogenic radionuclides in the environment: A review. *Journal of Environmental Radioactivity,* 6, 101(6), pp. 426-437.

IAEA 1999, International Atomic Energy Agency. & International Labour Office., 1999. *Occupational radiation protection.* s.l.:International Atomic Energy Agency.

Izmer, A. V., Boulyga, S. F. & Becker, J. S., 2003. Determination of129I/127i isotope ratios in liquid solutions and environmental soil samples by ICP-MS with hexapole collision cell. *Journal of Analytical Atomic Spectrometry,* 18(11), pp. 1339-1345.

Jacobs, J. L., 2015. *Diagnostic studies of ion beam formation in inductively coupled plasma mass spectrometry with the collision reaction interface,* PhD thesis

Jakubowski, N., 2008. *Analytical plasma ion sources for elemental mass spectrometry: Where are we coming from-where are we going to?.Journal of Analytical Atomic Spectrometry, Volume 23*, pp. 673-684.

Jerše, A., Raćimović, R., Maršić, N.K., Germ., M., Šircelj, H., Stibilj, V., 2018. Determination of iodine in plants by ICP-MS after alkaline microwave extraction. *Microchemical Journal,* 1 3, Volume 137, pp. 355-362.

Kalmykov, S. N., Aliev, R.A., Sapohnikov, D.Y., Sapozhnikov, Y.A., Afinogenov., A.M., 2004. Determination of Np-237 by radiochemical neutron activation analysis combined with extraction chromatography. *Applied Radiation and Isotopes,* 60(2-4), pp. 595-599.

Kerl, G., Sabine Becker A N D Hans-Joachim D I E T Z E, J. & Dannecker, W., 1996. *Determination of Iodine Using a Special Sample Introduction System Coupled to a Double-focusing Sector Field Inductively Coupled Plasma Mass Spectrometer, Journal of Analytical Atomic Spectrometry, Volume 11, pp. 723-726*

Komura, K. & Hamajima, Y., 2004. *Ogoya underground laboratory for the measurement of extremely low levels of environmental radioactivity: Review of recent projects carried out at OUL, Applied Radiation and Isotopes,* pp. 185-189.

Kučera, J., 2007. Methodological developments and applications of neutron activation analysis. *Journal of Radioanalytical and Nuclear Chemistry,* 273(2), pp. 273-280.

Kuritani, T. & Nakamura, E., n.d. Highly precise and accurate isotopic analysis of small amounts of Pb using 205 Pb-204 Pb and 207 Pb-204 Pb, two double spikes, Journal of Analytical Atomic Spectrometry, Volume 18, pp. 1464-1470

Kutschera, W., 2005. *Progress in isotope analysis at ultra-trace level by AMS, International Journal of Mass Spectrometry, Volume 242, pp. 145-160*

Lang, A. R., 2017. *Contamination and Decontamination of Steel Components,* PhD Thesis

Lariviere, D., Taylor, V. F., Evans, R. D. & Cornett, R. J., 2006. *Radionuclide determination in environmental samples by inductively coupled plasma mass spectrometry, Spectrochemica Acta Part B: Atomic Spectroscopy, Volume 61, pp. 877-904*

Larsen, M. M., Blusztajn, J. S., Andersen, O. & Dahllöf, I., 2012. Lead isotopes in marine surface sediments reveal historical use of leaded fuel. *Journal of Environmental Monitoring,* 11, 14(11), pp. 2893-2901.

Lehto, J., Räty, T., Hou, X., Paatero, J., Aldahan, A., Possnert, G., Flinkman, J., Kankaanpää, H., 2012. Speciation of 129I in sea, lake and rain waters. *Science of the Total Environment,* 1 3, Volume 419, pp. 60-67.

Li, K., Vogel, E. & Krähenbühl, U., 2009. Measurement of I-129 in environmental samples by ICP-CRI-QMS: Possibilities and limitations. *Radiochimica Acta,* 97(8), pp. 453-458.

Livens, F. R. & Loveland, P. J., 1988. The influence of soil properties on the environmental mobility of caesium in Cumbria. *Soil Use and Management,* 4(3), pp. 69-75.

Łokas, E., Zawierucha, K., Cwanek, A., Szufa, K., Gaca, P., Mietelski, J.W., Tomankiewicz, E., 2018. The sources of high airborne radioactivity in cryoconite holes from the Caucasus (Georgia). *Scientific Reports,* 1 12.8(1).

Longerich, H., Fryer, B. & Strong, D., 1987. Determination of lead isotope ratios by inductively coupled plasma-mass spectrometry (ICP-MS). *Spectrochimica Acta Part B: Atomic Spectroscopy,* 1, 42(1-2), pp. 39-48.

Maeda, K., Sasaki, S., Kumai, M., Sato, I., Suto, M., Ohsaka, M., Goto, T., Sakai, H., Chigira, T., Murata, H., 2014. Distribution of radioactive nuclides of boring core samples extracted from concrete structures of reactor buildings in the Fukushima Daiichi Nuclear Power Plant. *Journal of Nuclear Science and Technology,* 3 8, 51(7-8), pp. 1006-1023.

Makishima, A. & Nakamura, E., 2010. Precise isotopic determination of Hf and Pb at sub-nano gram levels by MC-ICP-MS employing a newly designed sample cone and a pre-amplifier with a 1012 ohm register. *Journal of Analytical Atomic Spectrometry,* 11, 25(11), pp. 1712-1716.

Makishima, A., Nath, B. N. & Nakamura, E., 2008. New sequential separation procedure for Sr, Nd and Pb isotope ratio measurement in geological material using MC-ICP-MS and TIMS. *Geochemical Journal,* 42(3), pp. 237-246.

Mason, L. H., Harp, J. P. & Han, D. Y., 2014. *Pb neurotoxicity: Neuropsychological effects of lead toxicity, Hindawi, Volume 2014, pages 8*

Matsunaka, T., Sasa, K., Sueki, K., Takahashi, T., Satuo, Y., Matsumura, M., Kinoshita, N., Kitagawa, J., Matsuzaki, H., 2016. Pre- and post-accident 129 I and 137 Cs levels, and 129 I/ 137 Cs ratios in soil near the Fukushima Dai-ichi Nuclear Power Plant, Japan. *Journal of Environmental Radioactivity,* 1 1, Volume 151, pp. 209-217.

May, T. W. & Wiedmeyer, R. H., 1998. *S A Atomic Spectroscopy A Table of Polyatomic Interferences in ICP-MS, Atomic Spectroscopy, Volume 19, pp. 150-155*

Meeks, A. M., Giaquinto, J. M. & Keller, J. M., 1998. *Application of ICP-MS radionuclide analysis to "Real World"samples of Department of Energy radioactive waste,* Journal of Radioanalytical and Nuclear Chemistry, Volume 234, pp. 131-136

Merz, S., Shozugawa, •. K. & Steinhauser, •. G., 2015. Effective and ecological half-lives of 90 Sr and 137 Cs observed in wheat and rice in Japan. *Journal of Radioanalytical and Nuclear Chemistry,* Volume 307.

Michel, R., Baraoui, A., Gorny, M., Jakob, D., Sachse, R., Tosch, L., Nies, H., Goroncy, I., Herrmann, J., Synal, H.A., Stocker, M., Alfimov, V., 2012. Iodine-129 and iodine-127 in European seawaters and in precipitation from Northern Germany. *Science of the Total Environment,* 1 3, Volume 419, pp. 151-169.

Miller, H., Croudace, I.W., Bull, J.M., Cotterill, C., Dix, J.K., Taylor, R., 2014. A 500 year sediment lake record of anthropogenic and natural inputs to windermere (English Lake District) using

double-spike lead isotopes, radiochronology, and sediment microanalysis. *Environmental Science and Technology,* 1 7, 48(13), pp. 7254-7263.

Miranda, M. G., Russell, B. & Ivanov, •. P., 2017. Measurement of 151 Sm in nuclear decommissioning samples by ICP-MS/MS. *Journal of Radioanalytical and Nuclear Chemistry,* Volume 316.

Moran, J. E., Oktay, S. D. & Santschi, P. H., 2002. Sources of iodine and iodine 129 in rivers. *Water Resources Research,* 8, 38(8), pp. 24-1-24-10.

Muramatsu, Y., Yoshida, S., Fehn, U., Amachi, S., Ohmomo, Y., 2004. *Studies with natural and anthropogenic iodine isotopes: Iodine distribution and cycling in the global environment, Journal of Environmental Radioactivity, Volume 74*, pp. 221-232.

Nakano, K., Shikamori, Y., Sugiyama, N. & Kakuta, S., n.d. *The ultratrace determination of iodine 129 in aqueous samples using the 7700x ICP-MS with oxygen reaction mode Application note, Agilent*

Neeb, K.-H., 1997. *Tile Hadiochernistry of Nuclear Power Plants with Light Water Reactors With a preface written by Gunter Marx,* Book

Niu, H., 1994, *Fundamental studies of the plasma extraction and ion beam formation processes in inductively coupled plasma mass spectrometry, PhD thesis*

O'brien, E., 2011. *Chronology of Leaded Gasoline / Leaded Petrol History, The Lead Group Incorporated*

Ohno, T., Muramatsu, Y., Shikamori, Y., Toyama, C., Okabe, N., Matsuaki, H., 2013. Determination of ultratrace ^{129}I in soil samples by Triple Quadrupole ICP-MS and its application to Fukushima soil samples. *Journal of Analytical Atomic Spectrometry,* 28(8), pp. 1283-1287.

Olesik, J. W. & Jiao, S., 2017. Matrix effects using an ICP-MS with a single positive ion lens and grounded stop: Analyte mass dependent?. *Journal of Analytical Atomic Spectrometry,* 1 5, 32(5), pp. 951-966.

Oliveira, A. A., Trevizan, L. C. & Nóbrega, J. A., 2010. *Iodine determination by inductively coupled plasma spectrometry.* Applied Spectroscopy Reviews, Volume 45, pp. 447-473

Parus, J. & Raab, W., 1988. Analysis of uranium and plutonium materials by radiometric methods. *International Journal of Radiation Applications and Instrumentation. Part,* 39(4), pp. 315-322.

Petrov, P., Russell, B., Douglas, D. N. & Goenaga-Infante, H., n.d. Interference-free determination of sub ng kg−1 levels of long-lived 93Zr in the presence of high concentrations (μg kg−1) of 93Mo and 93Nb using ICP-MS/MS, Analytical and Bioanalytical Chemistry, Volume 410, pp. 1029-1037

Potter, D., 2008. A commercial perspective on the growth and development of the quadrupole ICP-MS market, Journal of Analytical Atomic Spectrometry, Volume 23(5)

Qiao, J., Hansen, V., Hou, X., Aldahan, A., Possnert, G., 2012. Speciation analysis of 129I, 137Cs, 232Th, 238U, 239Pu and 240Pu in environmental soil and sediment. *Applied Radiation and Isotopes,* 8, 70(8), pp. 1698-1708.

Qiao, J., Shi, K., Hou, X., Nielsen, S., Roos, P., 2014. Rapid multisample analysis for simultaneous determination of anthropogenic radionuclides in marine environment. *Environmental Science and Technology,* 1 4, 48(7), pp. 3935-3942.

Reid, H. J., Bashammakh, A.A., Goodall, P.S., Landon, M.R., O'Connor, C., Sharp, B.L., 2008. Determination of iodine and molybdenum in milk by quadrupole ICP-MS. *Talanta,* 15 3, 75(1), pp. 189-197.

Rousis, N. I., Pasias, I. N. & Thomaidis, N. S., 2014. Attenuation of interference in collision/reaction cell inductively coupled plasma mass spectrometry, using helium and hydrogen as cell gases-application to multi-element analysis of mastic gum. *Analytical Methods,* 7 8, 6(15), pp. 5899-5908.

Rusconi, R., Forte, M., Caresana, M., Bellinzona, S., Cazaniga, M.T., Sgorbati, G., 2006. The evaluation of uncertainty in low-level LSC measurements of water samples. *Applied Radiation and Isotopes,* 10, 64(10-11), pp. 1124-1129.

Russell, B. C., Croudace, I. W. & Warwick, P. E., 2015. *Determination of 135Cs and 137Cs in environmental samples: A review, Analytica Chimica Acta, Volume 890, pp. 7-20*

Russell, B. C., Croudace, I. W., Warwick, P. E. & Milton, J. A., 2014. Determination of precise 135Cs/137Cs ratio in environmental samples using sector field inductively coupled plasma mass spectrometry. *Analytical Chemistry,* 2 9, 86(17), pp. 8719-8726.

Russell, B., García-Miranda, M. & Ivanov, P., 2017. Development of an optimised method for analysis of 90Sr in decommissioning wastes by triple quadrupole inductively coupled plasma mass spectrometry. *Applied Radiation and Isotopes,* 1 8, Volume 126, pp. 35-39.

Sahoo, S. K., Muramatsu, Y., Yoshida, S., Matsuaki, H., Rühm, W., 2009. Determination of 129I and 127I Concentration in Soil Samples from the Chernobyl 30-km Zone by AMS and ICP-MS. *Journal of Radiation Research,* 50(4), pp. 325-332.

Scarciglia, F. & Barca, D., 2017 A powerful tool for assessing distribution and fate of potentially toxic metals (PTMs) in soils: integration of laser ablation spectrometry (LA-ICP-MS) on thin sections with soil micromorphology and geochemistry, Enviornmental Science and Pollution Research International, Volume 24, pp. 9776-9790

Schmidt, A., Schnabel, C., Handl, J., Jakob, D., Michel, R., Synal, H.A., Lopez, J.M., Suter, M., 1998. *On the analysis of iodine-129 and iodine-127 in environmental materials by accelerator mass spectrometry and ion chromatography, Science Total Environment, Volume 223, pp. 131-156*

Shah, M., Wuilloud, R. G., Kannamkumarath, S. S. & Caruso, J. A., 2005. Iodine speciation studies in commercially available seaweed by coupling different chromatographic techniques with UV and ICP-MS detection. *Journal of Analytical Atomic Spectrometry,* 20(3), pp. 176-182.

Shelor, C. P. & Dasgupta, P. K., 2011. *Review of analytical methods for the quantification of iodine in complex matrices, Analytica Chimica Acta, Volume 702, pp. 16-36*

Shikamori, Y., Nakano, K., Sugiyama, N. & Kakuta, S., 2012. *The ultratrace determination of iodine 129 using the Agilent 8800 Triple Quadrupole ICP-MS in MS/MS mode, Agilent, Technical Note*

Shozugawa, K., Riebe, B., Clemens, W., Brandl., A., Steinhouser, G., 2016. Fukushima-derived radionuclides in sediments of the Japanese Pacific Ocean coast and various Japanese water samples (seawater, tap water, and coolant water of Fukushima Daiichi reactor unit 5). *Journal of Radioanalytical and Nuclear Chemistry,* Volume 307.

Smith, C. A., Martinez, M. A., Veirs, D. K. & Cremers, D. A., 2002. Pu-239/Pu-240 isotope ratios determined using high resolution emission spectroscopy in a laser-induced plasma. *Spectrochimica Acta - Part B Atomic Spectroscopy,* 57(5), pp. 929-937.

Snyder, G., Aldahan, A. & Possnert, G., 2010. Global distribution and long-term fate of anthropogenic129i in marine and surface water reservoirs. *Geochemistry, Geophysics, Geosystems,* 4.11(4).

Steinhauser, G., Brandl, A. & Johnson, T. E., 2014. *Comparison of the Chernobyl and Fukushima nuclear accidents: A review of the environmental impacts, Science of The Total Environment, pp. 800-817*

Suárez, J. A., Espartero, A. G. & Rodríguez, M., 1996. Radiochemical analysis of 129I in radioactive waste streams. *Nuclear Instruments and Methods in Physics Research, Section A: Accelerators, Spectrometers, Detectors and Associated Equipment,* 1 2, 369(2-3), pp. 407-410.

Sugiyama, N. & Nakano, K., 2014. *Reaction data for 70 elements using O 2 , NH 3 and H 2 gases with the Agilent 8800 Triple Quadrupole ICP-MS Technical note,* Agilent

Suzuki, T., Kitamura, T., Kabuto, S., Togawa, O., Amano., 2006. High Sensitivity Measurement of Iodine-129/Iodine-127 Ratio by Accelerator Mass Spectrometry. *Journal of Nuclear Science and Technology,* 43(11), pp. 1431-1435.

Szidat, S., Schmidt, A., Handl, J., Jakob, D., Botsch, W., Michel, R., Synal, H.A., Schnabel, C., Suter, M., Lópe-Gutiérrez, J.M., Städe, W., 2000. *Iodine-129: Sample preparation, quality control and analyses of pre-nuclear materials and of natural waters from Lower Saxony, Germany, Nuclear Instruments and Methods in Physics Research Section B: Beam Interactions with Materials and Atoms, Volume 172, pp. 699-710*

Taddei, M. H., Macacini, J.F., Vicente, R., Marumo, J.T., Sakata, S., Terremoto, L.A.A., 2013. Determination of 63 Ni and 59 Ni in spent ion-exchange resin and activated charcoal from the IEA-R1 nuclear research reactor. *Applied Radiation and Isotopes,* 7, Volume 77, pp. 50-55.

Takaku, Y., Shimamura, T., Masuda, K. & Igarashi, Y., 1995. *Iodine Determination in Natural and Tap Water using Inductively Coupled Plasma Mass Spectrometry,* Analytical Science, Volume 11, pp. 823-827

Tanimizu, M., Sugiyama, N., Ponzevera, E. & Bayon, G., 2013. Determination of ultra-low 236U/238U isotope ratios by tandem quadrupole ICP-MS/MS. *Journal of Analytical Atomic Spectrometry,* 9, 28(9), pp. 1372-1376.

Tanner, S. D., Baranov, V. I. & Bandura, D. R., 2002. *Reaction cells and collision cells for ICP-MS: a tutorial review,* Spectrochimica Acta Part B, Atomic Spectroscopy, Volume 57, pp. 1361-1452

Taylor, R. N., Ishiuka, O., Michalik, A., Milton, J.A., Croudace, I.W., 2015. Evaluating the precision of Pb isotope measurement by mass spectrometry. *Journal of Analytical Atomic Spectrometry,* 1 1, 30(1), pp. 198-213.

Terrasi, F., Boumpane, R., D'Onofrio, A., Esposito, A, Gialanella, L., Marzaioli, F., Petraglia, A., Porzio, G., Sabbarese, C., Scolamacchia, F., Sirignano, C., 2018. AMS assessment of U-contamination of structural materials of the Garigliano NPP under decommissioning. *Journal of Environmental Radioactivity,* 1 7, Volume 187, pp. 144-150.

Thirlwall, M. F., 2002. Multicollector ICP-MS analysis of Pb isotopes using a 207pb-204pb double spike demonstrates up to 400 ppm/amu systematic errors in TI-normalization. *Chemical Geology,* 184(3-4), pp. 255-279.

Tian, X., Êkan, H., Barbaste, M. & Adams, F. C., 2000. Full Paper Accuracy and precision of lead isotope ratios in wines measured by axial inductively coupled plasma time of light mass spectrometry, Journal of Analyical Atomic Spectrometry, Volume 15, pp. 829-835

Todorov, T. I. & Gray, P. J., 2016. Analysis of iodine in food samples by inductively coupled plasma-mass spectrometry. *Food Additives and Contaminants - Part A Chemistry, Analysis, Control, Exposure and Risk Assessment,* 1 2, 33(2), pp. 282-290.

Trojanowicz, M., Kołacińska, K. & Grate, J. W., 2018. A review of flow analysis methods for determination of radionuclides in nuclear wastes and nuclear reactor coolants. *Talanta,* 1 6, Volume 183, pp. 70-82.

van Es, E. M., Russell, B. C., Ivanov, P. & Read, D., 2017. Development of a method for rapid analysis of Ra-226 in groundwater and discharge water samples by ICP-QQQ-MS. *Applied Radiation and Isotopes,* 1 8, Volume 126, pp. 31-34.

Vonderheide, A. P., Zoriy, M., Izmer, A., Muller, C., Pickhardt, C., Caruso, J., Ostapchuk, P., Becker, J.S., 2004. Determination of 90 Sr at ultratrace levels in urine by ICP-MS, Journal of Analytical Atomic Spectrometry, Volume 19, pp. 675-680

Walder, A. J. & Furuta, N., 1993. High-Precision Lead Isotope Ratio Measurement by Inductively Coupled Plasma Multiple Collector Mass Spectrometry. *analytical sciences,* 9(5), pp. 675-680.

Walling, S. A., Kinoshita, H., Bernal, S.A., Collier, N.C., Provis, J.L., 2015. Structure and properties of binder gels formed in the system Mg(OH) 2SiO 2H2O for immobilisation of Magnox sludge. *Dalton Transactions,* 7 5, 44(17), pp. 8126-8137.

Warwick, P. E., Russell, B. C., Croudace, I. & Zacharauskas, Ž., 2019. Evaluation of inductively coupled plasma tandem mass spectrometry for radionuclide assay in nuclear waste characterisation. *Journal of Analytical Atomic Spectrometry,* 34(9), pp. 1810-1821.

Woods, G., 2014. *Lead isotope analysis: Removal of 204 Hg isobaric interference from 204 Pb using ICP-QQQ in MS/MS mode Application note Geochemistry and isotope analysis,* Agilent, Application note

Wu, Z., Zhou, Y., Xu, N., Tao, L., 2013. Extractive electrospray ionization mass spectrometry for sensitive detection of gaseous radioactive iodine-129. *Journal of Analytical Atomic Spectrometry,* 28(5), pp. 697-701.

Xu, Y., Qiao, J., Hou, X., Pan, S., Roos., P., 2014. Determination of plutonium isotopes (238Pu, 239Pu, 240Pu, 241Pu) in environmental samples using radiochemical separation combined with radiometric and mass spectrometric measurements. *Talanta,* 15 2, Volume 119, pp. 590-595.

Yamazaki, E., Nakai, S., Sahoo, Y., Yokoyama, T., Mifune, H., Saito, T., Chen, J., Takagi, N., Hokanishi, N., Yasuda, A., 2014. Feasibility studies of Sn isotope composition for provenancing ancient bronzes. *Journal of Archaeological Science,* 1 12, Volume 52, pp. 458-467.

Yang, G., Tazoe, H. & Yamada, M., 2018. Improved approach for routine monitoring of 129I activity and 129I/127I atom ratio in environmental samples using TMAH extraction and ICP-MS/MS. *Analytica Chimica Acta,* 30 5, Volume 1008, pp. 66-73.

Yiou, F., Raisbeck, G. & Imbaud, H., 2004. *Extraction and AMS measurement of carrier free 129I/ 127I from seawater.* Nuclear Instruments and Methods in Physics Research Section B: Beam Interactions with Materials and Atoms, Volume 223-224, pp. 412-415.

Zhang, L., Hou, X., Cheng, P., Chen, N., Fan., Y., Liu, Q., 2018. Impact of North Korean nuclear weapons test on 3 September, 2017 on inland China traced by 14C and 129I. *Journal of Radioanalytical and Nuclear Chemistry,* 1 4, 316(1), pp. 383-388.

Zhang, L., Hou, X. & Xu, S., 2015. Speciation Analysis of 129I and 127I in Aerosols Using Sequential Extraction and Mass Spectrometry Detection. *Analytical Chemistry,* 7 7, 87(13), pp. 6937-6944.

Zhao, X. L., Litherland, A. E., Doupé, J. P. & Kieser, W. E., 2004. *The potential for AMS analysis of 10Be using BeF-. Nuclear Instruments and Methods in Physics Research Section B: Beam Interactions with Materials and Atoms, Volume 223-224*, pp. 199-204.

Zheng, J., Tagami, K., Bu, W., Uchida, S., Watanabe, Y., Kubota, Y., Fuma, S., Ihara, S., 2014. 135Cs/137Cs isotopic ratio as a new tracer of radiocesium released from the Fukushima nuclear accident. *Environmental Science and Technology,* 20 5, 48(10), pp. 5433-5438.

Zheng, J., Takata, H., Tagami, K., Aono, T., Fujita, K., Uchida, S., 2012. Rapid determination of total iodine in Japanese coastal seawater using SF-ICP-MS. *Microchemical Journal,* 1, 100(1), pp. 42-47.

Zulauf, A., Happel, S., Mokili, M.B., Bombard, A., Jungclas, H., 2010. *Characterization of an extraction chromatographic resin for the separation and determination of 36Cl and 129I.* Journal of Radioanalytical and Nuclear Chemistry, Volume 286, pp. 539-546.